

SUBMITTED UNDER CONTRACT N.  
11. 2 871 SUBMITTED AT NASA L...

IN 34-12  
NILES  
PRINT  
11/1531  
P-204

UNIVERSITY OF CALIFORNIA

Los Angeles

ANALYTICAL STUDY  
of the  
LIQUID PHASE TRANSIENT BEHAVIOR  
of a  
HIGH TEMPERATURE HEAT PIPE

A thesis submitted in partial satisfaction of the  
requirements for the degree Master of Science  
in Mechanical Engineering

by

Gregory Lawrence Roche

1988

(NASA-CR-187426) ANALYTICAL STUDY OF THE  
LIQUID PHASE TRANSIENT BEHAVIOR OF A HIGH  
TEMPERATURE HEAT PIPE M.S. Thesis  
(California Univ.) 204 p

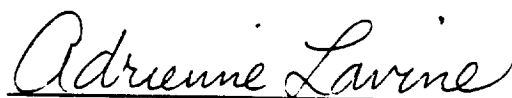
CSCL 200

N91-13644


Unclass

63/34 0317631

The thesis of Gregory Lawrence Roche is approved.



Adrienne G. Lavine



James M. McDonough



Ivan Catton, Committee Chair

University of California, Los Angeles

1988

PRECEDING PAGE BLANK NOT FILMED

## DEDICATION

This thesis is dedicated to my parents who have always given me their unconditional support.

## CONTENTS

Dedication .....	iii
List of Figures .....	vi
List of Symbols .....	viii
Acknowledgments .....	xv
Abstract of the Thesis .....	xvi
 <u>Chapter</u> .....	 <u>page</u>
I. Introduction .....	1
The Heat Pipe .....	1
The Problem .....	3
The Objectives .....	6
II. Theory of the Heat Pipe .....	8
Historical Perspective .....	8
Physical Operating Principles .....	9
Operating Limits .....	16
III. Heat Pipe Dynamics .....	24
Startup .....	25
Operating Transients .....	48
Shutdown .....	49
IV. The Solution .....	52
The Scope .....	52
The Configuration Studied .....	53
The Liquid Phase Mathematical Formulation .....	56
The Vapor Phase Mathematical Formulation .....	67
The Computational Implementation .....	71
V. Discussion of Results .....	83
Slow Startup Test .....	85
Sonic Limit Startup Test .....	92

VI.	Conclusions and Recommendations	95
	References	97

<u>Appendix</u>	<u>page</u>
A.	Liquid-Vapor Interface Conditions ..... 104
	Kinematic Surface Condition ..... 106
	Conservation of Mass ..... 107
	Continuity of Tangential Stress ..... 108
	Continuity of Normal Stress ..... 111
	Energy Boundary Condition ..... 113
B.	Axial Velocity Determination ..... 116
	Bulk Axial Velocity ..... 116
	Axial Velocity Distribution ..... 118
C.	Radial Velocity Determination ..... 125
	Radial Phase Change Velocity ..... 125
	Radial Velocity Distribution ..... 128
D.	Pressure Determination ..... 130
E.	Energy Equation Numerical Solution ..... 134
	General Numerical Formulation ..... 134
	Implementation of Boundary Conditions ..... 139
F.	Thermophysical Property Relations for Sodium ..... 149
G.	Computer Code Listing ..... 154

## LIST OF FIGURES

<u>Figure</u>	<u>page</u>
1. Representative Heat Pipe .....	2
2. Heat Pipe Applications in a Space Nuclear Power System .....	4
3. Axial Cross-Section of a Heat Pipe .....	10
4. Meniscus Due to Capillary Surface Tension Forces .....	13
5. Liquid and Vapor Pressure Gradients in a Heat Pipe .....	15
6. Heat Pipe Operating Limits .....	17
7. Three Modes of Heat Pipe Startup .....	26
8. Frontal Startup Temperature History of a Gas-Loaded Heat Pipe	30
9. Measured Vapor Temperatures During Startup .....	33
10. Startup Temperature History of Experimental Heat Pipe .....	35
11. Analytical Startup Prediction Map .....	39
12. Analytical Heat Pipe Startup as a Function of Time .....	41
13. Comparison of Analytical and Experimental Startup Data .....	46
14. Shutdown Temperature History of Experimental Heat Pipe .....	51
15. Heat Pipe with High Performance Composite Annular Wick .....	54
16. Cross Section of High Performance Annular Wick Configuration .	55
17. Algorithm Overview Flowchart .....	72
18. Algorithm Startup Flowchart .....	75
19. Algorithm Time Step Iteration Flowchart .....	77

20.	Algorithm Completion Flowchart .....	81
21.	Slow Startup Pressure Drop Results .....	87
22.	Slow Startup Liquid Pressure Drop Oscillations .....	88
23.	Slow Startup Heat Transfer Results .....	90
24.	Slow Startup Vapor Temperature Results .....	91
25.	Sonic Limit Startup Heat Transfer Results .....	93
26.	Sonic Limit Startup Vapor Temperature Results .....	94
27.	Liquid-Vapor Interface Physics .....	104
28.	Bulk Axial Velocity Control Volume .....	117

## LIST OF SYMBOLS

### ENGLISH SYMBOLS

- $A$  = area ( $m^2$ )
- $A_a$  = cross-sectional area of annulus ( $m^2$ )
- $A_l$  = cross-sectional area of liquid flow channel ( $m^2$ )
- $A_{lv}$  = cross-sectional area of liquid-vapor interface ( $m^2$ )
- $A_v$  = cross-sectional area of vapor space ( $m^2$ )
- $b, c, d$  = shape coefficients of axial velocity profile
- $c$  = speed of sound based on stagnation temperature ( $m/s$ )
- $C$  = heat capacity per unit length ( $J/kg \cdot K \cdot m$ )
- $c_v$  = specific heat at constant volume ( $J/kg \cdot K$ )
- $C_w$  = coefficient of wick porosity
- $D$  = diameter ( $m$ )
- $f$  = body force ( $N$ )
- $f_l$  = laminar duct flow friction coefficient
- $F_l$  = liquid flow friction coefficient ( $s/m^4$ )
- $h$  = enthalpy ( $J/kg$ )
- $h_x$  = axial grid step size ( $m$ )
- $h_r$  = radial grid step size ( $m$ )
- $h_{fg}$  = latent heat of vaporization ( $J/kg$ )
- $h_1$  = coefficient for determining radial phase change velocity



$i$	= cylindrical coordinates axial direction index
$j$	= cylindrical coordinates radial direction index
$k$	= cylindrical coordinates azimuthal direction index
$k$	= thermal conductivity ( $W/m \cdot K$ )
$k$	= time step size ( $s$ )
$K_n$	= Knudsen number
$l$	= length ( $m$ )
$L$	= overall heat pipe length ( $m$ )
$L_c$	= characteristic length ( $m$ )
$L_p$	= molecular mean free path ( $m$ )
$\dot{m}$	= mass flux ( $kg/s$ )
$M$	= mass ( $kg$ )
$M$	= molecular weight ( $kg/kgmole$ )
$\bar{n}$	= unit normal vector
$N$	= number of axial direction grid steps
$P$	= pressure ( $Pa$ )
$\bar{P}$	= total stress vector ( $N/m^2$ )
$q$	= heat flux ( $W/m^2$ )
$q_{in}$	= input heat flux ( $W/m^2$ )
$q_{max}$	= maximum input heat flux ( $W/m^2$ )
$q_0$	= heat flux at the liquid-vapor interface ( $W/m^2$ )
$q_{rad}$	= radiation heat flux ( $W/m^2$ )
$Q$	= heat transfer rate ( $W$ )
$Q_{cap}$	= capillary limit maximum heat transfer rate ( $W$ )

- $Q_{in}$  = heat transfer rate input to the evaporator ( $W$ )  
 $Q_{son}$  = sonic limit maximum heat transfer rate ( $W$ )  
 $r$  = cylindrical coordinate radial direction  
 $r_h$  = hydraulic radius ( $m$ )  
 $r^*$  = dimensionless radial coordinate  
 $R$  = radius ( $m$ )  
 $R_c$  = capillary radius of curvature ( $m$ )  
 $R_e$  = Reynolds number  
 $R_g$  = gas constant ( $J/kg \cdot K$ )  
 $R_p$  = wick pore radius ( $m$ )  
 $R_u$  = universal gas constant,  $8314 \text{ J/kgmole} \cdot K$   
 $R_v$  = radius of vapor space ( $m$ )  
 $R_1, R_2$  = radii of curvature of a meniscus surface ( $m$ )  
 $S$  = liquid-vapor interface surface shape function ( $m$ )  
 $S$  = molar entropy ( $W/kgmole \cdot K$ )  
 $t$  = time ( $s$ )  
 $t^{(n)}$  = time at discrete time level  $n$  ( $s$ )  
 $t^{(n+1)}$  = time at discrete time level  $n + 1$  ( $s$ )  
 $t^*$  = time at discrete time level  $t^{(n)} < t^* < t^{(n+1)}$  ( $s$ )  
 $\vec{t}$  = unit tangent vector  
 $T$  = temperature ( $K$ )  
 $T_c$  = critical temperature ( $K$ )  
 $T_r$  = reduced temperature ( $K$ )  
 $u$  = velocity component in axial direction ( $m/s$ )

$u^*$	= dimensionless velocity component in axial direction
$\vec{U}$	= velocity vector ( $m/s$ )
$\bar{U}$	= bulk axial velocity ( $m/s$ )
$\vec{U}_{lv}$	= liquid-vapor interface surface velocity ( $m/s$ )
$v$	= velocity component in radial direction ( $m/s$ )
$V$	= molar volume ( $m^3/mole$ )
$V$	= volume ( $m^3$ )
$V_0$	= liquid phase change radial velocity ( $m/s$ )
$V_{0v}$	= vapor phase change radial velocity ( $m/s$ )
$w$	= velocity component in the azimuthal direction ( $m/s$ )
$W_e$	= Weber number
$x$	= cylindrical coordinates axial direction coordinate ( $m$ )

## SUBSCRIPTS

$a$	= adiabatic region
$a$	= annulus
$c$	= condenser region
$c$	= critical property value
$cap$	= capillary
$e$	= environment radiation sink
$e$	= evaporator region
$eff$	= effective
$i$	= cylindrical coordinates axial direction index
$in$	= input

$j$  = cylindrical coordinates radial direction index  
 $JV$  = liquid-vapor interface radial grid index  
 $JW$  = pipe external wall radial grid index  
 $k$  = cylindrical coordinates azimuthal direction index  
 $l$  = liquid  
 $lv$  = liquid-vapor interface  
 $0$  = value at liquid-vapor interface  
 $p$  = wick pore  
 $\phi$  = cylindrical coordinates azimuthal direction  
 $pc$  = phase change  
 $r$  = cylindrical coordinates radial direction  
 $r$  = reduced property value  
 $rad$  = radiation  
 $s$  = liquid-vapor interface surface  
 $sat$  = thermodynamic saturation condition  
 $son$  = sonic  
 $v$  = vapor  
 $w$  = pipe wall  
 $w$  = wick screen wire  
 $x$  = cylindrical coordinates axial direction coordinate

## SUPERSCRIPTS

- $n$  = discrete time level index  
 $n + 1$  = discrete advanced time level index  
 $*$  = discrete intermediate time level index  
 $*$  = dimensionless value

## GREEK SYMBOLS

- $\alpha$  = thermal diffusivity ( $m^2/s$ )  
 $\gamma$  = ratio of principle specific heats  
 $\delta$  = annulus gap width,  $R_t - R_v$  ( $m$ )  
 $\delta_t$  = time step size ( $s$ )  
 $\Delta$  = difference  
 $\varepsilon$  = flow direction wick porosity  
 $\varepsilon$  = surface radiation emissivity  
 $K$  = wick permeability ( $m^2$ )  
 $\lambda$  = wavelength of capillary wave ( $m$ )  
 $\mu$  = dynamic viscosity ( $kg/m \cdot s$ )  
 $\nu$  = kinematic viscosity ( $m^2/s$ )  
 $\rho$  = density ( $kg/m^3$ )  
 $\sigma$  = surface tension coefficient ( $N/m$ )  
 $\sigma_{ik}$  = stress component ( $N/m^2$ )  
 $\sigma$  = Stefan-Boltzmann constant,  $5.6696 \times 10^{-8} W/m^2 \cdot K^4$   
 $\tau$  = input heat flux time parameter ( $s$ )  
 $\bar{\tau}$  = viscous shear force ( $N$ )

$\phi$  = cylindrical coordinates azimuthal direction (*radians*)

#### SPECIAL SYMBOLS

$\nabla$  = del operator

$\nabla_s$  = del operator on a surface

$\nabla^2$  = Laplacian operator

$\Delta P_{cap}$  = maximum capillary pressure across a meniscus surface (*Pa*)

$\Delta P_{pc}$  = phase change pressure jump (*Pa*)

## ACKNOWLEDGMENTS

Special recognition and thanks are extended to those individuals and institutions that have contributed to my graduate education. Professor Ivan Catton served as my advisor and helped to open my eyes. Professor James McDonough served on my thesis committee and introduced me to the art and science of numerical computation. Professor Adrienne Lavine served on my thesis committee and reminded me that learning can be fun.

The research represented by this thesis was partially supported by a grant from the Innovative Nuclear Space Power Institute. The UCLA Office of Academic Computing provided support through their excellent staff and facilities. Southern California Edison Company and Rockwell International provided tuition and other support during my employment with them.

I would like to especially thank Kathy Bishop for the understanding, the encouragement, and the positive mental attitude that have been so instrumental in enduring the graduate student experience.

ABSTRACT OF THE THESIS

ANALYTICAL STUDY

of the

LIQUID PHASE TRANSIENT BEHAVIOR

of a

HIGH TEMPERATURE HEAT PIPE

by

Gregory Lawrence Roche  
Master of Science in Mechanical Engineering  
University of California, Los Angeles, 1988  
Professor Ivan Catton, Chair

The transient operation of the liquid phase of a high temperature heat pipe is studied. The study was conducted in support of advanced heat pipe applications that require reliable transport of high temperature, high flux thermal energy over small temperature drops and significant distances under a broad spectrum of operating conditions.

The heat pipe configuration studied consists of a sealed cylindrical enclosure containing a capillary wick structure and sodium working fluid. The wick is



an annular flow channel configuration formed between the enclosure interior wall and a concentric cylindrical tube of fine pore screen.

The study approach is analytical through the solution of the governing equations. The energy equation is solved over the pipe wall and liquid region using the finite difference Peaceman-Rachford Alternating Direction Implicit numerical method. The continuity and momentum equations are solved over the liquid region by the integral method. The energy equation and liquid dynamics equations are tightly coupled due to the phase change process at the liquid-vapor interface. A kinetic theory model is used to define the phase change process in terms of the temperature jump between the liquid-vapor surface and the bulk vapor. Extensive auxiliary relations, including sodium properties as functions of temperature, are used to close the analytical system.

The solution procedure is implemented in a Fortran computer algorithm with some optimization features to take advantage of the IBM System/370 Model 3090 vectorization facility. Code output includes: temperatures of the pipe wall and liquid; velocities and pressures of the liquid; radii of curvature of the liquid-vapor interface meniscii; input, output, evaporation and condensation heat fluxes; sonic, entrainment, and capillary heat flux limits; and identification of operating limit violations.

The code was intended for coupling to a vapor phase algorithm so that the entire heat pipe problem could be solved. As a test of code capabilities, the vapor phase was approximated in a simple manner. The vapor was assumed to be quasisteady relative to liquid dynamics and uniform throughout specified control volumes. The simple treatment allowed demonstration of calculations,

but did not necessarily produce physically significant results. The kinetic theory phase change model was found to produce numerical stability and accuracy problems. The solution approach would also benefit from special treatment of the widely disparate length scales in the different coordinate directions. Cross-stream temperature gradients were found to be small such that a simplified solution approach taking advantage of this feature could be developed.

## Chapter I

### INTRODUCTION

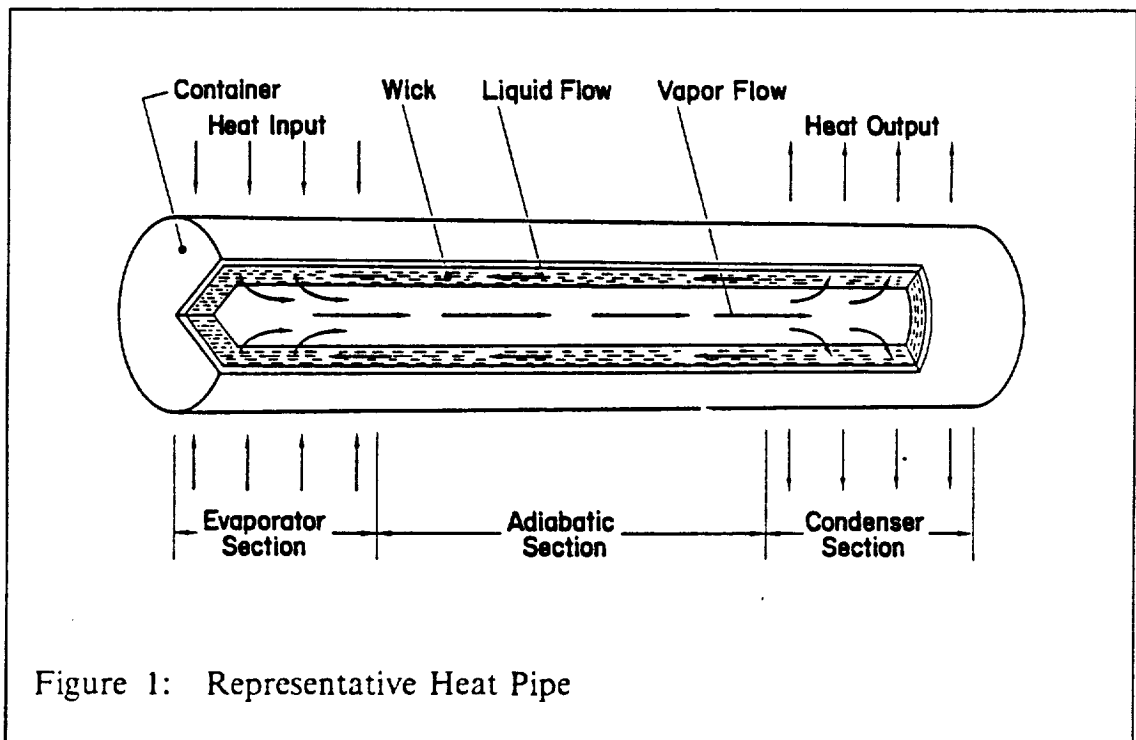
*“... a heat pipe may be regarded as a synergistic engineering structure which is equivalent to a material having a thermal conductivity greatly exceeding that of any known metal.”*

*G. M. Grover et al. 1964 [1]*

#### 1.1 THE HEAT PIPE

Transporting thermal energy at a high rate over a small temperature gradient is an important requirement for many heat transfer applications. One common method for meeting this requirement involves evaporation of a liquid at the heat source, transporting the resulting vapor to a heat sink for condensation, and replenishing the liquid through return of the condensate or provision of a continuous fresh liquid supply. The disadvantage of this approach is that generally work in the form of gravity or mechanical pumping must be performed on the system to maintain the supply of liquid. The heat pipe provides a passive alternative heat transfer system that accomplishes the same heat transfer functions without requiring external work.

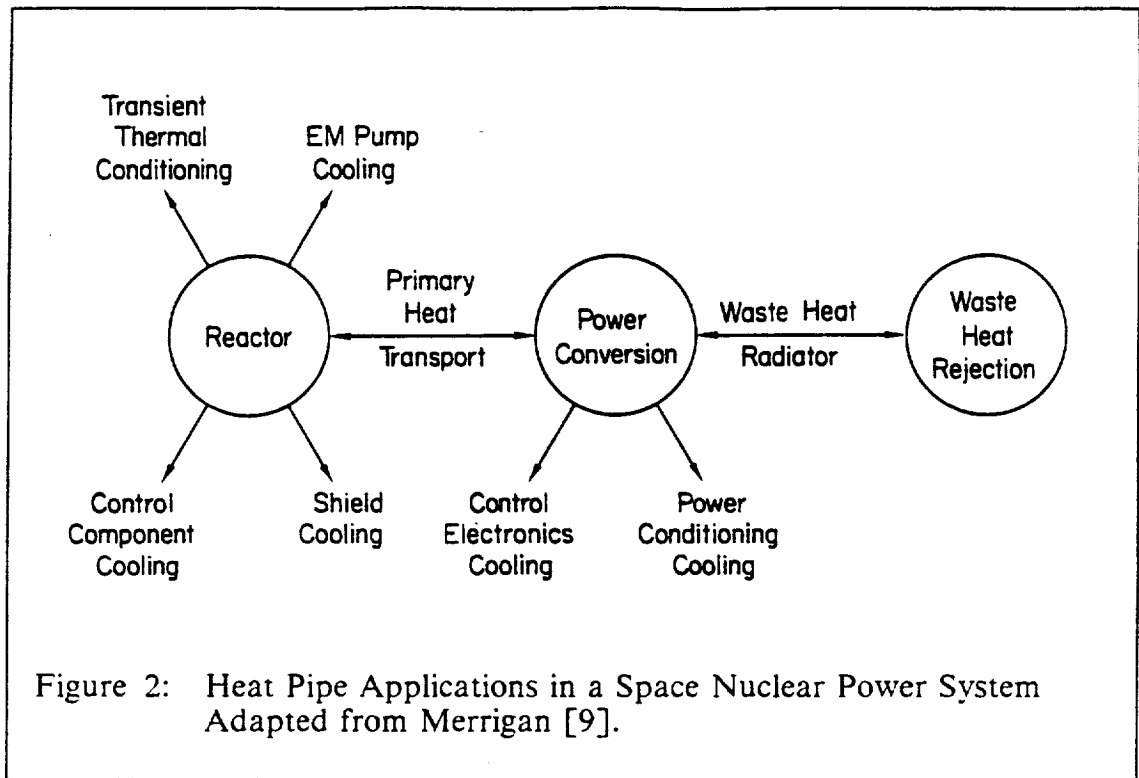
The heat pipe generally consists of a long sealed container that encloses a working fluid and a capillary wicking structure as shown in Figure 1. Heat added at the evaporator section causes a temperature increase and evaporation of the working fluid liquid phase. Mass addition to the vapor space and the temperature rise produce a vapor pressure gradient resulting in vapor flow from the heated evaporator to the cool condenser where condensation occurs. The condensate is returned to the heated end by the action of capillary forces in the wicking material. Since the primary mode of heat transfer is through the latent heat of vaporization, steady state operation is nearly isothermal even while maintaining a high heat transfer rate.



## 1.2 THE PROBLEM

Heat pipes are self-starting, self-regulating, high efficiency devices that operate passively. Unlike normal conducting materials, however, a heat pipe cannot be characterized by a single property such as an effective thermal conductivity. Rather, operation of the heat pipe is governed by the coupled laws of fluid dynamics and heat transfer as applied to each unique configuration.

There have been many advances in heat pipe design, theory and practice since the first experimental work performed by Grover in the early 1960's and the first quantitative analysis performed by Cotter in 1965[1][2] . There are now over 2000 heat pipe references in the literature[3] . There have been six international heat pipe conferences, and there are at least five heat pipe textbooks and design guides[4][5][6][7][8] . The scope of published information spans a broad range of theory, analysis, experiment, and application. However, the majority of these works are limited to steady state applications under highly idealized conditions. Comparatively little work has been done that addresses future heat transport requirements for applications that would benefit from the use of heat pipes. For example, space missions requiring high power supplies and reliable operation over a wide range of conditions may use nuclear generating systems. Such a system has a wide range of heat transfer requirements as shown in Figure 2 that may be met by heat pipes[9] . The heat transfer requirements range from high temperature, high flux primary heat transport to lower temperature secondary transport to heat transport for support equipment.



Primary heat transport channels reactor thermal energy to the power conversion system for production of electricity. Waste heat rejection transfers unuseable thermal energy to a radiator system for disposal to space. Support equipment heat transfer requirements include electromagnetic pump cooling, radiation shield cooling, control drum and motor cooling, and startup and shutdown thermal conditioning of liquid metal pumped heat transfer loops. As detailed designs are developed heat pipes may also be used in the control of power conditioning equipment, in control electronics cooling, and in low temperature waste heat rejection.

Heat transfer requirements unrelated to space nuclear power that may be met by heat pipes have also been identified. The leading edges of hypersonic

re-entry vehicles could be cooled and maintained isothermal by liquid metal heat pipes[10] . While the working fluid would normally be below the melting point, re-entry heat loads would melt the working fluid and initiate heat pipe operation. High temperature heat pipes have also been proposed for cooling and making isothermal the nozzles of rocket engines[11] .

Heat pipes may be the preferred design approach for many of these applications. Heat pipes offer a highly redundant system of independent flow paths. Passive operation can provide automatic handling of reactor decay heat as well as for restart after extended periods of inoperation without the need for stored power for pumps and controls. Heat pipes operate with minimal temperature drop such that high efficiency thermal radiation can be achieved. Heat pipes are able to transform thermal energy between high flux and low flux conditions at the pipe external boundaries.

While the range of benefits is impressive, many issues require further research. One of the most challenging issues is the transient operation of heat pipes. Transient heat pipe behavior has become the focus of recent research due to requirements for reliable operation over wide operating conditions. Consider the space-based nuclear power generating system. The system would be placed in orbit at temperatures below the melting point of the heat pipe working fluid. Placing the system in operation would require heat pipe startup from the frozen working fluid state. After achieving steady state operation, nominal changes in reactor power production, power conversion system operation, or heat rejection efficiency would result in transients requiring heat pipe response to load level changes. At some point due to maintenance

requirements or duty cycle, system shutdown would be required. The shutdown may be to temperatures below the working fluid melting point. The heat pipe must attain a state that permits eventual restart from the frozen or liquid state. The heat pipe may be required to operate for extended periods in a standby or low power level mode with occasional short bursts of full power operation.

Issues that must be resolved include determining the heat pipe response time, the ultimate capability of the heat pipe to handle the transient, and whether future operation is possible if the heat pipe is taken outside of design capabilities. The useable lengths of heat pipes must be determined, as well as optimal design configuration. Durability is an issue due to the cyclic nature of the application. Finally, the heat pipe problem must be reduced to a minimal set of parameters suitable for a system study with high fidelity results.

### **1.3 THE OBJECTIVES**

The purpose of this research is to develop an analytical model of the transient dynamics of the liquid phase in a high temperature heat pipe. This liquid phase model is intended to be coupled with a vapor phase model for the assessment of the potential for heat pipes to meet future heat transfer requirements covering a broad spectrum of transient operating conditions. These requirements are assumed to include high temperatures, high thermal flux, and reliable operation over long distances and small temperature drops. The model is intended to calculate the temperatures, velocities, and pressures



required to assess heat pipe transients. Transient operation characteristics of interest include the capability of a heat pipe to reach steady state operation following a change in operating conditions; the allowable magnitudes and rates of changes; the time required to respond to transient conditions; and the temperatures, velocities, and pressures encountered during transient operation.

## Chapter II

### THEORY OF THE HEAT PIPE

*“[The invention was to] cause absorption of heat, or in other words, the evaporation of the liquid to a point above the place where the condensation or the giving off of heat takes place without expending upon the liquid any additional work to lift the liquid to an elevation above the point at which condensation takes place.”*

*R. S. Gaugler 1944 [12]*

#### 2.1 HISTORICAL PERSPECTIVE

The predecessor of the heat pipe was developed in the mid 19th century by Angier Perkins [6]. The device, known as the Perkins Pipe, consisted of an unwicked sealed container in which heat transfer was accomplished through evaporation and vapor transport to a cool condensing point. Circulation of liquid was accomplished through gravitational forces. This device was a wickless heat pipe, known in current terminology as the thermosyphon.

The novel idea of using capillary forces to replace or supplement gravitational forces in circulating the working fluid is attributed to R. Gaugler in 1944[12] . The device was a true heat pipe consisting of a sealed container

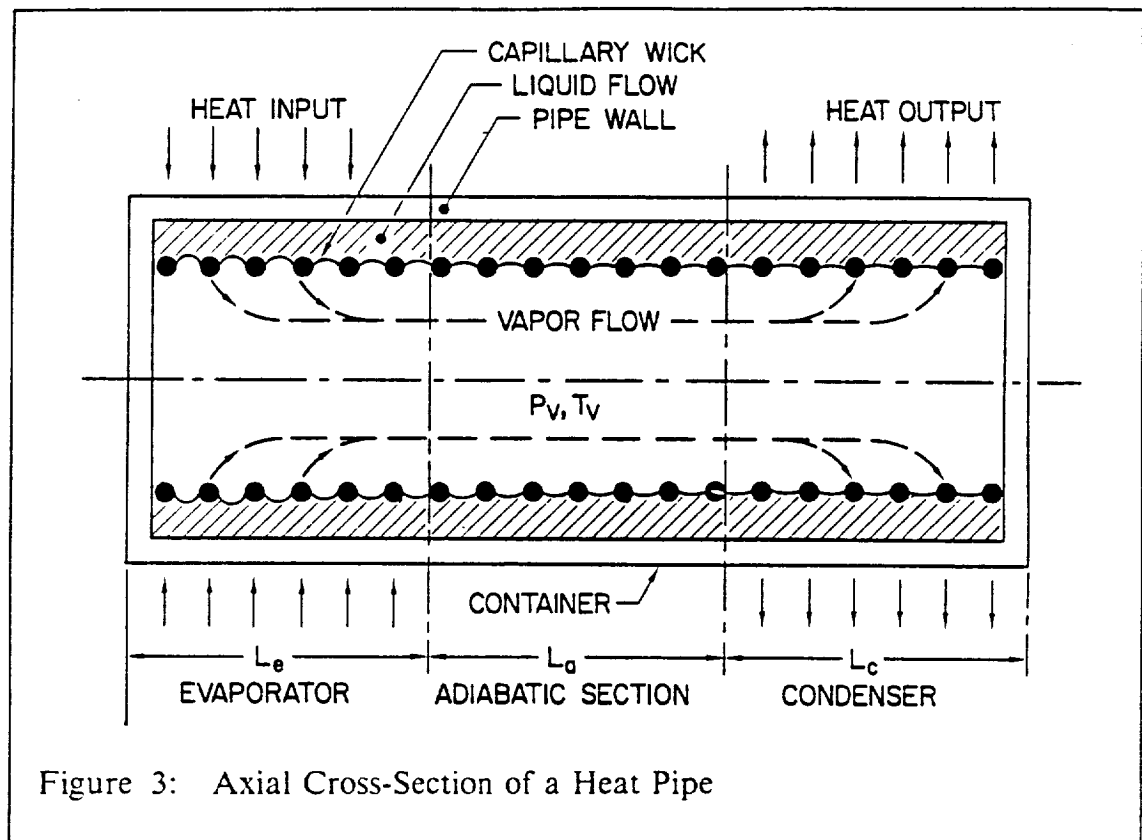
with capillary wick and working fluid. The invention was intended for use in the refrigeration industry but was not utilized.

The development of space power systems some twenty years after Gaugler's patent introduced a viable application for the capillary heat transfer device. The term heat pipe was introduced by Grover and his co-workers at Los Alamos Scientific Laboratory in 1963[13] . Limited experimental work by Grover in 1964 using water as the working fluid followed by liquid sodium showed the great promise of heat pipes in serving as highly efficient conductors [1]. The theoretical basis for heat pipe operation and analysis was first formulated by Cotter in 1965 [2].

## **2.2 PHYSICAL OPERATING PRINCIPLES**

The term heat pipe refers to a large class of heat transport devices. The operating principles provide great flexibility in tailoring the heat pipe design to a specific application. The fluid dynamics and heat transfer principles are integral to the specific design configuration such that each unique design requires a dedicated analysis. However, the general operating principles can be described in terms of the simple representative configuration shown in Figure 3.

A heat pipe generally consists of a long sealed container enclosing a working fluid and a capillary wick structure. The liquid and vapor have distinct flow paths, but share a common interface which allows them to communicate in all parts of the system. The quantity of working fluid is sufficient to at least



saturate the wicking material. The wick can be constructed of essentially any porous material: screen, gauze, sintered material, packed spheres, grooves in the container wall, perforated shields, etc. The heat pipe can use any working fluid that has a liquid and vapor phase at the operating temperature, that wets the wicking material, and is chemically compatible with the container and wick material. Proper selection of working fluid, container, and wick allow the heat pipe to be designed for specific temperature ranges: the cryogenic temperature range (0 to 150 K), the low temperature range (150 to 750 K), or the high temperature range (750 K and above).

A heat pipe generally has three distinct zones: the evaporator section, the adiabatic section, and the condenser section. The adiabatic section is optional and serves only to span the distance between the evaporator and condenser.

There are three basic types of heat transfer/fluid dynamics problems to consider:

1. Vapor flow in the core
2. Liquid flow in the wick
3. Phase transition between liquid and vapor

These three basic problems are coupled not only with each other but also with the specifics of the particular heat pipe design. Under static conditions with no heat flux, the liquid and vapor are under saturation equilibrium conditions. Thermal energy supplied to the evaporator is conducted across the container wall. Conduction and convection transport the heat to the liquid-vapor interface. The heat flux increases the liquid temperature which raises the liquid saturation vapor pressure. A pressure imbalance results between the liquid saturation vapor pressure and the pressure of the bulk vapor. If the pressure drop from the liquid saturation vapor pressure to the vapor phase pressure is larger than the pressure drop required for phase change, net evaporation will occur. The evaporating mass flux carries the thermal energy transferred to the liquid-vapor interface through the latent heat of vaporization. Mass injection and increased temperature raise the evaporator vapor phase pressure and establish pressure gradients that drive the vapor through the adiabatic region to the condenser. The pressure of the vapor in the condenser becomes higher than the liquid saturation vapor pressure. The

pressure imbalance results in net condensation on the cooler liquid if again the pressure drop is greater than that required for phase change. Since thermal energy is transferred in the form of latent heat of vaporization rather than sensible heat, high heat transfer rates can be achieved with low mass flow. If heat is transferred by high density, low velocity vapor the heat transfer is nearly isothermal due to the low vapor pressure gradient.

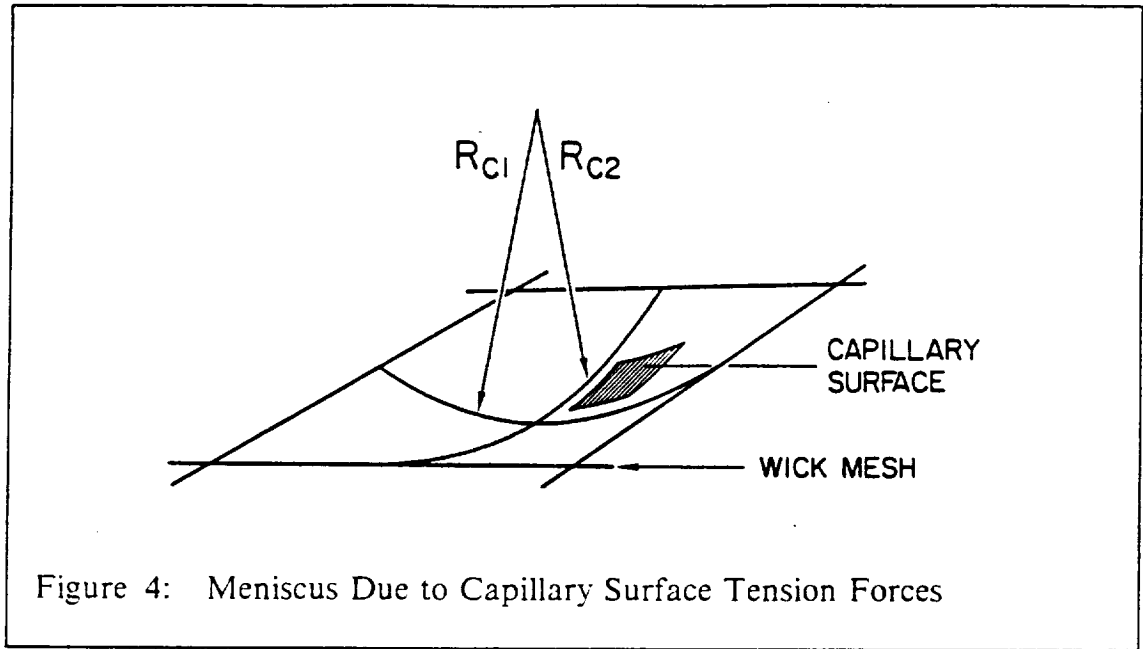
The condensate is returned to the evaporator through capillary pumping in the wick. As liquid evaporates, the liquid-vapor interface recedes into the wick. Pores in the wick form capillary structures in which a curved meniscus forms as shown in Figure 4 due to the pressure difference between the liquid and vapor across the surface and the action of surface tension forces. The Laplace-Young Equation relates surface curvature to the pressure jump across an equilibrium liquid-vapor interface[14]

$$P_v - P_l = \sigma \left( \frac{1}{R_1} + \frac{1}{R_2} \right) \quad (1)$$

where  $P_v$  is the vapor pressure,  $P_l$  is the liquid pressure,  $\sigma$  is the surface tension coefficient, and  $R_1$  and  $R_2$  are the principal radii of curvature of the meniscus surface. The liquid contact angle is taken in Equation 1 as zero for simplicity. The effects of phase transition can be included to take account of non-equilibrium systems

$$P_v - P_l + \Delta P_{pc} = \sigma \left( \frac{1}{R_1} + \frac{1}{R_2} \right) \quad (2)$$

where  $\Delta P_{pc}$  is the pressure difference due to the phase change transition.



As liquid recedes further into the wick, the radii of curvature decrease resulting in an increase in the liquid to vapor pressure jump and corresponding decrease in liquid pressure. The action in the condenser is the opposite process to that in the evaporator. Condensate tends to flood the wick such that the principal radii of curvature increase and the pressure difference between liquid and vapor decreases. If the wick is completely saturated such that the liquid forms a smooth flat surface across the wick at the liquid-vapor interface, then one principal radius of curvature is essentially infinite in length while the other is set by the dimension of the vapor space

$$P_v - P_l + \Delta P_{pc} = \frac{\sigma}{R_v} \quad (3)$$

where  $R_v$  is the radius of the vapor space.  $\Delta P_{pc}$  is generally small relative to other pressure drops in the system and can be neglected. The quotient  $\sigma/R_v$  is

small relative to  $P_v$  such that the pressure jump  $P_v - P_l$  for the flooded wick can be neglected relative to other pressure drops in the system. The liquid and vapor pressures for a flooded wick can then be taken as being essentially equal as in the case of a completely planar interface.

The variation along the length of the pipe of the radii of curvature coupled with the vapor pressure gradient results in a liquid pressure gradient ~~the~~ drives the liquid from the condenser to the evaporator. Typical pressure gradients in the liquid and vapor are shown in Figure 5. These pressure gradients show that continuous circulation of the working fluid and corresponding heat transfer can be maintained. However, there are certain operating limits governed by fluid dynamics and heat transfer theory. Knowledge of these limits imposed by fundamental theory is required to assure heat pipe operation.



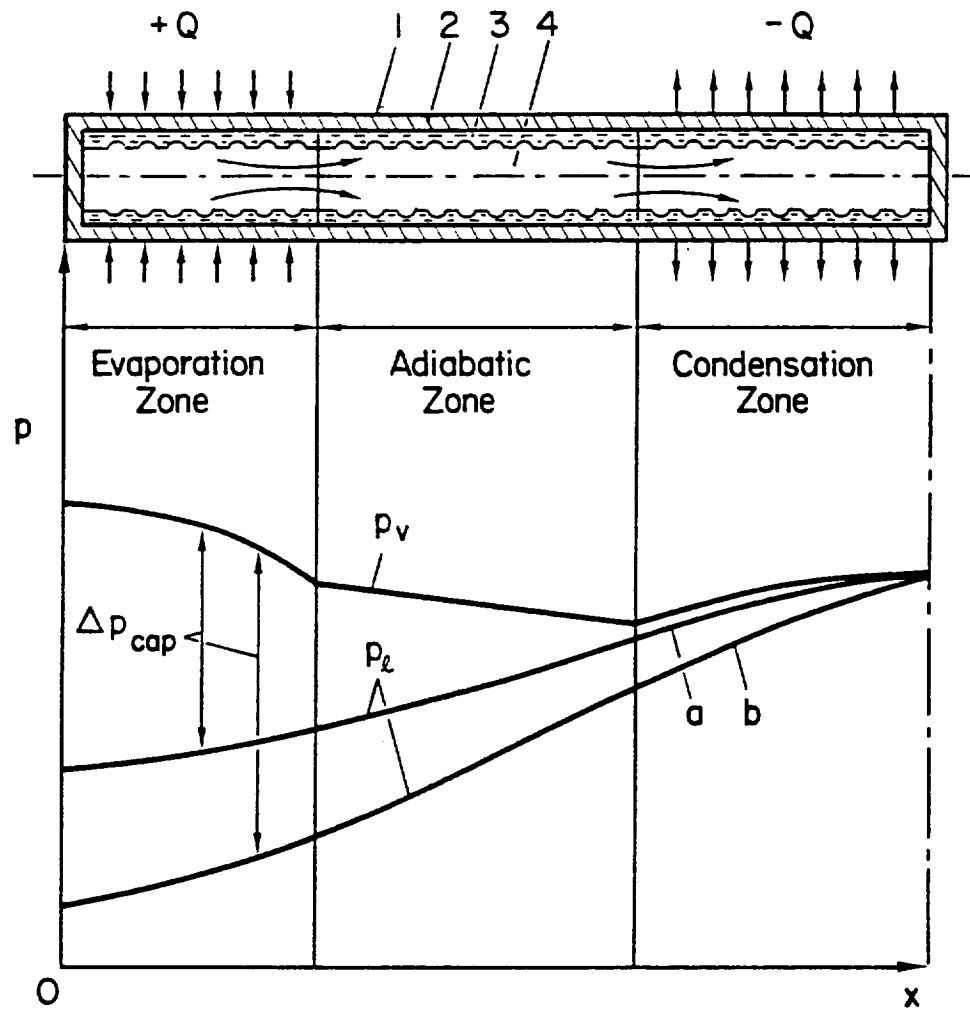


Figure 5: Liquid and Vapor Pressure Gradients in a Heat Pipe  
 a ) Negligible Gravity  
 b ) Gravity Opposed  
 Adapted from Ivanovskii et al. [4]

## 2.3 OPERATING LIMITS

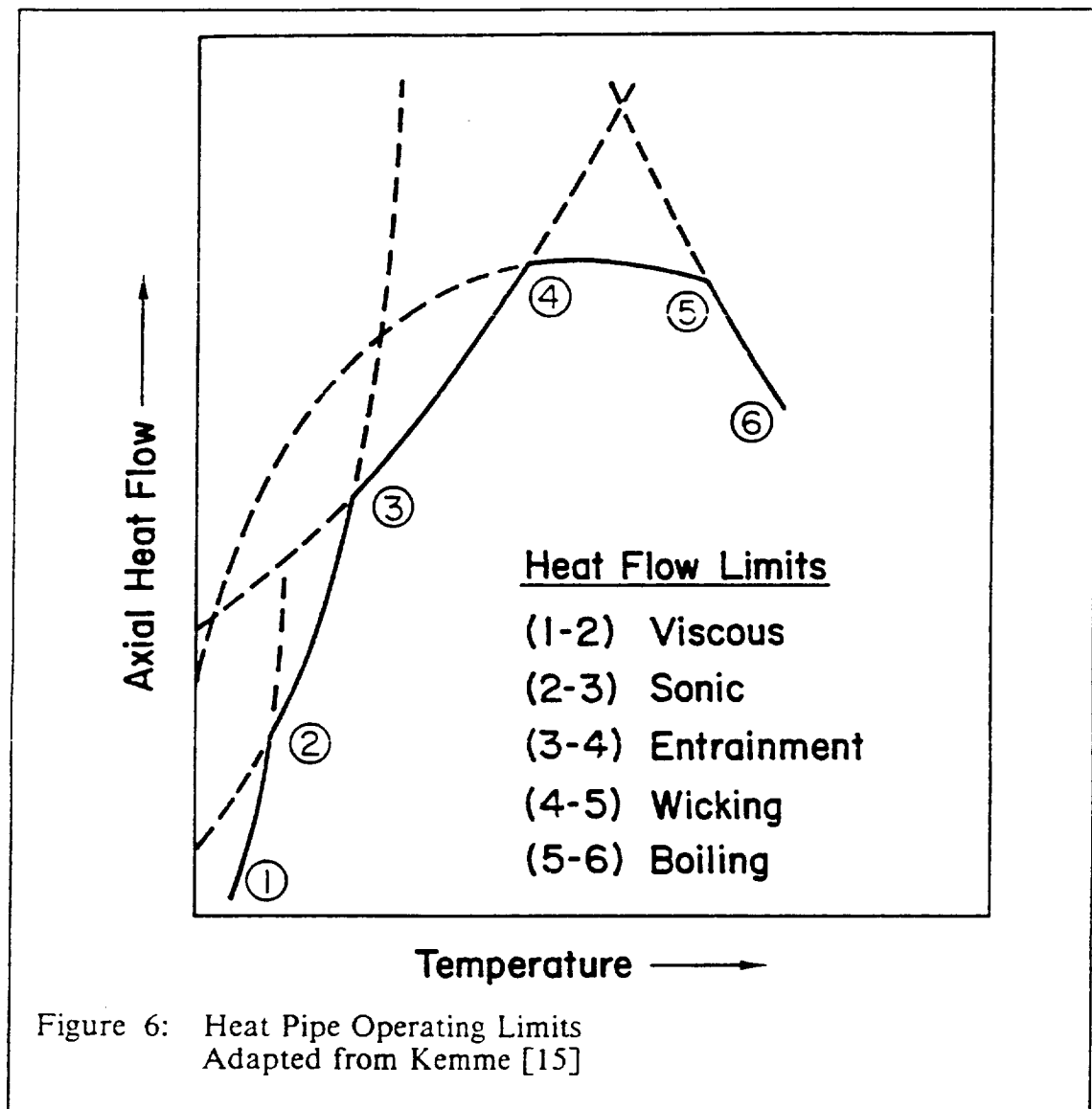
A heat pipe behaves like a structure of very high thermal conductance, but is constrained by the principles of fluid dynamics and heat transfer. These operating constraints depend additionally on thermophysical properties of the working fluid, container and wick, design configuration, and the coupling of the heat pipe to the environment for heat addition and removal. The commonly accepted limits discussed in the literature and shown in Figure 6 include [4][15] :

1. Viscous Limit
2. Sonic Limit
3. Entrainment Limit
4. Capillary Limit
5. Boiling Limit

As shown in Figure 6, the limits have overlapping regions of influence such that knowledge of all limits is required to assess a heat pipe for a specific application.

### 2.3.1 *Viscous Limit*

The viscous limit refers to vapor pressure losses due to friction forces. The viscous limit is generally associated with operation at low vapor pressures and temperatures when vapor density is low. The viscous limit is particularly noted in heat pipes with long condenser sections. Under these circumstances, the vapor pressure at the end of the condenser may be low enough to be effectively



zero in considering the maximum possible vapor pressure drop available to drive the vapor flow. The low possible pressure drop results in a low possible heat transport capability. The viscous limit is not necessarily a failure of the pipe to operate, but a limit on the heat transfer capability under specific conditions.

### 2.3.2 *Sonic Limit*

The sonic limit refers to vapor flow attaining the speed of sound in some part of the pipe. This condition is generally a concern during startup when the vapor has low pressure and large specific volume. The vapor velocity at the evaporator exit is high even for low heat transfer rates and can reach sonic velocity. Mass flow rate is then choked at the point where sonic velocity is attained such that downstream pressure changes are not transmitted upstream. Since mass flow is choked, the axial heat transfer rate cannot be increased by improving heat removal in the condenser. In fact, improved condenser heat removal would actually prolong the sonic condition since the pipe would be prevented from heating up through storage of sensible heat. Large axial temperature gradients develop as the evaporator heats up faster than the condenser. The heat transfer associated with the sonic limit can be approximated as a function of vapor properties at the point of sonic velocity by [5]

$$Q_{son} = \frac{\rho_v h_{fg} A_v c}{\sqrt{2(1 + \gamma)}} \quad (4)$$

where  $\rho_v$  is vapor density,  $c$  is the speed of sound corresponding to stagnation temperature,  $h_{fg}$  is the latent heat of vaporization,  $A_v$  is the vapor flow cross-sectional area, and  $\gamma$  is the ratio of principal specific heats.

The sonic limit ordinarily does not result in heat pipe failure but is a transition condition from low vapor pressure to normal operating pressure. As shown in Figure 6, sonic limit can prevent the heat pipe from reaching more

severe limitations that can disrupt heat pipe operation such as the capillary limit.

### 2.3.3 *Entrainment Limit*

The entrainment limitation is brought about by the capture of condensate in the wick by the counterflowing vapor. The process is similar to a body of water agitated by high velocity winds into waves which propagate until liquid is torn from the wave crests. In a similar manner, high velocity vapor in the heat pipe can tear liquid from the wick. The entrained liquid is carried with the vapor back into the condenser. Entrainment acts to increase the working fluid circulation rate. However, an increase in heat transfer occurs only if the liquid absorbs sensible energy prior to entrainment since phase change latent heat is not involved. Since sensible energy transport is much less efficient than transport of latent heat, the increased fluid circulation rate does not sufficiently increase heat transfer to meet the heat transport requirements. Fluid circulation increases until capillary pressure cannot accommodate the flow rate. Formation of hot spots and dryout of the evaporator region results.

The occurrence of entrainment is a result of vapor inertia forces overcoming liquid surface tension forces. Onset of entrainment is generally assumed to occur when the ratio of viscous forces to liquid surface tension forces, called the Weber number  $We$ , is on the order of unity, where [4]

$$We = \frac{\rho_v u_v^2 \lambda}{2\pi\sigma} \quad (5)$$

where  $u_v$  is the vapor velocity axial component and  $\lambda$  is the wavelength of a capillary wave. The capillary wave is a difficult to determine function of the liquid-vapor interface surface and the geometry of the surface pores. The entrainment limit heat transfer can be approximated as [5]

$$Q_{ent} = A_v h_{fg} \sqrt{\frac{\sigma \rho_v}{2 r_{h,p}}} \quad (6)$$

where  $r_{h,p}$  is the hydraulic radius of the wick pores at the liquid-vapor interface surface.

#### 2.3.4 Capillary Limit

Continuous circulation of working fluid is required for steady state heat pipe operation. The liquid circulation is maintained by capillary pressure forces developed in the wick structure at the liquid-vapor interface. The capillary pressure forces  $\Delta P_{cap}$  must be sufficient to balance pressure drops in the vapor flow, the liquid flow, and phase transition

$$\Delta P_{cap} \geq \Delta P_v + \Delta P_l + \Delta P_{pc} \quad (7)$$

As heat transferred by the pipe increases, the working fluid circulation rate also increases resulting in larger pressure drops in the flow paths. The maximum heat transfer capability is determined by the maximum capillary pressure force that can be attained by the wick. If the heat transfer is increased further, liquid flow rate cannot be increased to meet the higher demand. Evaporation will cause the liquid to recede into the wick resulting in

dryout and interruption of the working fluid circulation. The pipe will develop hot spots where liquid has dried out. The wicking limit is usually encountered at high vapor pressure when almost all pressure drop is in the liquid [15].

A simple expression can be derived relating the capillary heat transfer limit to operating conditions [5]

$$\left. \frac{\Delta P}{\Delta x} \right|_{cap} = -F_l Q_{cap} \quad (8)$$

where  $F_l$  is the liquid flow coefficient of friction,  $Q_{cap}$  is the capillary heat transfer limit, and  $\left. \frac{\Delta P}{\Delta x} \right|_{cap}$  is the pressure gradient at the capillary limit.

By assuming liquid and vapor pressures are equal at the end of the condenser, Equation 1 can be evaluated at the two extremes of the pipe

$$[P_v - P_l]_{x=0} - [P_v - P_l]_{x=L} = [P_v - P_l]_{x=0} = \frac{2\sigma}{R} \quad (9)$$

where the assumption has been made that the capillary radii of curvature are equal,  $R_1 = R_2 = R$ .

The capillary pressure drop limit over the length of the pipe occurs when the minimum capillary radii of curvature along the pipe are equal to the pore radius,  $R = R_p$ , so that at the capillary limit

$$\Delta P_{cap} = \frac{2\sigma}{R_p} \quad (10)$$

and Equation 8 can be written

$$Q_{cap} = -\frac{2\sigma}{LF_l R_p} \quad (11)$$

where  $L$  is the pipe length and the frictional coefficient is given by

$$F_l = \frac{\mu_l}{K A_l h_{fg} \rho_l}$$

where  $A_l$  is the liquid flow cross-sectional area,  $\mu$ ,  $h_{fg}$ , and  $\rho$  are the kinematic viscosity, latent heat of vaporization, and density, respectively, and  $K$  is the wick permeability given by

$$K = \frac{2 \varepsilon r_h^2}{f_l Re_l}$$

with  $\varepsilon$  the flow direction porosity,  $r_h$  the hydraulic radius, and  $f_l Re_l$  the friction factor-Reynolds number product for laminar duct flow.

### 2.3.5 Boiling Limit

The boiling limit refers to the occurrence of nucleate boiling in the wick structure. While many convection systems are enhanced by nucleate boiling, formation of vapor bubbles can block flow passages in wicks and cause localized hot spots. The resulting increased circulation rate can exceed the capillary capabilities of the pipe and disrupt operation. Boiling limit is highly dependent on the working fluid thermophysical properties. A working fluid with low thermal conductivity such as water may easily boil in the wick structure, while a high conductivity working fluid such as liquid metal may efficiently conduct energy to the liquid-vapor interface and resist boiling[16] .



The extensive variables involved with boiling processes make the boiling limit the most difficult to accurately predict.

### Chapter III

## HEAT PIPE DYNAMICS

*“The quantitative details of the startup process are of minor interest.”*

*T. P. Cotter 1965 [2]*

Heat pipe dynamics are difficult to predict due to the complex fluid dynamics and heat transfer phenomena and the wide range of variables involved. These variables include pipe configuration, working fluid fill, initial temperature, the rate of change of heat addition to the evaporator, and condenser heat sink conditions. The important dynamic processes are also a function of the heat pipe operating state at each point during the transient. Transient operation can be considered in terms of three general regimes: startup; operating transients; and shutdown. The following sections discuss the physics of these regimes and the status of research in each area.

### 3.1 STARTUP

Heat pipe startup refers to the process of bringing a heat pipe from an initial static condition to steady state operation. The heat pipe working fluid may initially be in a frozen or liquid state. Heat pipe startup concerns include the conditions and time necessary to bring a heat pipe to operation, the conditions that hinder startup, and the dynamic behavior during the startup period.

#### 3.1.1 *Startup Physics*

There are various means to attain heat pipe startup from either liquid or frozen state. One reliable method is to isothermally warm or cool the entire pipe to the desired operating temperature and then gradually increase the input heat flux. Isothermal conditioning of the entire heat pipe may not be practical, particularly for the long heat pipes required for future applications such as for reactor core heat removal. Other methods of startup can be grouped according to the three general startup modes as shown in Figure 7.

Uniform startup corresponds to Figure 7(a). Uniform startup occurs when the density of the vapor is high at the initial temperature. The working fluid is completely melted. Heat applied to the evaporator results in vapor pressure gradients that initiate working fluid circulation. The high vapor density and pressure result in a high rate of heat transfer with a low vapor pressure drop. Since axial temperature drop is a function of vapor pressure drop, the axial

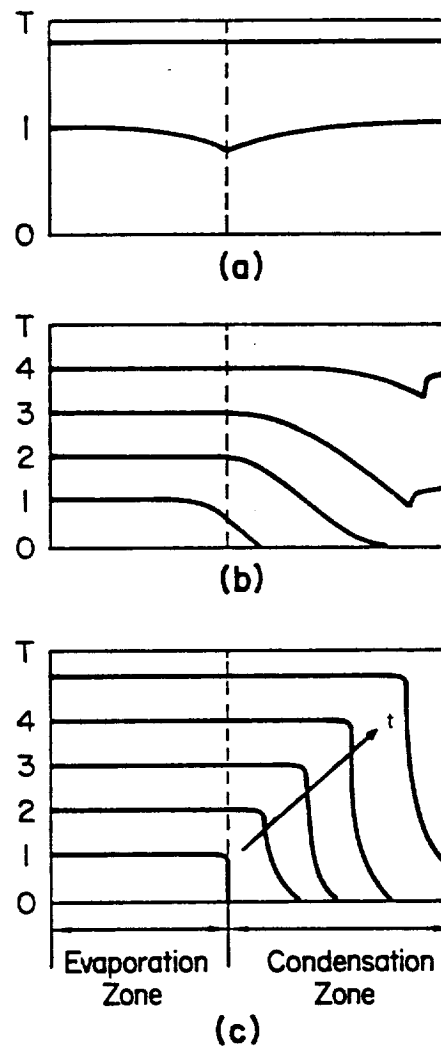


Figure 7: Three Modes of Heat Pipe Startup  
 (a) Uniform Startup  
 (b) Frontal Startup  
 (c) Frontal Startup with Noncondensible Gas  
 Adapted from Ivanovskii et al. [4]

temperature gradient is also small. Heat pipe response is smooth and relatively quick.

Frontal startup is shown in Figure 7(b). Frontal startup occurs when the vapor density at the initial temperature is low such that vapor flow is free molecular. Free molecular flow refers to the molecular mean free path exceeding the diameter of the vapor channel. At low vapor pressure the molecular mean free path is large so that interaction between vapor molecules is rare. The nature of flow is determined mainly by collisions of vapor molecules with the pipe walls. Evaporator heating raises vapor pressure in the evaporator so that vapor begins to flow as a continuum when the molecular mean free path becomes small compared to the vapor channel diameter. Vapor in the condenser is still low density and free molecular, so that there is little axial heat flux. A transition region exists between evaporator and condenser. Vapor compressibility effects become important since vapor flow may reach supersonic velocities. Since axial temperature drop is determined by vapor pressure drop, evaporator temperatures will initially be much higher than in the condenser. Condensation of liquid drops occurs in the vapor space during the rapid expansion through the transition region. The transition regime occurs at intermediate mean free paths such that collisions between vapor molecules and collisions with the wall are of the same order of magnitude such that both types of interactions determine the flow. The entrainment limit may be reached due to the viscous stress from high vapor velocity tearing liquid from the wick.

The heat pipe temperature and vapor pressure increase since the sonic limit restricts the flow of latent heat and forces the retention of sensible heat. At high vapor pressure the molecular mean free path is small so that vapor

molecules interact frequently and determine the nature of flow as continuous. The condenser temperature will then increase until the pipe becomes almost isothermal. Startup is completed as with a uniform startup.

Vapor flow regimes are determined by vapor temperature and pressure. For a sodium heat pipe, Ivanovskii et al. found free molecular flow from the melting point to 250 °C, transition flow from 250 to 400 °C, and continuous flow above 400 °C [4]. Criteria were suggested for bounding the flow regimes based on the Knudsen number:

$$K_n = \frac{L_p}{L_c} \quad (12)$$

where  $L_p$  is the molecular mean free path and  $L_c$  is a characteristic dimension for vapor flow in a heat pipe such as the vapor channel diameter  $D_v$ . The suggested boundaries are given as:

$\frac{L_p}{D_v} > 1.0$	Free Molecular Flow
$0.01 < \frac{L_p}{D_v} < 1.0$	Transition Flow
$\frac{L_p}{D_v} < 0.01$	Continuum Flow

Startup may fail to occur if initial vapor pressure is low and the thermal resistance between condenser and heat sink is low. Low thermal resistance maintains a good flow of heat out of the pipe so that the pipe does not retain

the energy to raise the overall pipe temperature. Low vapor pressure results in compressibility effects and possible sonic conditions. Startup may fail due to the entrainment limit. The pipe may be successfully started from low vapor pressure if there is a high thermal resistance at the sink-container interface. While vapor flow may reach the sonic limitations, the condenser temperature will gradually rise and raise the vapor pressure so that normal operation is achieved.

The working fluid may originally be in a frozen state. Heat introduced to the evaporator progressively melts the working fluid to the empty vapor space. Evaporation occurs to essentially a vacuum such that free molecular flow occurs above the melting and solid working fluid. Vapor molecules that condense on the frozen fluid will then refreeze. Heat pipe startup can be prevented if evaporation and subsequent condensing and freezing of working fluid occurs at a faster rate than the melting for replenishing the supply. The rate of heat input is an important consideration in achieving startup, as well as maintaining the condenser insulated so that heat is kept in the pipe to melt the working fluid.

A heat pipe pressurized with a noncondensable gas may also undergo frontal startup as shown in Figure 7(c). A gas loaded heat pipe is useful as a temperature regulator or as a thermal diode. The presence of noncondensable gas is also known to aid the startup of a heat pipe from a low initial vapor pressure. As working fluid evaporates, a diffuse vapor-gas transition region occurs creating a thermal front and forming a compressed gas plug in the condenser.[17] . Additional evaporation further compresses the gas such that

eventually only part of the condenser vapor space is plugged by gas. The length of this inactive condenser zone is a function of the vapor pressure dependence on temperature. Since the vapor is in a near saturation condition, the vapor pressure is directly related to the vapor temperature. The axial temperature distribution therefore provides an accurate description of the corresponding vapor conditions[18] . A qualitative axial distribution for frontal startup of a heat pipe with noncondensable gas is shown in Figure 8.

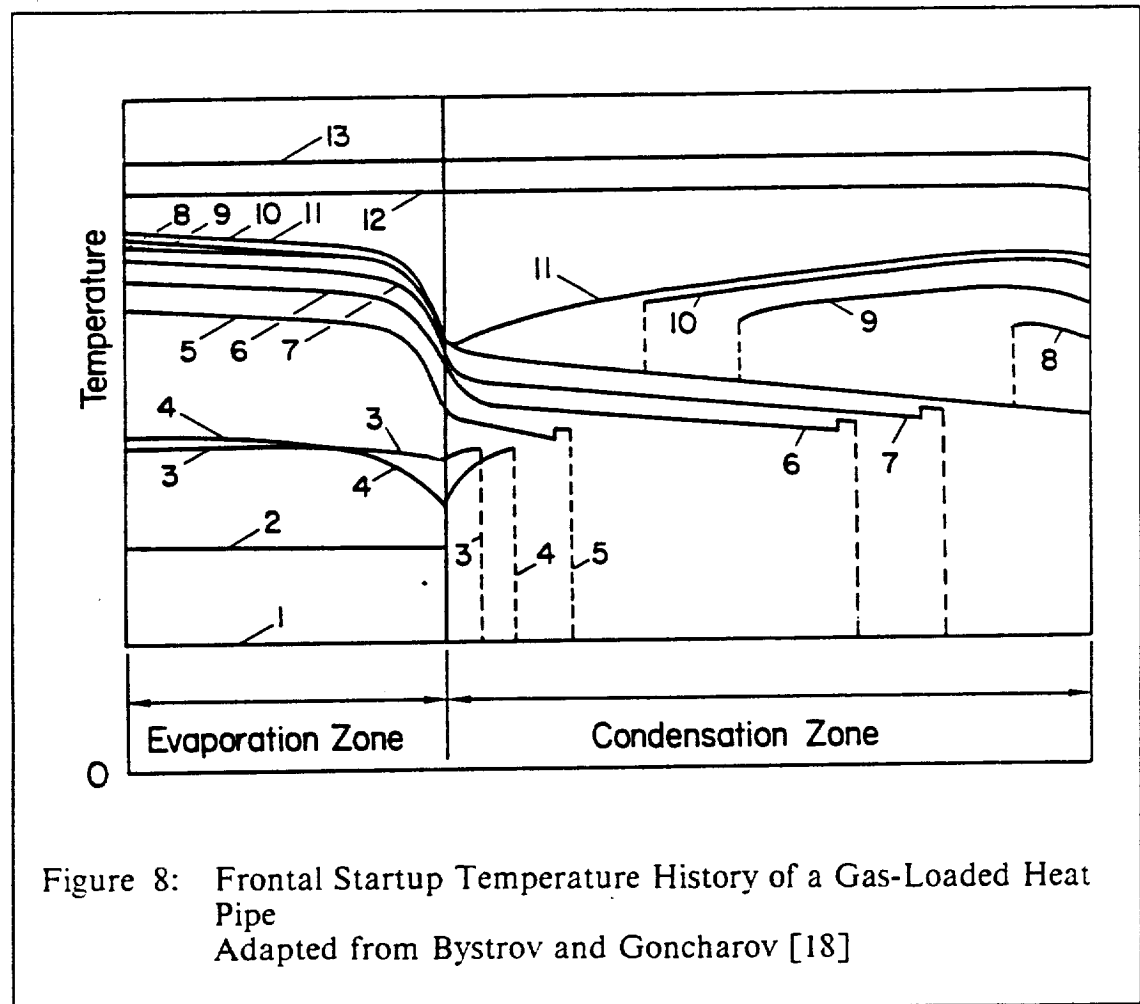


Figure 8: Frontal Startup Temperature History of a Gas-Loaded Heat Pipe  
Adapted from Bystrov and Goncharov [18]



The heat pipe is initially at a uniform temperature represented by curve 1. A uniform applied heat flux causes a uniform warming of the evaporator as represented by curve 2. The noncondensable gas overpressure is assumed to suppress evaporation during the initial warming period. As the temperature in the evaporator reaches curve 3, intense evaporation begins. The mass addition sweeps the noncondensable gas into the condenser. Sonic velocity is reached at the evaporator-condenser boundary. The vapor velocity corresponding to curve 3 is slowed to subsonic after the evaporator exit due to the buffering effect of the noncondensable gas. The velocities corresponding to curves 4 and 5 reach supersonic conditions at the evaporator exit as shown by the sharp temperature drop. Subsequent pressure and temperature recovery occur at the noncondensable gas front.

As vapor pressure increases the noncondensable gas front is compressed further into the condenser. Supersonic flow occurs over the length of the active condenser as shown by curves 6 and 7. Non-isothermal conditions during this period of sonic limited operation can be very pronounced. The shock front adjustment from supersonic to subsonic velocity gradually moves to the end of the condenser. The shock front reflects back to the evaporator as represented by curves 8 through 10. The vapor speeds during this process are sonic at the choked evaporator outlet, supersonic in the condenser up to the shock, and subsonic after the shock. As shown by curve 11, continued warming raises the vapor pressure and eliminates the shock conditions. While initially a large axial temperature drop persists, the heat pipe eventually

reaches near isothermal conditions as shown by curves 12 and 13. High heat transfer rates occur during this period of near isothermal conditions.

### **3.1.2 *Experimental Startup Studies***

Experimental studies were performed by Ivanovskii et al. on the temperature distribution along a heat pipe during startup [4]. The experiments were performed with sodium heat pipes with and without noncondensable gas added to the vapor space. The entire inventory of working fluid was solid at the beginning of the experiments. The experiments studied the frontal startup mode. Temperature measurements made in the vapor core are shown in Figure 9.

Curves 1 through 5 show that axial heat transfer to the condensation zone is negligible during initial heating of the evaporator. As the temperature increases, the flow of vapor molecules from the evaporator to condenser increases. The authors state that curves 5 and 6 represent free molecular and transition flow regimes. The flow regime can be seen to be a function of local axial conditions.

Curves 6 through 9 represent operation at the sonic limit with supersonic flow in the condenser due to low vapor pressure and high condensation rate. A shock front occurs corresponding to the abrupt temperature drop at the transition from supersonic velocity to zero velocity at the end of the condensing zone. Non-isothermal conditions during sonic limited operation can be seen to exceed 300 °C. Continuum vapor flow begins with curve 8.

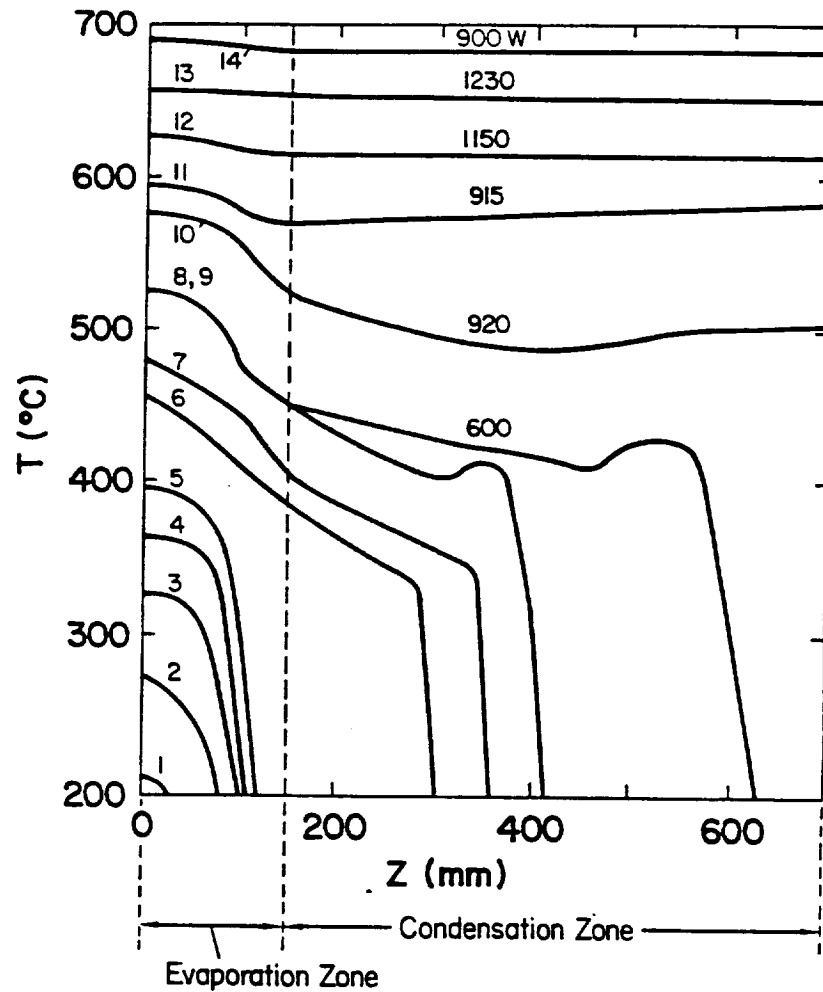


Figure 9: Measured Vapor Temperatures During Startup  
Adapted from Ivanovskii et al. [4]

Curves 10 through 14 represent steady operation below the sonic limit. The authors point out that the degree of isothermal operation depends on the vapor pressure. The extent of isothermal operation increases with decreasing ratio of heat transferred to the sonic limit. Heat pipe operation is essentially isothermal for the large vapor pressures represented by curves 12 through 14.

The time dependence of the startup was not reported, although the authors state without definition or elaboration that the warmup time was ninety minutes.

Experiments were performed at Los Alamos Scientific Laboratory on a heat pipe with molybdenum container using lithium as the working fluid[19][20] . The intent of the program was to address questions pertaining to the operation and performance characterization of high length-to-diameter ratio heat pipes under conditions of high radiation loading. Startup times and power handling capability, shutdown behavior with radiation sink temperatures below the freezing point of the working fluid, and accuracy of presently used performance models were specific questions addressed.

Starting from a uniform temperature of approximately 300 K, the heat pipe evaporator was brought to a uniform temperature of 1350 K over a period of forty minutes. The temperature was then held constant by adjusting the input power as the melt front progressed along the heat pipe. Total time to bring the heat pipe to temperature was approximately three hours. Peak power throughput was 15 kW. The temperature history of a typical condenser thermocouple (located 106 cm from the evaporator end) is shown in Figure 10. The interesting characteristic is the sharp thermal front between the melted and solid regions of the pipe.

Transient operation of low temperature heat pipes has been studied experimentally by Colwell et al. for several years[21][22][23] . Experimental studies concerned a heat pipe with circumferential and central slab wick using Freon 11 as the working fluid. Testing was performed in temperature ranges

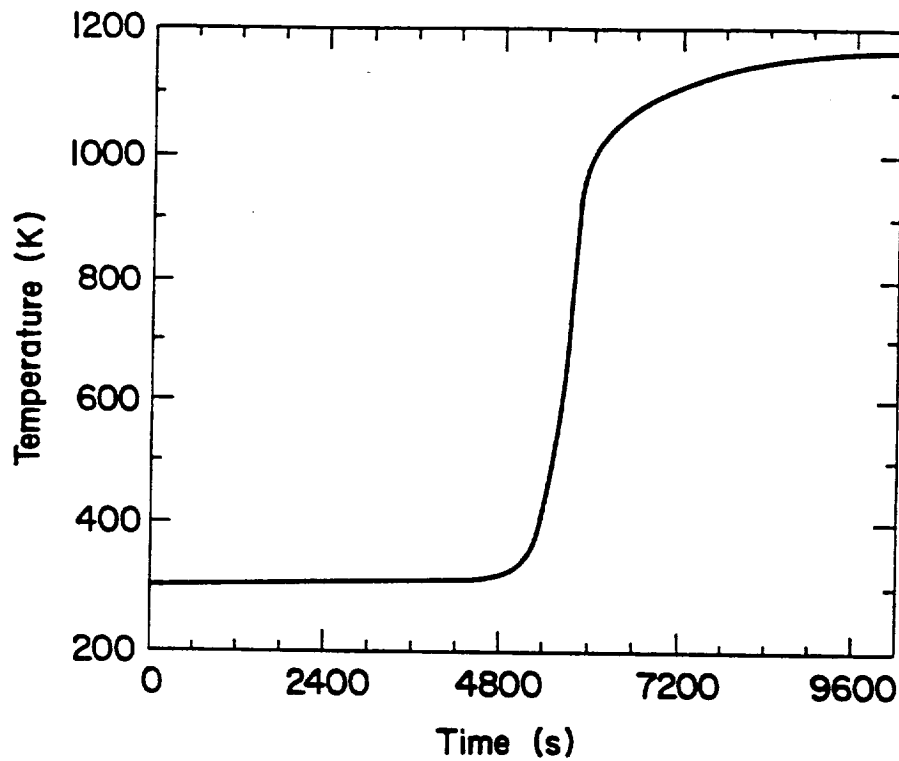


Figure 10: Startup Temperature History of Experimental Heat Pipe  
Adapted from Merrigan et al. [19]

from ambient room conditions to well above the working fluid critical point. The heat pipe was found to operate very smoothly at modest heat transfer rates with temperatures well below critical. Abrupt changes in coolant flows, heating rates, and inlet coolant temperatures were easily accommodated. Liquid temperatures were nearly uniform in the slab wick and only small gradients existed in the vapor. Measured vapor pressures were very close to saturation pressures corresponding to measured temperatures. Steady state was generally reached within ninety minutes for the specific configuration and

testing performed. Testing conducted at temperatures near the critical temperature identified more dynamic conditions in the heat pipe than at the lower temperatures. Partial and complete drying of the wick were encountered. Experiments were also performed to study the rewetting capabilities of the wick after dryout. Under some conditions steady operation was achieved even with a portion of the evaporator wick dried. Rewetting could sometimes be accomplished depending on the change in boundary conditions. Rewetting was found to be very difficult to accomplish after the wick completely dried. A significant lag time was encountered in rewetting the wick.

Mathematical models were formulated to describe the experimental results[24] . The model for a fully wetted wick was based on the assumptions that heat is transferred by conduction through the container wall and liquid saturated wick, thermal resistances associated with phase change are negligible, and vapor space temperature is uniform. A finite difference code using the Alternating Direction Implicit method was used to solve the conduction equation. The vapor temperature was determined from a simple heat balance at the liquid-vapor interface. Under saturated wick conditions the transient conduction equation with variable properties predicted performance accurately. A lumped parameter one dimensional momentum equation was used for cases in which the wick was not completely saturated. The mathematical model did not agree with experiments for transients involving a partially dried wick. General trends and end steady state conditions were qualitatively predicted, but with large temporal errors. A

calculation time step of five seconds was used, although the authors state that a time step of up to twenty seconds could be used.

### 3.1.3 *Analytical Startup Studies*

The first apparent study of heat pipe transients was reported by Cotter in 1967[25] . A one dimensional analysis was performed of a heat pipe at uniform initial temperature  $T_1$  which is heated to steady state operating conditions at temperature  $T_2$  and heat flux  $Q_2$ . A uniform heat flux  $Q_{in}$  is supplied to the evaporator during startup.  $Q_{in}$  may vary with time depending on the type of startup to be considered. A slow startup consists of increasing  $Q_{in}$  to  $Q_2$  so slowly that the pipe essentially passes through a series of steady states. A rapid or pulsed startup occurs for  $Q_{in} = 0$  at time  $t = 0$  and  $Q_{in} = Q_2$  for time  $t > 0$ . By considering the pipe as a one dimensional object with temperature  $T$  a function of axial location  $x$  and time  $t$ , Cotter derived energy equations for the evaporator and condenser regions

$$\begin{aligned} -A \frac{\partial}{\partial x} \left( k_{eff} \frac{\partial T}{\partial x} \right) + C \frac{\partial T}{\partial t} &= \frac{Q_{in}}{l_e} && \text{for the evaporator} \\ &= \frac{-Q_2}{l_c} \frac{T - T_1}{T_2 - T_1} && \text{for the condenser} \end{aligned} \quad (13)$$

where the effective thermal conductivity in the axial direction is  $k_{eff}$ ,  $A$  is the pipe cross-sectional area,  $C$  is the heat capacity per unit length, and  $l_c$  is the condensation zone length.

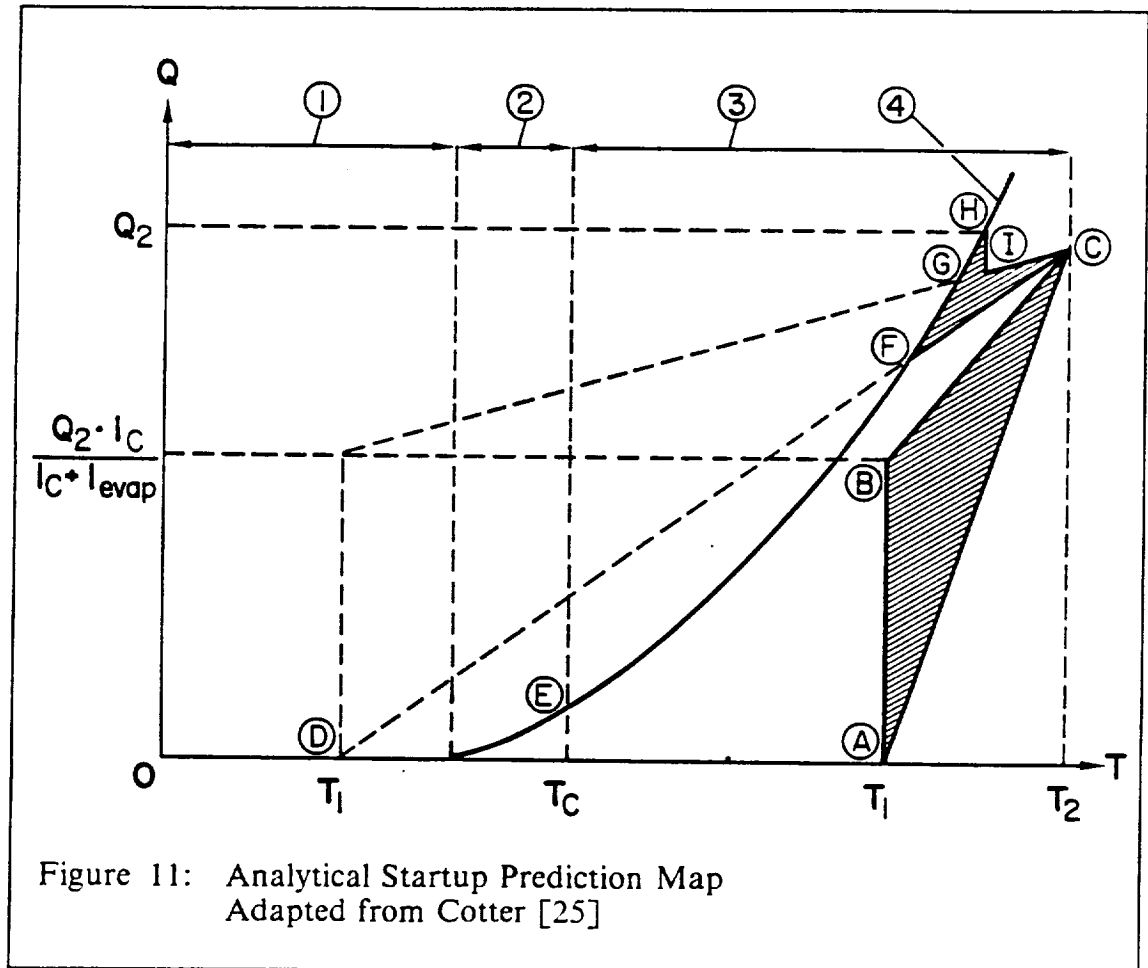
Equation 13 suggests two different characteristic times. The first,  $Cl_c(T_2 - T_1)/Q_2$ , is related to the heat input required to raise the pipe temperature from initial value  $T_1$  to final value  $T_2$ . This first characteristic time is given as on the order of 10 to 100 seconds.

The second characteristic time,  $Cl_c^2/k_{eff}A$ , is related to the axial heat transport rate. This time is inversely proportional to the effective thermal conductivity. At low vapor temperature and corresponding low vapor pressure, the molecular mean free path is large compared to the pipe diameter so that heat transfer is primarily due to conduction in the pipe wall and liquid. The second characteristic time under these conditions is given as on the order of  $10^3$  seconds. As the vapor pressure increases, convective heat transfer of latent heat becomes of comparable magnitude to thermal conduction. As the vapor temperature reaches a temperature range of 100 to 200 °C, the transition to continuum vapor flow is completed. The effective thermal conductivity increases rapidly such that the second characteristic time is typically less than one second.

Cotter performed a first approximation analysis based on the relative magnitudes of the characteristic times with the results shown in Figure 11. Let  $T_c$  be the temperature at which continuum vapor flow is established. Due to the large characteristic time, heat transfer is neglected wherever the temperature is below  $T_c$ . Wherever the temperature in a region exceeds  $T_c$ , heat transfer is so rapid that the entire region has uniform temperature. By considering the bounds set by rapid startup and slow startup Cotter solved a system of equations for startup from various initial temperatures  $T_1$ . Startup



from a high vapor pressure in which  $T_1 > T_c$  results in a uniform startup and the hot zone extends over the entire length of the pipe. The uniform startup is plotted as line segment AC in Figure 11. Solution for the rapid startup is plotted as line BC in Figure 11. Any startup program lying within the region ABC is expected to be successful.



Startup from low vapor pressure with  $T_1 < T_c$  will have no initial axial heat transport as represented by point D in Figure 11. The evaporator heats up until  $T = T_c$  at point E. The sonic limit line of curve 4 is followed above  $T_c$  to point F. A slow startup will follow curve FC until steady state operation is

reached at point  $C$ . A rapid startup follows a slightly peculiar path. The heated zone reaches the end of the condenser on the interval  $GH$ , where  $G$  is the intersection of the sonic limit curve and curve  $GC$ . At point  $H$ ,  $Q_{son} = Q_2$ , but  $T_2$  has not been reached. The heat pipe continues to heat up such that the path  $H - I - C$  is followed. The startup regime for a pipe at initial temperature below  $T_c$  is then the curve  $DEF$  and the region  $FGHIC$ .

The heat transfer variation with time was expressed by Cotter using a one dimensional approximation. Heat supplied to the evaporator was expressed as the exponential function

$$Q_{in} = Q_2[1 - \exp(-t/t_0)] \quad (14)$$

where  $t_0 = C/k_{eff}$ . With  $t_Q = Cl_c(T_2 - T_1)/Q_2$ , the variation of heat transfer with time is given by

$$Q(t) = Q_2 \left\{ 1 - \frac{1}{\frac{t_Q}{t_0} - 1} \left[ \frac{t_Q}{t_0} \exp\left(\frac{-t}{t_Q}\right) - \exp\left(\frac{-t}{t_0}\right) \right] \right\} \quad (15)$$

The qualitative behavior of Equation 15 for a range of heating rates is shown in Figure 12.

Researchers have followed Cotter's startup analysis with approaches that have ranged from the simple to the complex. The simple end of the spectrum includes the adaptation of generalized thermal analyzer programs to include heat pipe transients[26][27]. The intermediate range of complexity includes lumped parameter approaches, while the high end of complexity involves solution of the full system of governing equations.

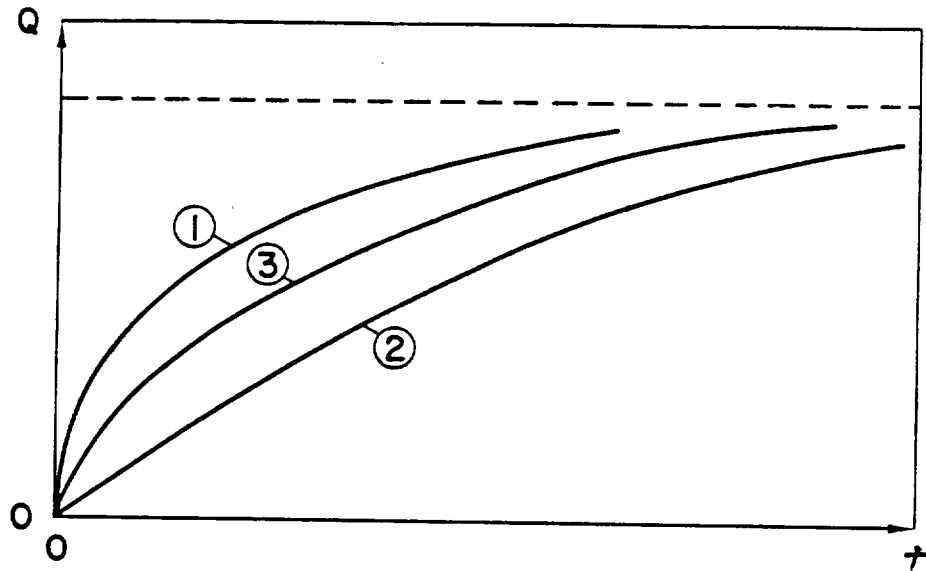


Figure 12: Analytical Heat Pipe Startup as a Function of Time  
 ( 1 ) Rapid Startup  
 ( 2 ) Intermediate Startup  
 ( 3 ) Slow Startup  
 Adapted from Cotter [25]

Published lumped parameter transient studies include two studies of thermosyphons. A thermosyphon is similar to a heat pipe in that heat is transferred in a closed container through the latent heat of vaporization of the working fluid. The two devices are dissimilar in the mechanism for returning the liquid phase to the evaporating region of the device. A thermosyphon uses gravitational force to accomplish liquid return while a heat pipe uses capillary forces that are either opposed by gravity, supplemented by gravity, or are gravity free. The similarities between devices make analysis of thermosyphons of interest in the study of heat pipes.

A simple lumped parameter formulation for thermosyphon transients was developed by Dikiy et al.[28] . The thermosyphon considered was actually simplified from the usual configuration since the vapor flow paths and liquid flow paths were assumed to be separate and isolated so that communication between the countercurrent liquid and vapor was not considered. Heat and mass balances were formulated for liquid, vapor, evaporator wall, and condenser wall. Empirical relationships were used in defining heat transfer coefficients for the condensation and evaporation processes. The result of derivations was a first order nonlinear differential equation for temperature as a function of time. Results of the numerical integration of the governing differential equation show transient processes that occur smoothly over a period of approximately thirty seconds.

Reed and Tien developed a lumped parameter model of a thermosyphon that included the effects of liquid-vapor interaction[29] . Control volume equations were developed for conservation of mass, momentum, and energy in the liquid; mass, momentum and energy in the vapor core; and overall system mass and energy. Auxiliary empirical and analytical relations were used for specifying wall and interfacial shear stresses and the liquid film heat transfer coefficient. The lumped parameter model compared well with steady state experimental data. Transient experimental data were not available for comparison. The primary significance of the approach was that a single model was found to be able to predict most operating parameters and operating limits, making it useful for inclusion in a systems analysis formulation.

A lumped parameter approach was used by Beam et al. to investigate heat pipe response to pulsed startups[30][31] . A pulsed startup refers to applying a step increase in heat flux to a static heat pipe. The authors address the questions of whether a heat pipe will reach normal operation after applying the pulse, and the time required to rewet a wick that partially dries during the startup. The time variation of heat pipe temperature was expressed as an exponential function. The authors also developed a model to describe the dryout and rewetting of wicks. Two types of pulsed startups were considered. In the first the mean temperature of the transport section was maintained constant at the initial temperature so that thermal storage in the system was negligible. This test addressed the ability of the heat pipe to respond immediately to pulsed heating with no thermal storage. In the second, the heat pipe temperature was allowed to increase so that thermal storage was appreciable. The lumped parameter model was compared to experimental data from a copper-water heat pipe with a homogeneous screen wrap wick. Three experimental responses to pulsed startup were identified. The wick in the evaporator may accommodate the pulse heat flux without drying; partial dryout may occur followed by rewetting; or dryout may occur without rewetting. The authors conclude liquid in a screen wick can respond almost instantaneously to a change in pressure gradient. The heat pipe was found to be able to transport a pulsed heat load equal to the capillary pumping limit without drying and without thermal storage.

Experimental and analytical work addressing startup with and without noncondensable gas was performed by Bystrov and Goncharov [18]. Two

analytical approaches were attempted. In the first, conservation of mass, momentum and energy equations for vapor were written as one dimensional averaged over the vapor channel cross-section. Phase change from evaporation and condensation was based on kinetic theory. The vapor phase equations were solved separately for the evaporator and condenser zones with appropriate matching conditions at the boundary between zones. The liquid phase solution method depended on whether the working fluid was initially frozen or solid. The non-steady heat conduction equation was used for the solid case with a heat balance to describe melting. The one dimensional equations of motion for a flux of variable mass were used for the liquid phase. The area of liquid flow was taken as constant. Heat supply and rejection were through radiation boundary conditions.

The resulting numerical solution routine required extremely small time steps on the order of  $10^{-5}$  to  $10^{-7}$  second for stability. The equations governing the liquid phase had better stability characteristics such that time steps of  $10^{-2}$  second could be used. The authors note that these characteristics have advantages when the vapor flow is subsonic. The vapor can be taken as uniform due to large time scale differences.

The small time steps required for vapor were prohibitive for a complete transient analysis. The authors developed a revised approach consisting of lumped parameter heat balances that avoided calculation of detailed temperature distributions. The kinetic model of interphase mass transfer was also eliminated to avoid the stability problems. The authors solved the heat balance equations, one dimensional conservation of mass, momentum and

energy for the vapor, conservation of mass and momentum for the liquid, and supplemental equations to maintain operation within known operating limits.

The comparison of analytical and experimental results for a heat pipe with noncondensable gas is shown in Figure 13. The startup exhibits frontal behavior as noncondensable gas is swept into the condenser. The region furthest in the condenser has a large lag time showing the low diffusion of vapor into the gas. Initially the evaporator warms uniformly while there is little axial heat transfer since the noncondensable gas suppresses evaporation. A substantial axial temperature gradient in excess of 400 °C occurs due to sonic conditions at the evaporator outlet.

A detailed computer model of transient heat pipe performance has been under development at Los Alamos Scientific Laboratory[32] . The model is intended to include startup from frozen state with provision for free molecule flow through steady state operating conditions. Vapor flow is modeled as one dimensional and compressible with friction and mass addition from the wick. The Kachina method is used for solving the governing equations. The authors state mass addition from the wick is the most difficult aspect to simulate. Mass transfer rate based on kinetic theory was found to produce high effective mass transfer coefficients that required very small time steps for explicit integration. This problem was circumvented by using a simplified wick model for computing temperature and saturation pressure at the wick surface. Mass transfer rates based on this locally computed wick surface temperature are used in the vapor core solution and later in the full wick solution. The wick model (liquid flow) is solved using the SIMPLER method. Freezing and

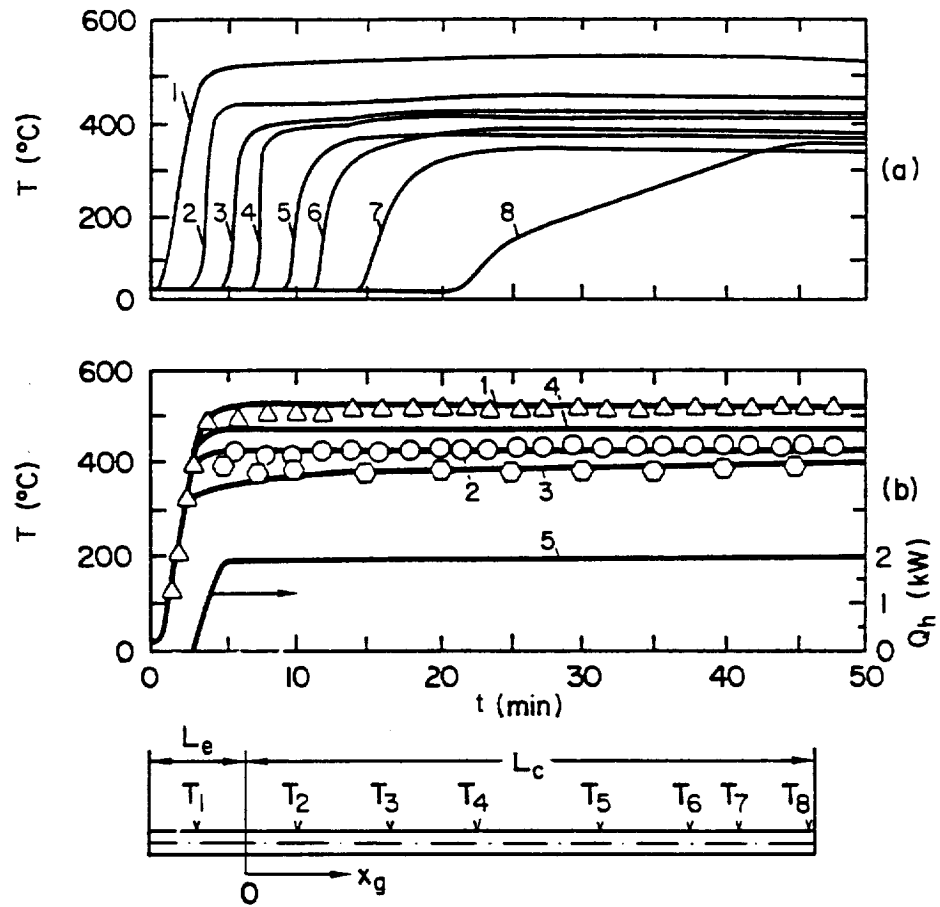


Figure 13: Comparison of Analytical and Experimental Startup Data  
a ) Experimental Temperature Fields  
b ) Experimental and Analytical Data  
1. Evaporator Surface Temperature  
2. Condenser Surface Temperature  
3. Condenser Average Temperature  
4. Evaporator Exit Temperature  
5. Heat Transfer  
Adapted from Bystrov and Goncharov [18]

thawing are treated by an enthalpy balance. Radial temperature of the wick/groove/wall structure is solved implicitly at each axial location. Axial direction integration is performed explicitly. Implicit radial integration is used



due to the high radial conductances and the small radial dimensions. The model was run for ten computational steps on a Compaq Deskpro II computer. Execution on a Cray computer was expected to require thirty minutes of processor time per hour of actual time simulated.

Analytical work by Peery and Best was performed to address rapid transients in a heat pipe[33] . The heat pipe simulated was a 200 cm long rectangular aluminum container with a homogeneous slab screen wick and water working fluid. Continuity and momentum were solved as one dimensional while energy was solved as two dimensional. The computations were fully implicit in time with property variations a function of temperature. The liquid and vapor flows were solved individually with coupling through a kinetic phase change model. The authors began computations with a time step of  $1 \times 10^{-4}$  seconds and increased the time step to  $6.4 \times 10^{-3}$  seconds. The model broke down for time steps larger than  $6.4 \times 10^{-3}$  seconds. At three seconds into the transient, the condensation rate increased to become approximately equal to the evaporation rate. Convergence then became a problem and the transient was terminated. The code was expensive to use since one second of transient required one hour of CPU time on a CDC Cyber 825 computer. The authors conclude that the kinetic theory phase change model caused the requirement for small time steps and resulting computational expense.

### 3.2 OPERATING TRANSIENTS

Operating transients involve power changes during nominal operating conditions. There are several transient conditions of interest. A heat pipe may operate at low power standby mode but be required to quickly respond to reach full power operation. A heat pipe may also be required to perform load following functions depending on changing conditions at the power conversion system. Reactor control also may require changes of heat generation that would have to be handled by the heat pipe system.

The physics of interest for these situations depends on the initial condition, the rate of change and magnitude of input power, and condenser conditions. A heat pipe operating in standby mode at low vapor pressure may encounter the sonic limit while powering up. Large temperature gradients and complex vapor dynamics would develop. After passing through sonic limited operation, or for a heat pipe initially operating at high vapor pressure, the capillary, entrainment, and boiling limits are of concern.

While physical processes are similar to those encountered during a startup, very limited work has been performed to address issues or characterize transient performance. The previously discussed study performed by Ivanovskii et al. and shown in Figure 9 included some work in the operating transient regime. Curves 11 through 14 are the axial temperature profiles at different axial power levels. These curves show the temperature characteristics of a quasisteady process since the input heat flux was intentionally varied slowly with time. The issues concerning more dynamic processes remain to be resolved. Issues requiring resolution involve the allowable rate of change of

input heat flux, the magnitude of input heat flux, the time required for the heat pipe to respond to a transient, and the capability to buffer small scale transients that occur at the heat sink and source.

### 3.3 SHUTDOWN

The dynamics of heat pipe shutdown are important since subsequent restart depends on the final shutdown condition. Shutdown may be to a liquid or frozen state. Depending on the means of attaining shutdown, wick depriming may occur due to non-uniform conditions. Shrinkage voids may occur as the liquid begins to freeze. Shrinkage may also cause tearing of the delicate capillary wick structure. The tear would result in a larger capillary surface and corresponding reduction in capillary pumping capability.

These issues are illustrated in the single identified study that addresses heat pipe shutdown dynamics [19] [20]. Shutdown tests were performed at Los Alamos Scientific Laboratory on a high temperature heat pipe with annular wick and lithium working fluid. A temperature profile taken 8 minutes 30 seconds after power shutoff is shown in Figure 14. Lithium near the evaporator end of the condenser has reached the solidification point while lithium in the evaporator is almost 240 K above the melting point. An attempted restart of the pipe after complete lithium solidification failed due to voids in the annular flow region. The authors concluded the voids were a result of shrinkage of the working fluid during freezing due to non-uniform cooldown rates. Subsequent tests were performed in which a more uniform

cooldown rate was attempted. The temperature difference between the hottest and coolest point at onset of solidification was reduced to approximately 140 K. Subsequent restart tests were performed successfully. The authors concluded the critical issues include the axial location where freezing first occurs during shutdown, and the ability of the wick structure to accommodate working fluid shrinkage in the region furthest from the condenser and liquid pool following establishment of the freeze plug. The restart capability of a given radiation coupled design was found to be strongly dependent on the external geometry and thermal environment of the heat pipe as well as on the heat pipe internal design itself.

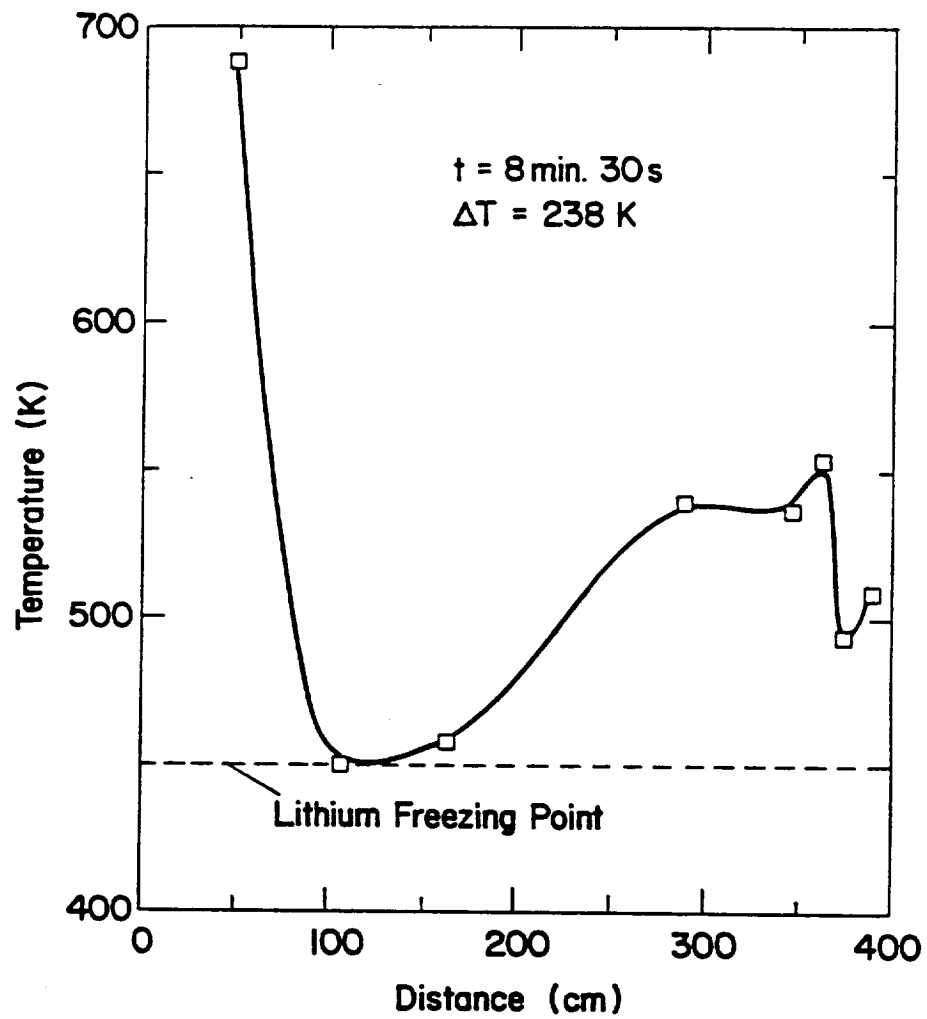


Figure 14: Shutdown Temperature History of Experimental Heat Pipe  
Adapted from Merrigan et al. [19]

## Chapter IV

### THE SOLUTION

*“The simple derivation is left as an exercise for the interested reader.”*

*Engineering Textbooks*

#### 4.1 THE SCOPE

As previously discussed, most research in heat pipe dynamics has focused on the startup transient. An experimental investigation has also been performed for the shutdown transient. Only modest efforts have been expended to date that consider operational transients. These efforts generally address two issues: the capability to achieve nominal operation under specified conditions, and the resulting axial temperature distribution. The processes are assumed to occur quasisteadily such that time dependent characteristics are not considered. Despite these research efforts, a comprehensive analytical model does not exist that captures the physical processes while being economical enough for required computations.

The objective of this study is to develop an analytical model of the liquid phase of a high temperature heat pipe. The model is intended to be coupled to a vapor phase model for the complete solution of the heat pipe problem. The mathematical equations are formulated consistent with physical processes while allowing a computationally efficient solution. The model simulates time dependent characteristics of concern to the liquid phase, including: input, phase change, and output heat fluxes, liquid temperatures, container temperatures, liquid velocities, and liquid pressures.

#### **4.2 THE CONFIGURATION STUDIED**

This research considers requirements for high temperature, high thermal flux operation with heat transport over long distances and small temperature drops. These requirements indicate the need for a heat pipe with a high performance composite wick. A composite wick consists of small pores at the liquid-vapor interface and large pores in the direction of bulk liquid flow. Recall that the maximum capillary pumping capability is limited by the largest capillary surface at the liquid-vapor interface as shown by Equation 1. The small pores at the liquid-vapor interface establish a high capillary pumping capability that drives the circulation of working fluid. The larger pores in the direction of flow provide a low resistance flow path for the liquid.

The heat pipe selected for this study uses an annular wick configuration as shown in Figure 15. The annular wick is an excellent configuration for liquid metals, is popular for experimental work, and involves geometry easily

modeled in cylindrical coordinates [15,19,20]. The wick configuration consists of several layers of fine pore screen pressed together and concentrically installed in the pipe to form an annular flow channel as shown in Figure 16. The annulus forms the low resistance flow channel while the fine pore screen tube forms the high pumping capability boundary between the liquid and vapor regions.

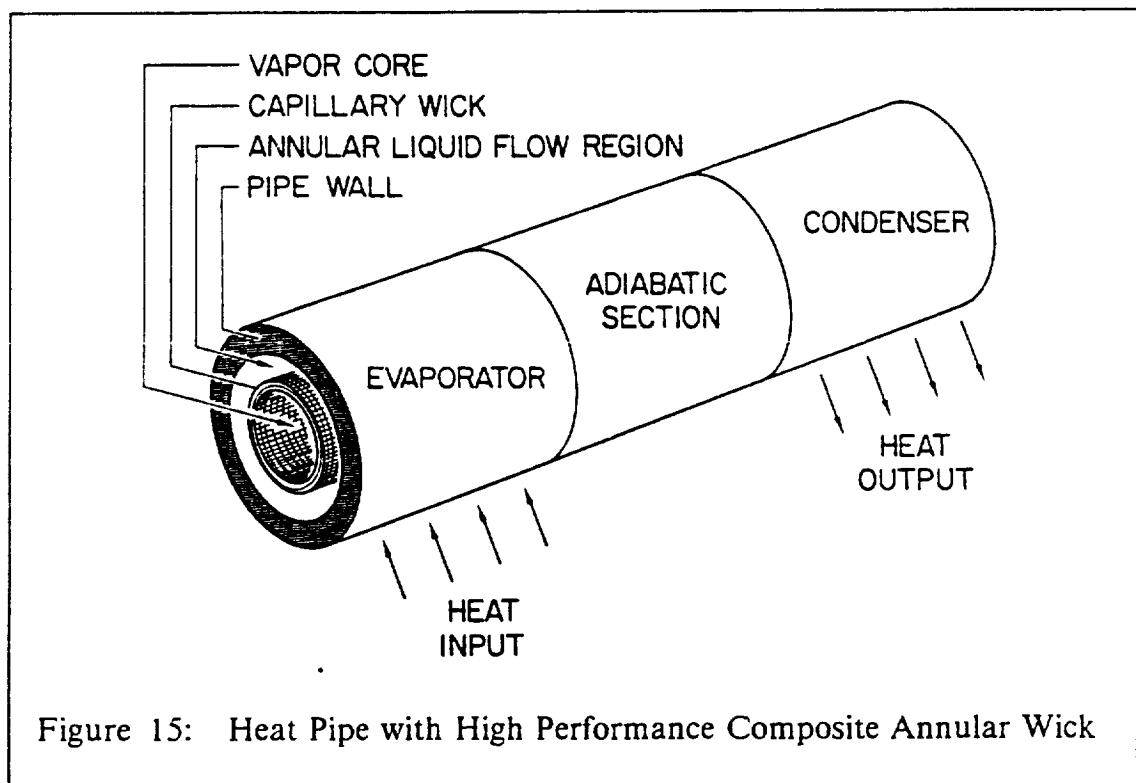


Figure 15: Heat Pipe with High Performance Composite Annular Wick

The capillary wick introduces some analytical although not conceptual difficulty. A thin screen tube consisting of several layers of pressed screen forms a tortuous flow channel with no slip conditions on the surface of the screen wires. Explicit analysis of the flow including consideration of the large number of wire surfaces involved would be difficult if at all practical



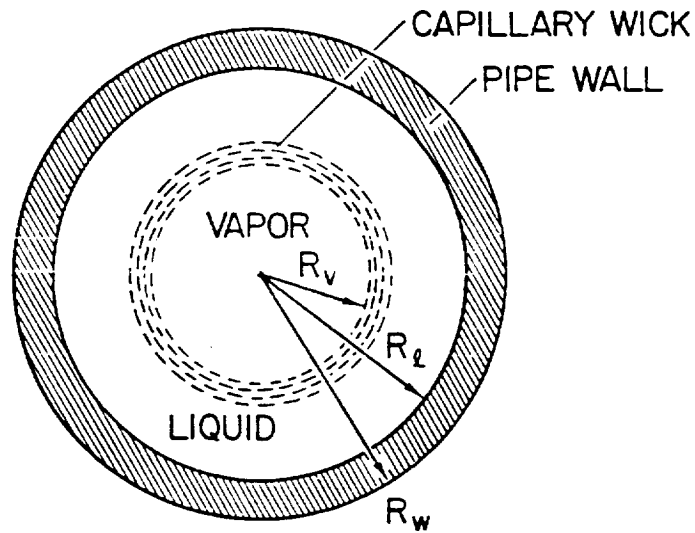


Figure 16: Cross Section of High Performance Annular Wick Configuration

considering the goal of performing transient analysis. A macroscopic approach such as Darcy's Law for flow in a porous medium could be used to alleviate the complexity. However the axial flow in the pressed screen is expected to be small relative to axial flow in the open annular channel. Indeed, the very purpose of the annular composite wick configuration is to provide a low resistance flow channel in the annulus for circulation of liquid. The screen tube is used only to provide a fine capillary surface at the liquid-vapor interface. The screen tube can then be approximated as a single layer of screen with a characteristic pore size. Flow normal to the screen is restricted by a characteristic specified porosity, while tangential flow is governed by alternating free slip and no slip conditions. The free slip condition provides the

tangential shear communication between the liquid and vapor phases. The wick is approximated then as an infinitesimally thin porous surface.

### **4.3 THE LIQUID PHASE MATHEMATICAL FORMULATION**

#### **4.3.1 *Assumptions***

The governing equations to be presented below will be reduced by recognizing unique characteristics of the system to be analyzed. The system is assumed to operate in an essentially gravity free environment. Other body forces such as those due to translational and rotational acceleration will also be neglected.

The heat pipe is assumed to be installed with azimuthal symmetry in the particular application. The thermal energy source adds heat uniformly around the evaporator circumference while the heat sink extracts heat uniformly around the condenser circumference. The resulting uniform conditions in the azimuthal direction imply there are no velocity components or gradients in the azimuthal direction.

Liquid flow in a heat pipe wick is generally low speed, laminar, and incompressible. Since the liquid flow field is relatively simple and the cross-stream dimension of the liquid region is much smaller than the streamwise dimension, the cross-stream (i.e., radial) pressure gradient is assumed to be negligible. Also since the flow is low speed and incompressible, viscous energy dissipation can be neglected.

In summary, the assumptions to be used for reducing the governing equations are:

1. Negligible body forces:  $f_r = f_x = 0$
2. Azimuthal symmetry
  - a. No azimuthal flow:  $w = 0$
  - b. No azimuthal gradients:  $\frac{\partial \bullet}{\partial \phi} = 0$
3. Negligible radial pressure gradient:  $\frac{\partial P}{\partial r} = 0$
4. Negligible viscous dissipation
5. Incompressible liquid:  $\frac{\partial \rho_l}{\partial P} = 0$
6. Laminar liquid flow

Thermophysical properties are considered to be uniform functions evaluated at a reference temperature. The reference temperature is assumed to change slowly with time such that properties can be treated as constants in the governing equations.

#### **4.3.2 Governing Equations**

Temperatures of the heat pipe container and the temperatures, pressures, and velocities of the liquid phase are required to describe the dynamic behavior of the liquid phase of a high temperature heat pipe under transient operating conditions. The governing equations describing the behavior of these parameters consist of the conservation of mass, momentum, and energy.

#### 4.3.2.1 Conservation of Mass

The full condition governing conservation of mass of an incompressible fluid is

$$\frac{\partial u}{\partial x} + \frac{\partial v}{\partial r} + \frac{1}{r} \frac{\partial w}{\partial \phi} + \frac{v}{r} = 0 \quad (16)$$

where  $u$  is the velocity in the axial ( $x$ ) direction,  $v$  is the radial ( $r$ ) velocity, and  $w$  is the azimuthal direction ( $\phi$ ) velocity. Imposing the assumption of azimuthal symmetry reduces Equation 16 to the familiar two dimensional form

$$\frac{\partial u}{\partial x} + \frac{\partial v}{\partial r} + \frac{v}{r} = 0 \quad (17)$$

#### 4.3.2.2 Conservation of Radial Momentum

Full conservation of radial momentum for an incompressible fluid with constant properties is given by

$$\begin{aligned} \frac{\partial v}{\partial t} + \frac{\partial uv}{\partial x} + \frac{\partial v^2}{\partial r} + \frac{1}{r} \frac{\partial wv}{\partial \phi} - \frac{w^2}{r} + \frac{v^2}{r} = \\ - \frac{1}{\rho} \frac{\partial P}{\partial r} + v \left( \frac{\partial^2 v}{\partial x^2} + \frac{\partial^2 v}{\partial r^2} + \frac{1}{r^2} \frac{\partial^2 v}{\partial \phi^2} + \frac{1}{r} \frac{\partial v}{\partial r} - \frac{2}{r^2} \frac{\partial w}{\partial \phi} - \frac{v}{r^2} \right) + f_r \end{aligned} \quad (18)$$

where  $t$  is the time,  $\rho$  is density,  $P$  is pressure, and  $\nu$  is kinematic viscosity. By assuming negligible radial pressure gradient, the conservation of radial momentum equation is replaced by

$$\frac{\partial P}{\partial r} = 0 \quad (19)$$

Under this approximation the radial momentum equation is not used to define liquid dynamics so that pressure is determined from the continuity equation and the axial momentum equation.

#### 4.3.2.3 Conservation of Axial Momentum

Conservation of axial momentum for an incompressible fluid with constant properties is given by

$$\begin{aligned} \frac{\partial u}{\partial t} + \frac{\partial u^2}{\partial x} + \frac{\partial uv}{\partial r} + \frac{1}{r} \frac{\partial uw}{\partial \phi} + \frac{uw}{r} = \\ - \frac{1}{\rho} \frac{\partial P}{\partial x} + v \left( \frac{\partial^2 u}{\partial x^2} + \frac{\partial^2 u}{\partial r^2} + \frac{1}{r^2} \frac{\partial^2 u}{\partial \phi^2} + \frac{1}{r} \frac{\partial u}{\partial r} \right) + f_x \end{aligned} \quad (20)$$

Assuming negligible body forces, azimuthal symmetry and no radial pressure gradient reduces Equation 20 to

$$\frac{\partial u}{\partial t} + \frac{\partial u^2}{\partial x} + \frac{\partial uv}{\partial r} + \frac{uw}{r} = - \frac{1}{\rho} \frac{dP}{dx} + v \left( \frac{\partial^2 u}{\partial x^2} + \frac{\partial^2 u}{\partial r^2} + \frac{1}{r} \frac{\partial u}{\partial r} \right) \quad (21)$$

#### 4.3.2.4 Conservation of Energy

Full conservation of energy for an incompressible, constant property fluid is given by

$$\begin{aligned} \rho c_v \left[ \frac{\partial T}{\partial t} + u \frac{\partial T}{\partial x} + v \frac{\partial T}{\partial r} + \frac{w}{r} \frac{\partial T}{\partial \phi} \right] = \\ k \nabla^2 T + 2\mu \left\{ \left( \frac{\partial u}{\partial x} \right)^2 + \left( \frac{\partial v}{\partial r} \right)^2 + \left[ \frac{1}{r} \left( \frac{\partial w}{\partial \phi} + v \right) \right]^2 \right\} + \\ \mu \left\{ \left[ \frac{\partial v}{\partial x} + \frac{\partial u}{\partial r} \right]^2 + \left[ \frac{\partial w}{\partial x} + \frac{1}{r} \frac{\partial u}{\partial \phi} \right]^2 + \left[ \frac{1}{r} \frac{\partial v}{\partial \phi} + r \frac{\partial}{\partial r} \left( \frac{w}{r} \right) \right]^2 \right\} \end{aligned} \quad (22)$$

Neglecting viscous dissipation and assuming azimuthal symmetry results in

$$\frac{\partial T}{\partial t} + u \frac{\partial T}{\partial x} + v \frac{\partial T}{\partial r} = \alpha \left( \frac{\partial^2 T}{\partial x^2} + \frac{\partial^2 T}{\partial r^2} + \frac{1}{r} \frac{\partial T}{\partial r} \right) \quad (23)$$

The conservation of mass and momentum equations are solved subject to the boundary conditions using the integral formulation developed in Appendices B, C, and D. The conservation of energy equation is solved using the finite difference numerical formulation developed in Appendix E. The computational implementation of the solution approach is given in Section 4.5.2.

#### **4.3.3 Boundary Conditions**

The heat pipe boundary conditions can be considered as either external or internal. The external conditions refer to the communication of the heat pipe external surface with the surrounding environment. The internal conditions are of two types: fluid-solid and fluid-fluid. The fluid-solid conditions refer to the interaction between the liquid and either the pipe internal surface or the wick. Fluid-fluid conditions govern the interaction between the liquid and vapor phases.

##### **4.3.3.1 External Boundary Conditions**

The heat pipe external boundary can be divided into three convenient regions as shown in Figure 15. The evaporator region absorbs heat from the environment, the adiabatic region exchanges no heat with the environment,

and the condenser rejects heat to the environment. The evaporator surface is assumed to be exposed to a known surface heat flux condition, while the condenser exchanges heat through radiation<sup>1</sup> to a sink of known temperature[34] . The conditions on the pipe external wall are then

AXIAL RANGE	RADIAL RANGE	CONDITION
$0 \leq x \leq L_e$	$r = R_w$	$-k \frac{\partial T}{\partial r} = q_{in}(x, t)$
$L_e < x < L_e + L_a$	$r = R_w$	$\frac{\partial T}{\partial r} = 0$
$L_e + L_a \leq x \leq L$	$r = R_w$	$-k \frac{\partial T}{\partial r} = q_{rad}$

where  $q_{in}$  is specified and  $q_{rad}$  is to be determined from  $q_{rad} = \epsilon \sigma (T_w^4 - T_e^4)$  assuming environmental sink temperature  $T_e$  is known.

---

<sup>1</sup> The condenser could generally exchange heat with the environment through conduction, radiation, and convection. However, the study of radiation loaded elements is of current research interest for space based applications [9].

Long heat pipes with large evaporator and condenser circumferential surface areas relative to the surface area of pipe endcaps will normally have negligible effects due to conduction in the end caps. With this assumption, the boundary conditions are:

AXIAL RANGE	RADIAL RANGE	CONDITION
$x = 0$	$R_i \leq r \leq R_w$	$\frac{\partial T}{\partial x} = 0$
$x = L$	$R_i \leq r \leq R_w$	$\frac{\partial T}{\partial x} = 0$



#### 4.3.3.2 Internal Boundary Conditions

Solid-fluid surfaces correspond to the heat pipe container internal wall interface with the working fluid, and the capillary wick interface with the fluid. The pipe wall conditions are no slip and matching temperature gradient. The conditions are:

AXIAL RANGE	RADIAL RANGE	CONDITION
$x = 0$	$R_v \leq r \leq R_l$	$u = 0$ $v = 0$ $\frac{\partial T_l}{\partial x} = 0$
$x = L$	$R_v \leq r \leq R_l$	$u = 0$ $v = 0$ $\frac{\partial T_l}{\partial x} = 0$
$0 \leq x \leq L$	$r = R_l$	$u = 0$ $v = 0$ $k_l \frac{\partial T_l}{\partial r} = k_w \frac{\partial T_w}{\partial r}$
$0 \leq x \leq L$	$r = R_v$	See Section 4.3.3.3

#### 4.3.3.3 Liquid-Vapor Interface Conditions

The liquid-vapor interface of the heat pipe is the most difficult feature to analyze. The interface serves as the medium for communication between the liquid and vapor along the entire axial length of the pipe. The flow characteristics are distinctly different between the respective liquid and vapor sides of the interface. The interface is subjected to physical phenomena through the action of surface tension that is generally not considered in the liquid or vapor flow fields.<sup>2</sup> The general liquid-vapor interface conditions are reduced in Appendix A to the following forms used in this analysis.

#### KINEMATIC SURFACE CONDITION

$$\vec{U}_{lv} = 0 \quad (24)$$

where  $\vec{U}_{lv}$  is the velocity of the liquid-vapor interface surface.

#### CONSERVATION OF MASS

$$\rho_v V_{0v} = \rho_l V_{0l} \quad (25)$$

---

<sup>2</sup> The vapor and liquid regions are each assumed to be a single phase such that multi-phase phenomena in these bulk flow regions are not considered. Entrainment of liquid by shearing action of the vapor, condensation in the bulk vapor, and vapor bubble formation in the liquid are common examples of departures from the single phase assumption. These phenomena are outside the scope of the present analysis.

where  $V_{0v}$  is the vapor radial phase change velocity and  $V_{0l}$  is the liquid radial phase change velocity. In future uses,  $V_0$  will refer to the liquid phase change velocity unless for clarity  $V_{0l}$  is used.

## CONTINUITY OF TANGENTIAL STRESS

As discussed in Appendix A, the tangential stress condition provides an important coupling relation between the liquid and vapor phases. Since the vapor phase solution is not included in this study, as a first approximation the vapor tangential shear stress will be neglected and replaced with the axial velocity no slip condition

$$u_0 = 0 \quad (26)$$

## CONTINUITY OF NORMAL STRESS

$$P_v - P_l + \rho_v V_{0v}(V_{0v} - V_{0l}) + 2 \left[ \mu_l \frac{\partial v_l}{\partial r} - \mu_v \frac{\partial v_v}{\partial r} \right] = \sigma \left( \frac{1}{R_1} + \frac{1}{R_2} \right) \quad (27)$$

## CONTINUITY OF THERMAL FLUX

$$C_w \rho_v V_{0v} h_{fg} = -k_l \frac{\partial T_l}{\partial r} \quad (28)$$

where

$$C_w = \left[ \frac{D_p}{D_p + D_w} \right]^2$$

The term  $C_w$  accounts for the effective liquid-vapor interface surface area due to the presence of the wick pores of diameter  $D_p$  and of the screen wires of diameter  $D_w$ .

## SUPPLEMENTAL RELATIONS

Supplemental relations can be used to derive relations between the liquid and vapor at the interface. Using the kinetic theory for interphase mass transfer[35] and the Clausius-Clapeyron Equation[36] , the following expression is derived in Appendix C for the radial liquid velocity at the liquid-vapor interface

$$\begin{aligned} V_0 &= \sqrt{\frac{M}{2\pi R_u}} \left[ \frac{\rho_v}{\rho_l} h_{fg} \right] [T_v^{-3/2}] (T_v - T_s) \\ &= h_1 [T_v^{-3/2}] (T_v - T_s) \end{aligned} \quad (29)$$

The interphase heat flux can be expressed by using the continuity equation and substituting Equation 29 in Equation 28

$$q_0 = C_w \sqrt{\frac{M}{2\pi R_u}} \left[ \rho_v h_{fg}^2 \right] [T_v^{-3/2}] (T_v - T_s) \quad (30)$$

#### 4.4 THE VAPOR PHASE MATHEMATICAL FORMULATION

Heat pipe dynamics are strongly dependent on the vapor phase so that complete solution of the heat pipe problem requires solution of the full system of vapor phase governing equations. The intent of this research was to develop a computational algorithm for liquid phase dynamics that would be combined with a vapor phase algorithm. Development of the vapor phase algorithm encountered extreme difficulties such that a vapor code was not available for complete checkout of both the liquid and vapor codes[37] . An approximation of the vapor phase was developed to permit demonstration of the liquid phase code operation.

The characteristics of vapor flow allow some simplification in developing the approximate model. In general the vapor response is orders of magnitude faster than the liquid response such that the vapor can possibly be treated as quasisteady in a liquid time scale reference [18]. The vapor is also assumed to be uniform in a selected control volume. A mass balance on the control volume for a single arbitrary time step gives

$$M_v^{(n+1)} = M_v^{(n)} - \delta_t \dot{m}_v \quad (31)$$

where  $M_v$  is the total vapor mass at a given discrete time,  $\delta_t$  is the time step size, and  $\dot{m}_v$  is the net mass flux due to evaporation and condensation. The sign of  $\dot{m}_v$  is taken such that evaporation, which has a negative velocity, produces mass addition, while condensation produces mass extraction from the vapor space.

Solution of Equation 31 can be used to fix the vapor state. The solution is dependent on the phase change process, which is a function of the heat pipe operating limits. This study will consider restriction only due to the sonic limit. The solution is then dependent on whether the pipe operation is subsonic or sonic limited.

#### 4.4.1 Subsonic Vapor Operation

Subsonic operation is assumed to occur such that the vapor is uniform at a given time step. The mass balance control volume is then the entire vapor space. The net phase change mass transfer can be expressed as

$$\dot{m}_v = \int_0^L \rho_v V_{0v} C_w 2 \pi R_v dx \quad (32)$$

Using the continuity equation (Equation 25) and the kinetic energy formulation for  $V_0$  (Equation 29) gives

$$\dot{m}_v = C_w R_v \sqrt{\frac{2\pi}{R_g}} \rho_v h_{fg} \left[ L T_v^{-1/2} - T_v^{-3/2} \int_0^L T_s dx \right] \quad (33)$$

where  $T_v$  is the uniform vapor temperature,  $T_s$  is the liquid-vapor interface surface temperature, and  $R_g$  is the gas constant for the working fluid of interest. As a first approximation, all parameters except the temperatures in Equation 33 are assumed to be at time level  $t^n$ .

Substituting Equation 33 in Equation 31 and dividing by the fixed volume of the vapor space  $V$  gives

$$\rho_v^{(n+1)} = \rho_v^{(n)} \left\{ 1 - \frac{\delta_t C_w R_v}{4} \sqrt{\frac{2\pi}{R_g}} h_{fg} \left[ L T_v^{-1/2} - T_v^{-3/2} \int_0^L T_s dx \right] \right\} \quad (34)$$

As shown in Appendix F, the Clausius-Clapeyron Equation can be solved for the vapor density to give

$$\rho_v = \left[ \frac{h_{fg}}{T \left( \frac{dP}{dT} \right)_{sat}} + \frac{1}{\rho_l} \right]^{-1} \quad (35)$$

All parameters except temperature are again assumed to be from time level  $t^{(n)}$ .

Equations 34 and 35 can be equated to produce a nonlinear expression for  $T_v$  in terms of time level  $t^{(n)}$  properties and time level  $t^{(n+1)}$  liquid-vapor interface surface temperatures. The equation can be solved using Newton's method.

#### 4.4.2 *Sonic Limit Operation*

The sonic limit condition is a restriction on axial mass and heat transfer. This restriction implies that the entire vapor space cannot be treated as uniform. The vapor space will be approximated as two control volumes. The first control volume is the vapor space of the evaporator. The second control volume consists of the combined vapor space of the adiabat and condenser regions. The two control volumes communicate through the axial vapor transport corresponding to sonic limited operation. The control volume mass balance for the evaporator is

$$M_{ve}^{(n+1)} = M_{ve}^{(n)} - \delta_t \dot{m}_{ve} - \delta_t \dot{m}_{son} \quad (36)$$

and for the adiabat-condenser is

$$M_{vc}^{(n+1)} = M_{vc}^{(n)} - \delta_t \dot{m}_{vc} + \delta_t \dot{m}_{son} \quad (37)$$

where  $\dot{m}_{son}$  is the sonic limit axial vapor flux. The sonic limit mass flux can be derived from the sonic limit heat transfer given by Equation 4. Solving for mass transfer of sodium vapor produces

$$\dot{m}_{son} = \pi R_v^2 \sqrt{\frac{5R_g}{16}} \rho_v \sqrt{T_v} \quad (38)$$

The phase change mass flux for each control volume is found from Equation 32 with limits of integration corresponding to the respective control volume. The evaporator control volume has phase change mass flux of

$$\dot{m}_{ve} = \int_0^{L_e} \rho_v V_{0v} C_w 2 \pi R_v dx \quad (39)$$

or

$$\dot{m}_{ve} = C_w R_v \sqrt{\frac{2\pi}{R_g}} \rho_v h_{fg} \left[ L_e T_v^{-1/2} - T_v^{-3/2} \int_0^{L_e} T_s dx \right] \quad (40)$$

Phase change mass flux for the adiabat-condenser control volume is

$$\dot{m}_{vc} = \int_{L_e}^L \rho_v V_{0v} C_w 2 \pi R_v dx \quad (41)$$

or



$$\dot{m}_{vc} = C_w R_v \sqrt{\frac{2\pi}{R_g}} \rho_v h_{fg} \left[ (L - L_e) T_v^{-1/2} - T_v^{-3/2} \int_{L_e}^L T_s dx \right] \quad (42)$$

Equations 36 and 37 can be solved using Equations 38, 40, and 42 for the vapor density during sonic limit conditions for each of the control volumes. Using the Clausius-Clapeyron Equation as in the subsonic case produces a nonlinear expression for vapor temperature in each control volume that can be solved with Newton's method.

## 4.5 THE COMPUTATIONAL IMPLEMENTATION

The governing equations, boundary conditions, property relations, and supplemental equations were coded for solution in a Fortran computer program. The calculations are performed at discrete grid points in the liquid and pipe wall. For clarity, the program first will be presented in a top level sense to establish the overall sequence of calculation. The detailed algorithm will then be discussed. Equations presented in other sections of the thesis are repeated when discussed below for convenience.

### 4.5.1 *Computational Algorithm Overview*

Overall organization of the program is shown in the flowchart in Figure 17. The algorithm begins by setting various parameters and initializing conditions. The time stepping section is then entered. Operating limits and property dependent parameters are updated. The input heat flux is updated as is the

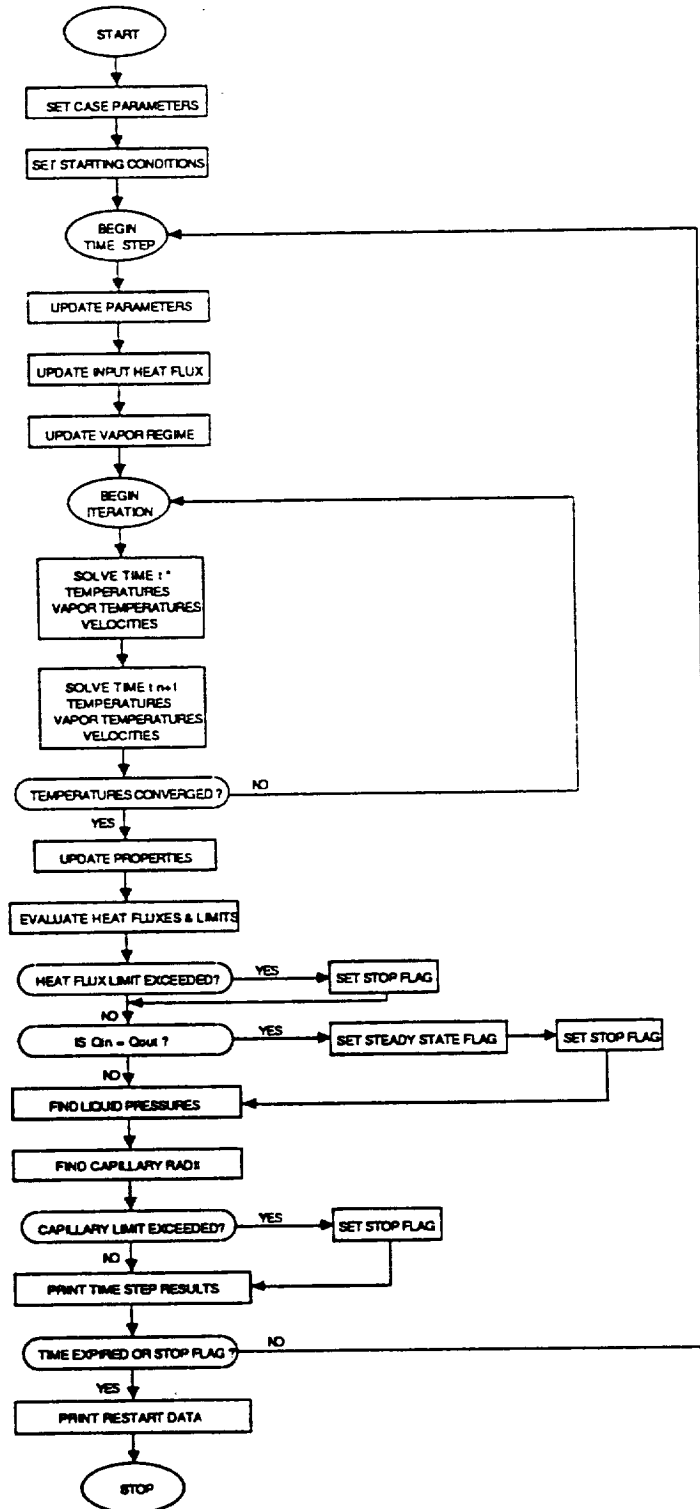


Figure 17: Algorithm Overview Flowchart

vapor regime. The iteration section is then entered. The first partial time step ( $t^*$ ) is solved for liquid and pipe temperatures, vapor temperature, and liquid velocities. The same steps are then repeated for the second partial time step ( $t^{(n+1)}$ ). Iterations are repeated on the first and second time split equations until temperatures of the liquid surface and container wall have converged to a user specified tolerance. After time step convergence the thermophysical properties are updated. Heat transfer limits are determined. Input, output, evaporation, and condensation heat transfer rates are calculated. The capillary limit heat transfer is calculated and compared to evaporation heat transfer. A stop flag is set if the limit is exceeded. A steady state test is performed by comparing input and output heat fluxes. Flags are set if steady state is reached. The liquid pressure gradient and liquid pressures are evaluated. The capillary radii are determined from vapor pressure, liquid pressure, and phase change velocities. Capillary radii are checked for the capillary pumping limit. A stop flag is set if the capillary limit is exceeded. Time step data are printed, and the program advances to the next time step unless a stop flag was issued or time has expired. If calculations are to be terminated, restart data are printed to a restart file which can be used to continue the calculations in a later run.

#### 4.5.2 *Computational Algorithm Details*

The detailed program can be considered in three broad sections: the startup section, the iteration section, and the completion section. The startup section shown in Figure 18 begins the calculation cycle. Calculations can be performed beginning from a time zero condition or in restart mode to continue calculations of a previous case. The algorithm begins by setting common and dimension areas, and reading input data. Input data consist of the restart option flag, time step size, grid step sizes, vapor space radius, wick pore radius, screen wire radius, environment heat sink radiation temperature, and initial heat pipe temperature. The restart option flag controls the program initialization steps so that for a restart case, the program will initialize with the appropriate data from the previous case. Geometry parameters are calculated. Time parameters controlling the duration of the calculations are set. Data output print control parameters are set. Heat pipe surface radiation characteristics are set as are input heat flux control parameters used in Equations 44 and 45. Thermophysical properties of the pipe wall material and sodium working fluid properties are initialized. Combinations of various constants used repeatedly throughout the code are calculated to reduce total arithmetic. Peaceman-Rachford ADI parameters used by Equations 134 and 135 in Appendix E are initialized. Operating limits are initialized, and temperature and velocity fields are initialized. Startup data are printed, and control passes to the beginning of the time steps in the iteration section.

The iteration section shown in Figure 19 begins the time step and performs iterations between temperatures and velocities until acceptable convergence is

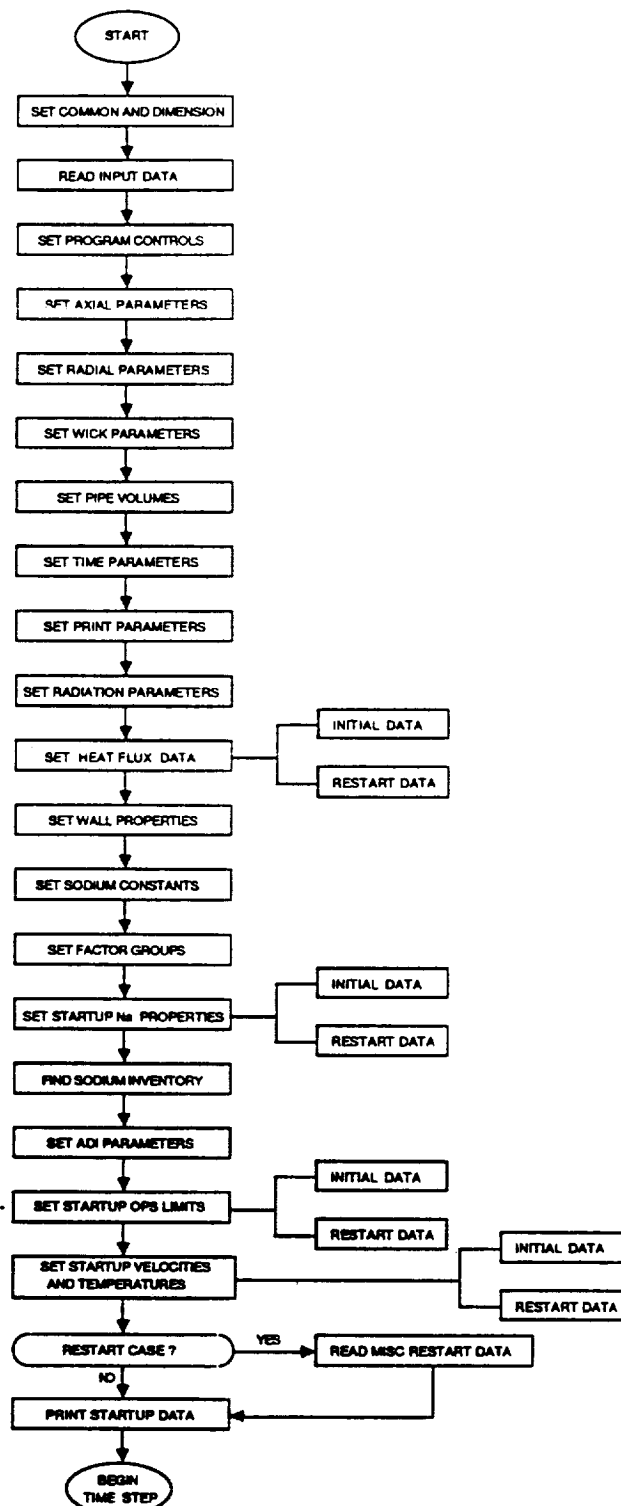


Figure 18: Algorithm Startup Flowchart

achieved. Property dependent operating limits and ADI parameters are updated. Input heat flux is updated for the new time step. The input heat flux profile and time dependence are user defined functions given by Equations 44 and 45

$$q_{in} = \frac{1}{2} q_{\max} \left\{ 1 - \sin \left[ \pi \left( \frac{t}{\tau} + \frac{1}{2} \right) \right] \right\} \quad (44)$$

$$t > \tau$$

$$q_{in} = q_{\max} \quad (45)$$

An option is included to smooth the abrupt step change of heat input at the evaporator-adiabat boundary. The vapor operating regime is checked using Equation 38

$$\dot{m}_{son} = \pi R_v^2 \sqrt{\frac{5R_g}{16} \rho_v \sqrt{T_v}} \quad (38)$$

Operation is subsonic if axial heat transfer is below the sonic limit and is sonic limited otherwise.

Iterations are set up by saving data from the just completed time step and using these data as the initial guess for the next time step. Iterations are performed by first solving for time  $t^*$  liquid and container temperatures. The finite difference Peaceman-Rachford Alternating Direction Implicit method is used to solve the energy equation in two partial time steps. The first partial time step is solved using Equation 134 from Appendix E

$$A_1 T_{ij-1}^* + A_2 T_{ij}^* + A_3 T_{ij+1}^* = B_1 T_{i-1,j}^{(n)} + B_2 T_{ij}^{(n)} + B_3 T_{i+1,j}^{(n)} \quad (134)$$

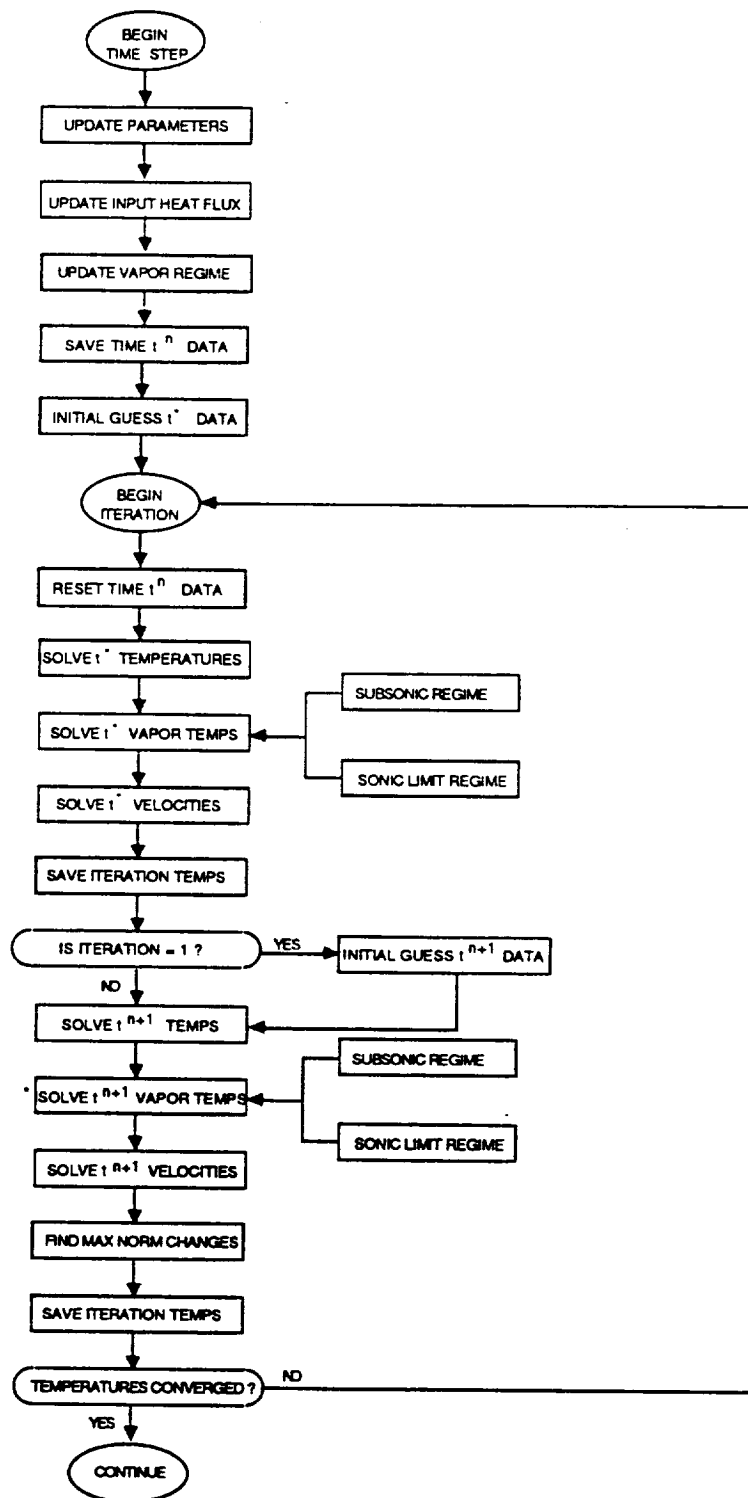


Figure 19: Algorithm Time Step Iteration Flowchart

Implementation details are provided in Appendix F. The method essentially involves solution by integrating the energy equation for a partial time step (time  $t^*$ ) in the radial direction, and then integrating for the remaining time step (time  $t^{(n+1)}$ ) in the axial direction.

The first time split liquid temperatures are then used to find time  $t^*$  vapor temperatures. Depending on whether the vapor is subsonic or sonic limited, control passes to the appropriate subroutine to use Newton's method to solve the vapor temperature equation. Subsonic vapor temperature is determined from Equations 34 and 35

$$\rho_v^{(n+1)} = \rho_v^{(n)} \left\{ 1 - \frac{\delta_t C_w R_v}{4'} \sqrt{\frac{2\pi}{R_g}} h_{fg} \left[ L T_v^{-1/2} - T_v^{-3/2} \int_0^L T_s dx \right] \right\} \quad (34)$$

$$\rho_v = \left[ \frac{h_{fg}}{T \left( \frac{\partial P}{\partial T} \right)_{sat}} + \frac{1}{\rho_l} \right]^{-1} \quad (35)$$

Sonic limited vapor temperatures are determined from Equation 35 above and Equations 36 and 37

$$M_{ve}^{(n+1)} = M_{ve}^{(n)} - \delta_t \dot{m}_{ve} - \delta_t \dot{m}_{son} \quad (36)$$

$$M_{vc}^{(n+1)} = M_{vc}^{(n)} - \delta_t \dot{m}_{vc} + \delta_t \dot{m}_{son} \quad (37)$$

Based on vapor temperatures and liquid-vapor interface surface temperatures the liquid phase change velocity is calculated from Equation 29



$$\begin{aligned}
V_0 &= \sqrt{\frac{M}{2\pi R_u}} \left[ \frac{\rho_v}{\rho_l} h_{fg} \right] [T_v^{-3/2}] (T_v - T_s) \\
&= h_l [T_v^{-3/2}] (T_v - T_s)
\end{aligned} \tag{29}$$

The bulk axial velocity distribution is calculated from the continuity equation and the liquid phase change velocity using Equation 84 from Appendix B

$$\bar{U}(i) = \frac{1}{2} \frac{A_{lv}}{A_a} \left[ V_0(1) + 2 \sum_{n=2}^{i-1} V_0(n) + V_0(i) \right] \tag{84}$$

Bulk axial velocity is transformed to a velocity profile using Equation 85 from Appendix B

$$u^* = a + b r^* + c r^{*2} + d r^{*3} \tag{85}$$

Finally, the radial velocity distribution is found from Equation 119 of Appendix C

$$\begin{aligned}
v(x,r) &= \frac{C_w V_0 R_v}{r} \left\{ 1 - \frac{2\delta}{R_l + R_v} \right. \\
&\quad \left. \left[ b \frac{R_v}{\delta} \frac{r^{*2}}{2} + \left( b + c \frac{R_v}{\delta} \right) \frac{r^{*3}}{3} + \left( c + d \frac{R_v}{\delta} \right) \frac{r^{*4}}{4} + d \frac{r^{*5}}{5} \right] \right\} \tag{119}
\end{aligned}$$

Calculations for the first time split are completed.

The second time split is set up by setting the temperatures and velocities for the first iteration of the  $(t^{(n+1)})$  time split equal to the time  $t^*$  values. The liquid and container temperatures, vapor temperatures, and velocities for the second partial time step  $(t^{(n+1)})$  are found as in the first time split with liquid and container temperatures found using ADI Equation 135. from Appendix E

$$A_4 T_{i-1,j}^{(n+1)} + A_5 T_{i,j}^{(n+1)} + A_6 T_{i+1,j}^{(n+1)} = B_4 T_{i,j-1}^* + B_5 T_{i,j}^* + B_6 T_{i,j+1}^* \quad (135)$$

The energy equation and the flow dynamics equations are tightly coupled at the liquid-vapor interface such that the solutions of each are interdependent. In addition, the equations contain nonlinear terms that required quasilinearization treatment, which requires iterations. Iterations are performed between temperatures and velocities until an acceptable convergence is achieved.

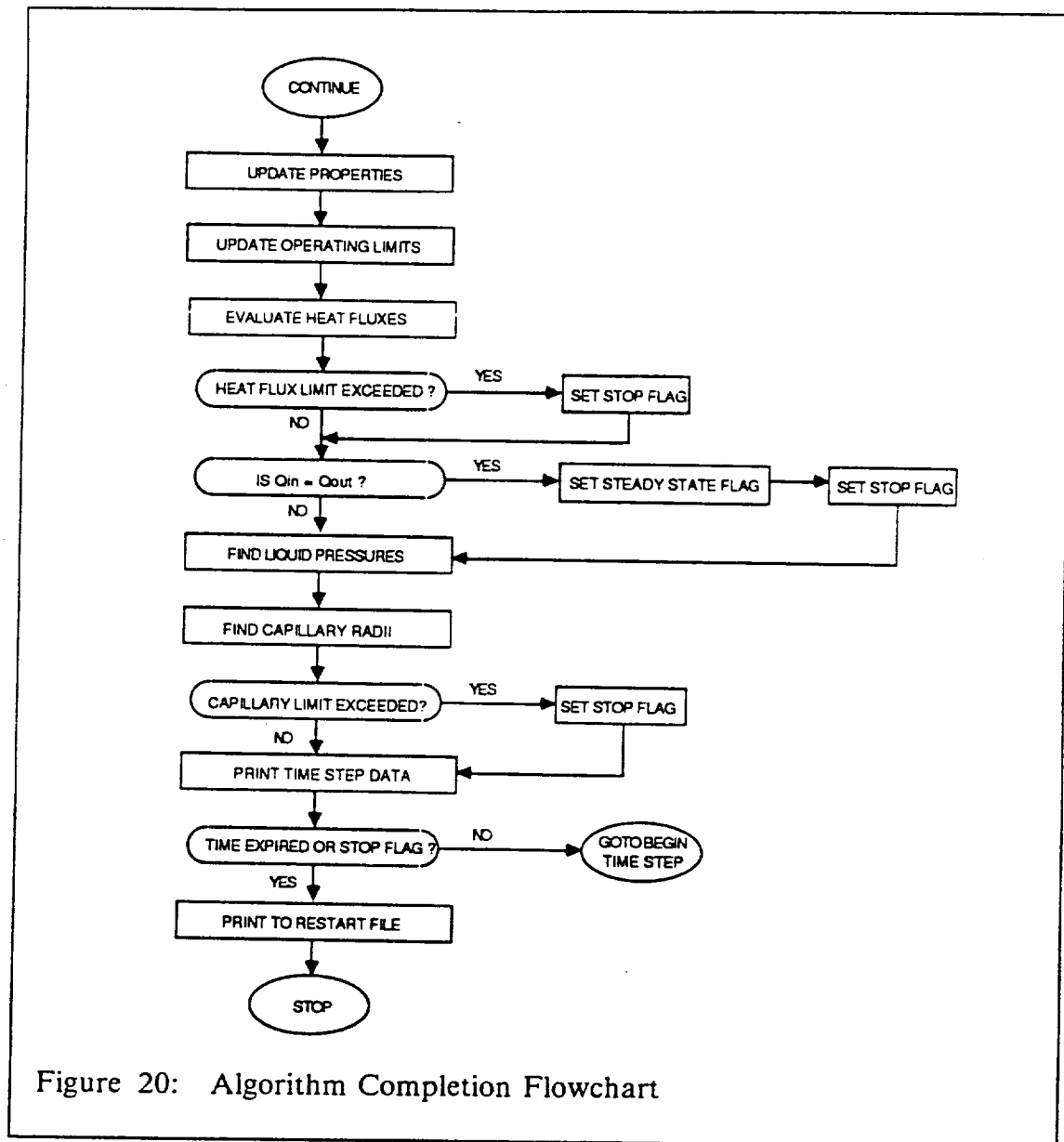
The completion section of the program shown in Figure 20 includes all remaining functions to complete the time step calculations and send control to the next time step or terminate execution. Thermophysical properties are updated based on the temperature conditions using the relationships presented in Appendix F. A mass balance is performed to track working fluid inventory. The sonic limit heat transfer is determined from Equation 4

$$Q_{son} = \frac{\rho_v h_{fg} A_v c}{\sqrt{2(1 + \gamma)}} \quad (4)$$

Capillary limit heat transfer is determined from Equation 8

$$\left. \frac{\Delta P}{\Delta x} \right|_{cap} = - F_l Q_{cap} \quad (8)$$

Input, output, evaporation, and condensation heat transfer rates are evaluated. A stop flag is issued if the capillary limit is exceeded. Input heat transfer is compared with output heat transfer, and a steady state flag is issued if they are approximately equal.



Liquid pressures are found from Equation 126 in Appendix D from the axial momentum integral equation

$$\begin{aligned}
P_i^{(n+1)} = & P_{i+1}^{(n+1)} + P_{i+1}^{(n)} - P_i^{(n)} \\
& - \left[ \frac{\mu}{h_x} \bar{U}_{i-1} + \left( \gamma h_x - \frac{2\rho h_x}{k} - \frac{2\mu}{h_x} \right) \bar{U}_i + \frac{\mu}{h_x} \bar{U}_{i+1} \right]^{(n+1)} \\
& - \left[ \frac{\mu}{h_x} \bar{U}_{i-1} + \left( \gamma h_x + \frac{2\rho h_x}{k} - \frac{2\mu}{h_x} \right) \bar{U}_i + \frac{\mu}{h_x} \bar{U}_{i+1} \right]^{(n)}
\end{aligned} \tag{126}$$

The integration is performed by assuming liquid pressure and vapor pressure are equal at the end of the condenser ( $x = L$ ). Details of the numerical implementation are provided in Appendix D. The liquid-vapor interface radial momentum condition given by Equation 27 can be solved for the capillary radii of curvature to give

$$R_c = \frac{2\sigma}{P_v - P_l + (\rho_l V_0)^2 \left[ \frac{1}{\rho_v} - \frac{1}{\rho_l} \right] + 2\mu_l \frac{\partial V_0}{\partial r}} \tag{43}$$

The total liquid pressure drop is compared to the maximum possible capillary pumping capability of the wick given by Equation 10

$$\Delta P_{cap} = \frac{2\sigma}{R_p} \tag{10}$$

A stop flag is activated if the limit is exceeded. Data from the time step are printed, and the next time step is initiated unless a stop flag has been activated or time for the case has expired. Data from the final time step are dumped to a restart file, and execution is terminated.

## Chapter V

### DISCUSSION OF RESULTS

*“It is of highest importance in the art of detection to be able to recognise out of a number of facts which are incidental and which vital. Otherwise your energy and attention must be dissipated instead of being concentrated.”*

*Sherlock Holmes in The Adventure of the Reigate Squire*

Capabilities of the computational algorithm were tested by running two heat pipe startup cases. The heat pipe dimensions were chosen to be consistent with the experimental device described by Merrigan et al. up to the limit of the uniform grid used in this analysis [19][20]. The experimental heat pipe in that study used lithium as the working fluid and an annular wick configuration. The annular region for liquid flow was formed between the pipe interior wall and a porous concentric tube constructed of 7.25 layers of pressed screen. The high temperatures involved required the container to be constructed from the refractory alloy molybdenum. The heat pipe geometry parameters used in this analytical study compared to the actual parameters are (see Figures 15 and 16):

Parameter	Actual	Approximate
Heat Pipe Internal Length ( $L$ )	4.0	4.0 m
Evaporator Length ( $L_e$ )	0.4 m	0.4 m
Condenser Length ( $L_c$ )	3.0 m	3.0 m
External Diameter ( $D_w$ )	1.90 cm	1.886 cm
Internal Diameter ( $D_l$ )	1.60 cm	1.598 cm
Vapor Space Diameter ( $D_v$ )	1.49 cm	1.490 cm
Effective Wick Pore Diameter ( $D_p$ )	53 $\mu\text{m}$	53 $\mu\text{m}$

where the effective wick pore diameter was experimentally determined from surface tension measurements.

An axial grid step size of  $h_x = 0.2$  m and a radial grid step size of  $h_r = 1.1 \times 10^{-4}$  m were used. The computational grid consisted of 21 axial grid steps and 20 radial grid steps. The grid mapping to the heat pipe configuration is:

Radial Liquid Space	$1 \leq j < 6$
Radial Pipe Wall	$6 \leq j \leq 20$
Axial Evaporator Region	$1 \leq i \leq 3$
Axial Adiabatic Region	$3 < i < 6$
Axial Condenser Region	$6 \leq i \leq 21$

Numerical experimentation showed that the code is highly sensitive to time step size. Too large a time step produced an inconsistent temperature at the

liquid-vapor interface. The temperature was inconsistent in that the temperature gradient at the surface changed sign relative to the gradient of the interior liquid. For example, in the evaporator energy is conducted from the pipe wall to the liquid-vapor interface. The liquid-vapor surface temperature should be the lowest temperature in the radial conduction path in order for the energy to reach the surface. Too large a time step will produce a physically questionable surface temperature that is greater than the temperature of the interior liquid. Too large a time step was also found to cause oscillations in the pressure calculations.

The time step size was selected by running a series of calculations for three hundred time steps each with gradually decreasing step sizes. A time step size of  $\delta_t = 2 \times 10^{-3}$  second was found to eliminate inconsistent liquid-vapor interface temperatures, but did not completely remove pressure oscillations. A time step size of  $\delta_t = 1 \times 10^{-3}$  second removed the pressure oscillations for the three hundred time steps calculation. This time step was used in the calculations.

## **5.1 SLOW STARTUP TEST**

A startup test was devised to supply input energy to the evaporator such that the heat pipe would warm up without reaching the sonic limit. This test was to check overall program implementation. Input heat flux was supplied according to the function

$$t \leq \tau$$

$$q_{in} = \frac{1}{2} q_{max} \left\{ 1 - \sin \left[ \pi \left( \frac{t}{\tau} + \frac{1}{2} \right) \right] \right\} \quad (44)$$

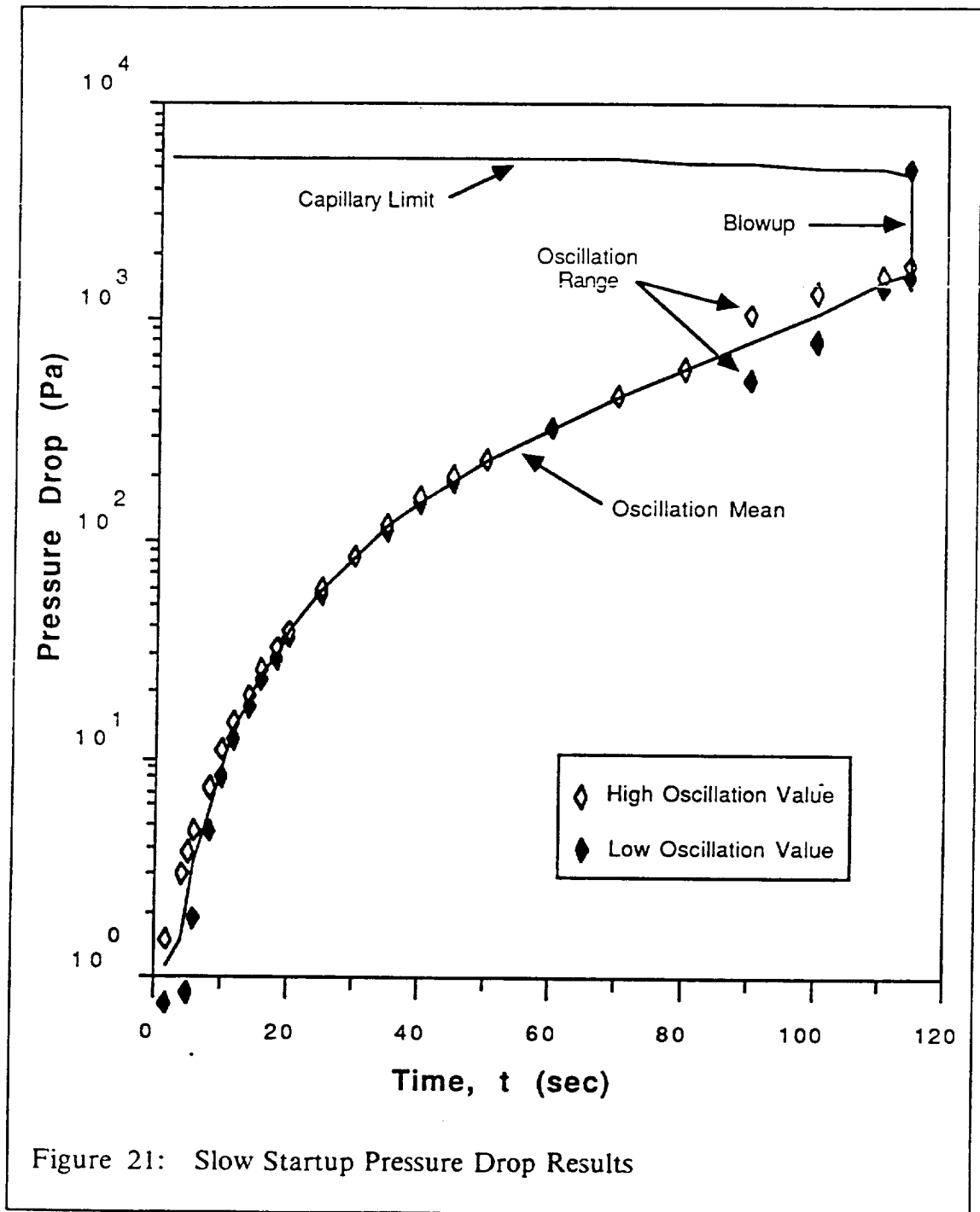
$$t > \tau$$

$$q_{in} = q_{max} \quad (45)$$

where  $q_{max}$  is the maximum input heat flux and  $\tau$  is the time stretching parameter that controls how quickly  $q_{in}$  reaches  $q_{max}$ . In this test,  $q_{max} = 1 \times 10^6 \text{ W/m}^2$  and  $\tau = 300$  seconds corresponding to a five minute period for the input heat flux to reach the maximum.

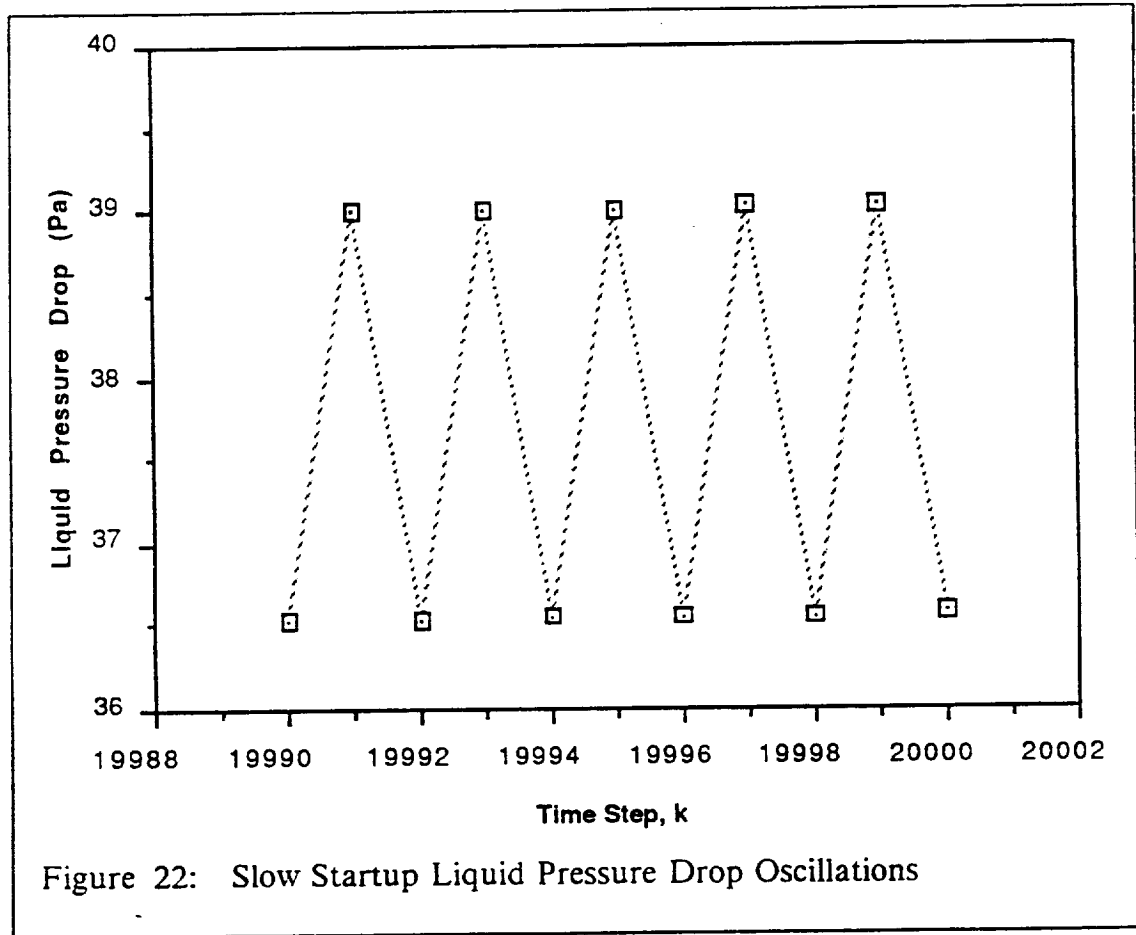
Calculations were performed for 114,193 time steps, or a period slightly greater than 114 seconds. The run was terminated at this time since the liquid pressure drop exceeded the capillary pumping limit. The liquid pressure drop and the capillary pumping limit as functions of time are shown in Figure 21. Analysis of the results shows that the capillary pumping limit was exceeded due to a large jump in pressure drop at a single time step. Figure 21 also shows that the pressure calculations had been experiencing oscillations with usually small amplitudes of approximately 2.5 Pa. The oscillations began after the 300 time steps used to verify the adequacy of the time step size of  $1 \times 10^{-3}$  second. The liquid pressure drop curve is drawn through the centers of the oscillation ranges in Figure 21. The oscillations become very large at  $t = 90$  seconds, but begin to decay until the large jump occurs at approximately 114 seconds.





The pressure oscillations are presented in detail in Figure 22. The liquid pressure drop is plotted for eleven consecutive time steps for

$19,990 \leq k \leq 20,000$ , corresponding to the time around time  $t = 20$  seconds in Figure 21. The oscillations are of essentially constant amplitude and well behaved until time  $t > 80$  seconds as shown in Figure 21.



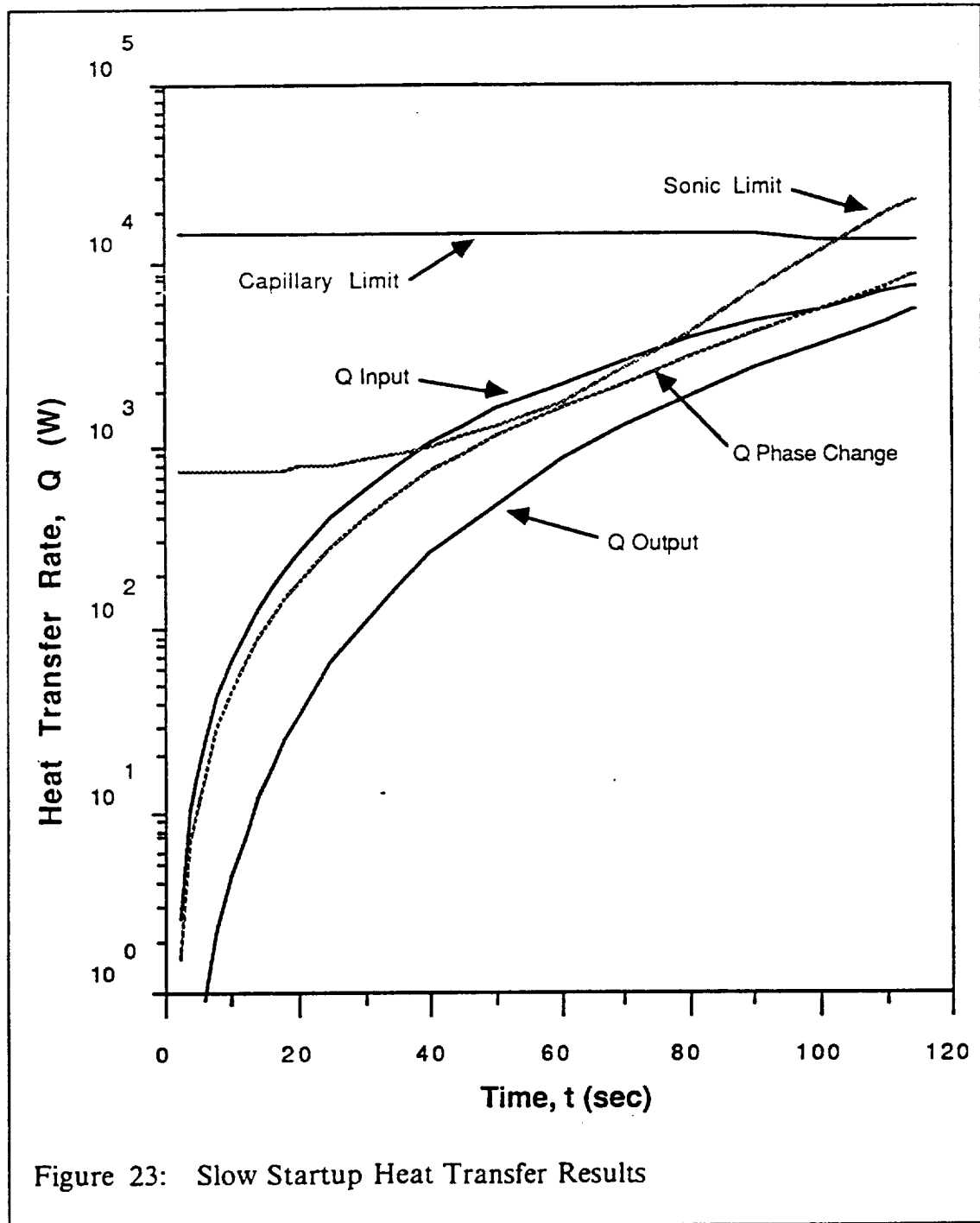
Power transfer as a function of time is shown in Figure 23. While the input power briefly exceeds the sonic limit line, the phase change heat transfer remains below the sonic limit. At approximately 103 seconds into the transient, the sonic limit exceeds the capillary limit so that the capillary limit becomes the controlling heat transport limit. At approximately 105 seconds, the unlikely result is produced that the phase change heat transfer exceeds the

input heat transfer. With the exception of this anomaly, the heat transfer curves are well behaved, smooth functions of time. In addition, the phase change heat transfer is well below the capillary limit heat transfer at the point when liquid pressure drop jumps to exceed the capillary pumping limit. The cause of the liquid pressure drop jump is not apparent from the heat transfer curves.

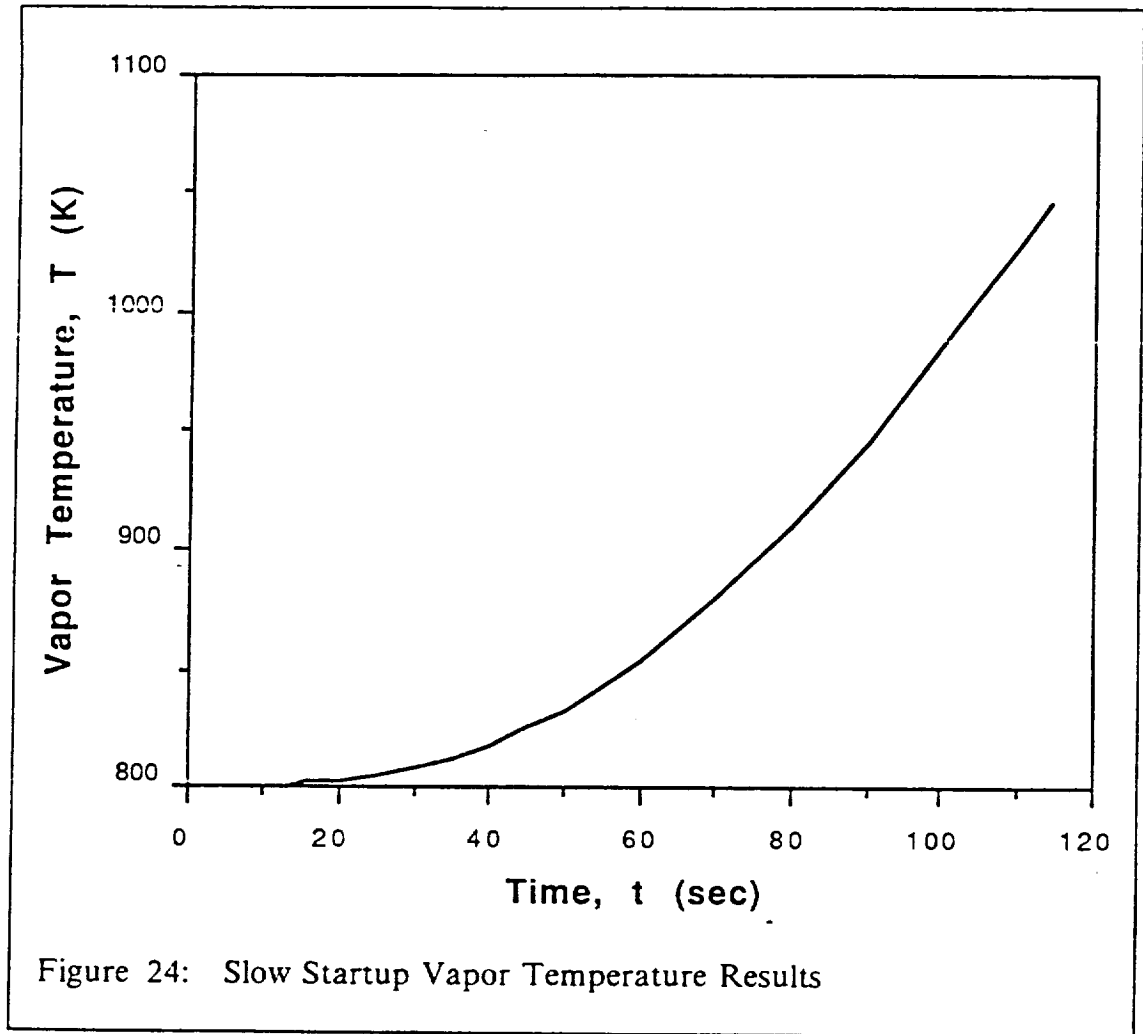
The vapor temperature as a function of time is shown in Figure 24. The vapor temperature is also a smooth, although rapidly increasing, function of time. The cause of the jump in liquid pressure drop is also not apparent from vapor temperature.

The pressure drop calculation can be seen in Figure 21 to produce oscillatory behavior with large sporadic oscillations for time greater than 80 seconds. The pressure calculations are a sensitive function of time step size. Numerical experimentation also showed that the pressure calculations are sensitive to property updates and changes in the liquid-vapor interface boundary conditions corresponding to the change between subsonic and sonic limited operation. Sensitivity to property updates was identified by varying the frequency at which updated properties are calculated.

There are many potential causes for the pressure oscillations. The pressure oscillations may be physical, but this possibility is remote considering the numerical sensitivities of the method. The time step size of  $1 \times 10^{-3}$  second may have been too large. If this is the case, a smaller time step may not be acceptable considering the cost of computations for a transient process that occurs over a period of tens of minutes. The oscillations may have resulted



from the derivation in Appendix B of the axial velocity profile in which the shape is determined by neglecting the temporal terms in the momentum

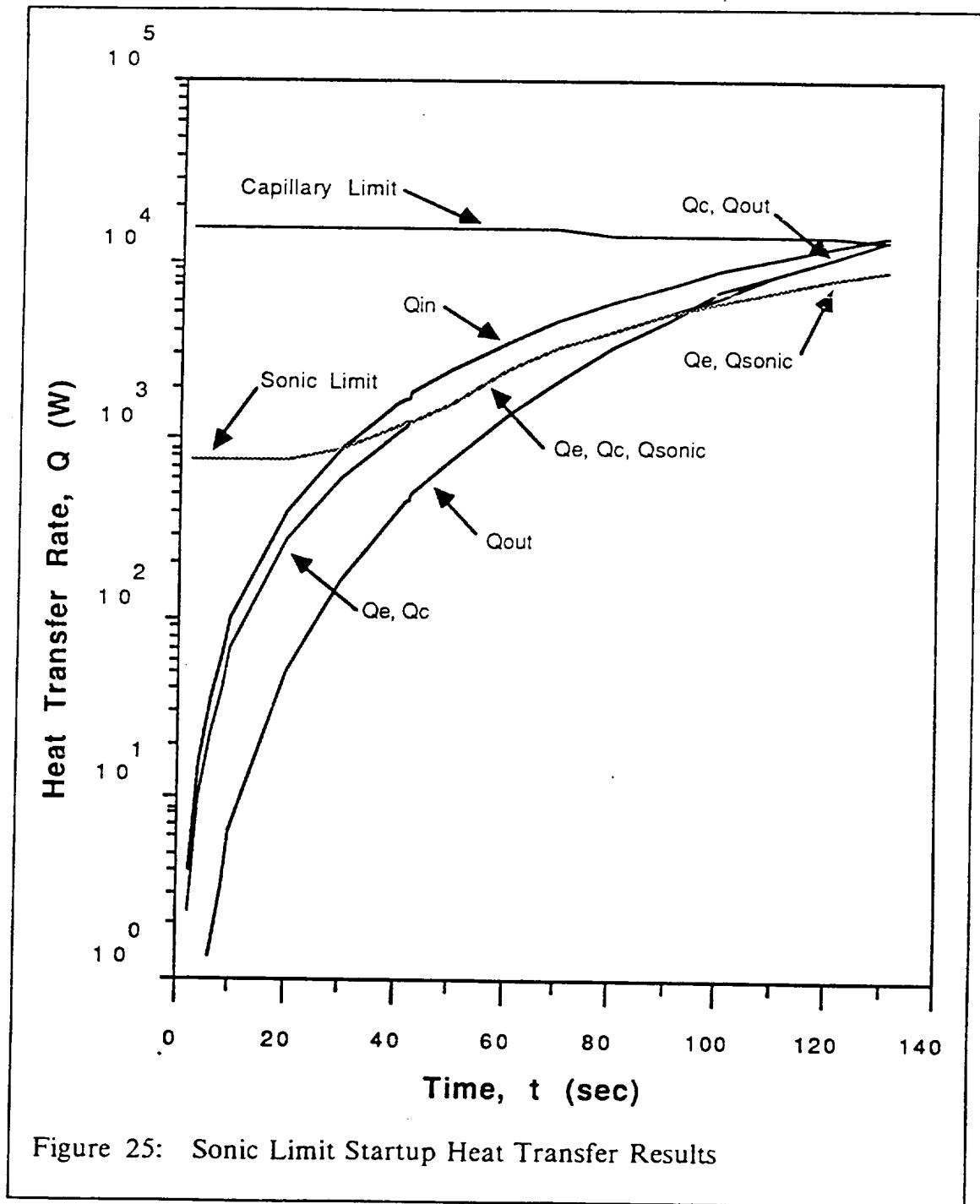


equation. The pressure calculations are also based on the convenient assumption that the minimum liquid pressure occurs at the end of the condenser, although this assumption is not generally valid for the wide range of operating conditions encountered during a startup transient.

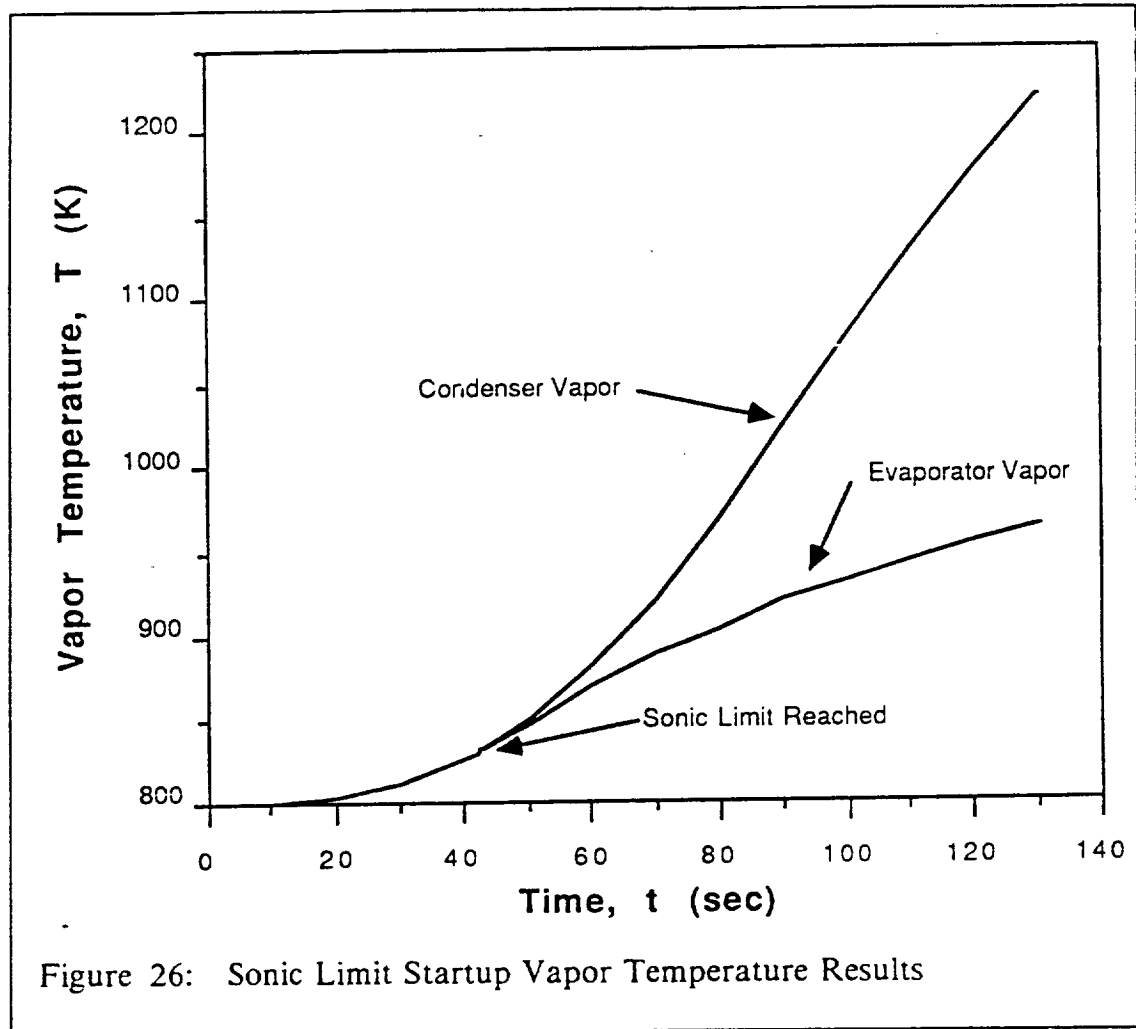
## 5.2 SONIC LIMIT STARTUP TEST

A startup test was performed to test algorithm calculation of sonic limited operation. Using again  $\tau = 300$  seconds, the maximum input heat flux was increased to  $q_{\max} = 1.5 \times 10^6 \text{ W/m}^2$  to assure the phase change heat transfer would reach the sonic limit. Heat transfer results are shown in Figure 25.

Input power exceeds the sonic limit at 20 seconds, and remains above the sonic limit through the duration of the test of 130 seconds. The evaporation and condensation heat fluxes are essentially equal as the sonic limit is reached at approximately 40 seconds. Evaporation and condensation follow the sonic limit curve until 80 seconds. After 80 seconds, condensation heat flux increases above the sonic limit, while evaporation heat flux continues to follow the sonic limit curve. This unlikely result is a result of the inadequacies of the simple vapor model used to perform calculations. The vapor model unintentionally forces a high condensation rate, which forces the condenser temperature to increase rapidly due to the high thermal resistance of the radiation boundary condition on the condenser. This temperature effect is shown in Figure 26. The evaporator vapor temperature smoothly and gradually increases with time, while the condenser vapor temperature rapidly increases. The condenser temperature eventually increases sufficiently so that radiation heat transfer from the condenser becomes very efficient. At approximately 93 seconds, the output heat transfer exceeds the evaporation heat transfer, which is another unlikely result. Calculations are terminated at 130 seconds due to the condensation heat transfer exceeding the capillary heat transfer limit. While the capillary limit is not strictly a limit on condensation,



calculations had already passed beyond physical significance and the computational implementation had been demonstrated.





## Chapter VI

### CONCLUSIONS AND RECOMMENDATIONS

The heat pipe is a very complex device such that performing analysis of heat pipe transients is a difficult venture. The difficulty is due to the coupled liquid and vapor dynamics, the phase change process, the coupled heat transfer problem with nonlinear boundary conditions, the physical geometry, and the transient time requirement. This study has presented the full system of governing equations, including boundary conditions, required to solve the liquid phase heat pipe problem. A simplified solution was formulated by using certain assumptions and integrating the liquid dynamics equations.

The resulting formulation identified a key requirement for future research in solving the heat pipe problem. This study used a kinetic theory approach to model the phase change process as expressed by Equation 29. The model consists of a large coefficient multiplying a very small temperature difference. The model requires a very small time step for stability even with the simplifications used in this analysis. The large coefficient also transforms temperature differences that are otherwise beyond machine accuracy into computationally significant terms. Future research should investigate an alternative model for the phase change process.

Difficulty with geometry was encountered due to the widely disparate length scales in the different coordinate directions. The radial dimension

across the liquid is much smaller than the radial dimension across the pipe wall, which in turn is much smaller than dimensions in the axial direction. One approach to address this problem is to assume radial gradients are negligible. The radial pressure gradient was neglected in this study. This study also found small radial temperature gradients indicating that the radial thermal resistance is small. The drawback of this approach is the loss of fidelity with the true physics of the problem. A preferable approach may be to use a variable mesh grid with a to-be-determined simplified treatment of radial gradients. The variable mesh grid allows fine resolution in important regions with coarse resolution in the other regions. The simplified treatment of radial gradients would take advantage of the small radial gradients.

The long duration of transients presents a competing concern with model complexity. An overly complex model with high fidelity may be too computationally expensive for practical calculations of transients.

This study has also shown that the transient heat pipe problem is not amenable to a straightforward simplification such as is used for the vapor phase. The solution of the heat pipe transient problem requires a full solution of the liquid and vapor phases. This elusive solution is left to future efforts.

## REFERENCES

1. Grover, G. M., T. P. Cotter, and G. F. Erickson. "Structures of Very High Thermal Conductance," Journal of Applied Physics, Vol. 35, No. 6 (June 1964).
2. Cotter, T. P. Theory of Heat Pipes. Los Alamos Scientific Laboratory, Los Alamos, New Mexico, Report LA-3246-MS (1965).
3. Faghri, A. "Vapor Flow Analysis in a Double-Walled Concentric Heat Pipe," Numerical Heat Transfer, Vol. 10 (1986) pp. 583-595.
4. Ivanovskii, M. N., V. P. Sorokin, and I. V. Yagodkin. The Physical Principles of Heat Pipes. Oxford: Clarendon Press (1982).
5. Chi, S. W. Heat Pipe Theory and Practice: A Sourcebook. Washington: Hemisphere Publishing Corporation (1976).
6. Dunn, P., and D. A. Reay. Heat Pipes. New York: Pergamon Press, Third Edition (1982).
7. Brennan, P. J. and E. J. Kroliczek. Heat Pipe Design Handbook. Prepared by B & K Engineering, Inc. for NASA Goddard Space Flight Center, Greenbelt, Md., Contract No. NAS5-23406 (June 1979).

8. Edwards, D. K., G. L. Fleischman, and B. D. Marcus. Theory and Design of Variable Conductance Heat Pipes: Steady State and Transient Performance. Prepared by TRW for NASA Ames Research Center, Contract No. NAS2-5503 (December 1972).
9. Merrigan, M. A. "Heat Pipe Technology Issues," Space Nuclear Power Systems 1984. Proceedings of the First Symposium on Space Nuclear Power Systems, Albuquerque, New Mexico (January 11-13, 1984) ed. by M. S. El-Genk and M. D. Hoover. Malabar, Florida: Orbit Book Company, Inc., Vol. 2 (1985) pp. 419-426.
10. Camarda, C. J. Aerothermal Tests of a Heat-Pipe-Cooled Leading Edge at Mach 7. NASA Technical Paper 1320 (November 1978).
11. DeMeis, R. "Heat Pipe Cooled Rockets," Aerospace America, Vol. 25, No. 3 (March 1987).
12. Gaugler, R. S. Heat Transfer Device. U. S. Patent No. 2,350,348 (June 6, 1944).
13. Grover, G. M. Evaporation-Condensation Heat Transfer Device. U. S. Patent No. 3,229,759 (January 18, 1966).
14. Adamson, A. W. Physical Chemistry of Surfaces. Interscience Publishers Division, John Wiley and Sons (1960).

15. Kemme, J. E. Heat Pipe Design Considerations. Los Alamos Scientific Laboratory, Los Alamos, New Mexico, Report LA-4221-MS (1969). Presented at the 11th Heat Transfer Conference, Minneapolis, Minnesota (August 3-6, 1969).
16. Davis, W. R. and J. K. Ferrell. Evaporative Heat Transfer of Liquid Potassium in Porous Media. Presented at the AIAA/ASME Thermophysics and Heat Transfer Conference, Boston, Massachusetts (July 15-17, 1974).
17. Shukla, K. N. and K. S. Rao. "Heat and Mass Transfer in the Vapor-Gas Region of a Gas Loaded Heat Pipe," Z. angew. Math. u. Mech., Berlin, Vol. 63, No. 11 (1983) pp. 575-580.
18. Bystrov, P. I., and V. F. Goncharov. "Starting Dynamics of High-Temperature Gas-Filled Heat Pipes, " High Temperature, Vol. 21, No. 6 (Nov.-Dec. 1983) pp. 927-936.
19. Merrigan, M. A., E. S. Keddy, and J. T. Sena. Transient Performance Investigation of a Space Power System Heat Pipe. Los Alamos Scientific Laboratory, Los Alamos, New Mexico, Report LA-UR-86-1567 (1986). Presented at the AIAA/ASME 4th Joint Thermophysics and Heat Transfer Conference, Boston, Massachusetts (June 2-4, 1986).
20. Merrigan, M. A., E. S. Keddy, and J. T. Sena. Transient Heat Pipe Investigations for Space Power Systems. Los Alamos Scientific

- Laboratory, Los Alamos, New Mexico, Report LA-UR-85-3341 (1985).  
Presented at the SP-100 Program Integration Meeting, Denver, Colorado  
(September 19, 1985).
21. Colwell, G. S. "Transient Heat Pipe Operation in the Near Critical Region," Advances in Heat Pipe Technology. New York: Pergamon Press (1981) pp. 289-296.
  22. Colwell, G. S. and W. S. Chang. "Measurements of the Transient Behavior of a Capillary Structure Under Heavy Thermal Loading," International Journal of Heat and Mass Transfer, Vol. 27, No. 4 (1984) pp. 541-551.
  23. Colwell, G. S. and J. G. Hartley. Modeling of Transient Heat Pipe Operation. Georgia Institute of Technology. Prepared for NASA Langley, NASA Grant NAG-1-392, Semiannual Status Report, NASA-CR-175496 (February 1985), Semiannual Status Report (September 1985), Semiannual Status Report, NASA-CR-177143 (June 1986).
  24. Chang, W. S. and G. S. Colwell. "Mathematical Modeling of the Transient Operating Characteristics of a Low Temperature Heat Pipe," Numerical Heat Transfer, Vol. 8 (1985) pp. 169-186.
  25. Cotter, T. P. Heat Pipe Startup Dynamics. Presented at the Thermionic Conversion Specialist Conference, Palo Alto, California (October

- 30-November 1, 1967). 1967 IEEE Conference Record of the Thermionic Conversion Specialist Conference, pp. 42-45.
26. Cullimore, B. A. Modeling of Transient Heat Pipe Effects Using a Generalized Thermal Analysis Program. AIAA Paper 85-0938 (June 1985).
27. Ransom, V. H. ATHENA Heat Pipe Model Idaho National Engineering Laboratory. Presented at the 4th Symposium on Space Nuclear Power Systems, Albuquerque, New Mexico (January 12-16, 1987).
28. Dikiy, N. A., A. A. Mochalov, T. A. Yurchenko, and N. F. Panchenko. "A Mathematical Model of Transients in a Thermosyphon," Heat Transfer-Soviet Research , Vol. 17, No. 5 (Sep-Oct 1985).
29. Reed, J. G. and C. L. Tien. "Modeling of the Two-Phase Closed Thermosyphon," Journal of Heat Transfer, Vol. 109 (August 1987).
30. Ambrose, J. H., L. C. Chow, and J. E. Beam. "Transient Heat Pipe Response and Rewetting Behavior," Journal of Thermophysics, Vol. 1, No. 3 (July 1987).
31. Beam, J. E. Transient Heat Pipe Analysis Air Force Wright Aeronautical Laboratory, Wright-Patterson Air Force Base. Presented at the AIAA 20th Thermophysics Conference, Williamsburg, Virginia (June 19-21, 1985).

32. Costello, F. A., A. F. Montague, and M. A. Merrigan. Detailed Transient Model of a Liquid-Metal Heat Pipe. Los Alamos Scientific Laboratory, Los Alamos, New Mexico, Report LA-UR-86-1707 (1986). Presented at the AIAA/ASME 4th Joint Thermophysics and Heat Transfer Conference, Boston, Massachusetts (June 2-4, 1986).
33. Best, F. and J. Peery. Simulation of Heat Pipe Rapid Transients. Nuclear Engineering Department, Texas A & M University. Presented at the Transient Heat Pipe Workshop, Los Alamos Scientific Laboratory, Los Alamos, New Mexico (March 4-5, 1986).
34. Merrigan, M. A. Heat Pipe Design for Space Power Heat Rejection Applications. Los Alamos Scientific Laboratory, Los Alamos, New Mexico, Report LA-UR-86-1842-R (1986). Proceedings of the 21st Intersociety Energy Conversion Conference (August 1986).
35. Schrage, R. W. A Theoretical Study of Interphase Mass Transfer. New York: Columbia University Press (1953).
36. Callen, H. B. Thermodynamics. New York: John Wiley and Sons, Inc. (1960).
37. Klein, D. B. and I. Catton. Analysis of Heat Pipe Vapor Dynamics. University of California, Los Angeles, Report INSPI-IR-UCLA-87-01 (1987).



38. Batchelor, G. K. An Introduction to Fluid Dynamics New York: Cambridge University Press (1967).
39. Prosperetti, A. "Boundary Conditions at a Liquid-Vapor Interface," Meccanica, Vol. 14, No. 1 (March 1979) pp. 34-47.
40. Landau, L.D. and E. M. Lifschitz. Fluid Mechanics. New York: Pergamon Press (1959)
41. Fink, J. K., and L. Leibowitz. Thermophysical Properties of Sodium. Argonne National Laboratory, Argonne, Illinois Report ANL-CEN-RSD-79-1 (May 1979).
42. Foust, O. J. Sodium-NaK Engineering Handbook, Volume 1, Sodium Chemistry and Physical Properties. New York: Gordon and Breach (1972).

## Appendix A

### LIQUID-VAPOR INTERFACE CONDITIONS

The liquid-vapor interface is a complex boundary that allows communication between the liquid flow and vapor flow along the entire length of the heat pipe. The complexity of the interface physics can be conceptualized as shown in Figure 27. Solution for the flow field on one side of the boundary is dependent on the flow field on the other side of the boundary. The location and configuration of the interface surface fluctuates with operating conditions. The phase change process, including direction of phase change, is a function of conditions on both sides of the boundary. The interface can be seen to involve exchanges of mass, momentum, and energy.

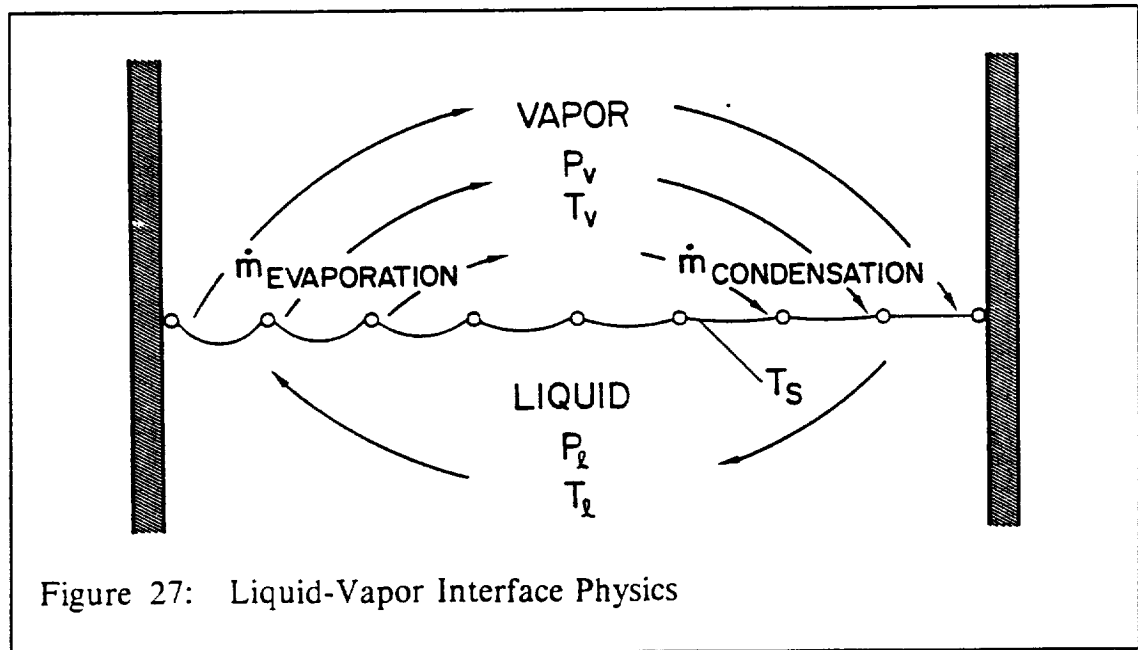


Figure 27: Liquid-Vapor Interface Physics

In general two transition relations are required to define the behavior of transportable quantities at material surfaces[38] . One relation is required to represent continuity of intensity of the appropriate quantity across the surface while the other relation represents continuity of the normal component of the flux vector across the surface.

The principles of continuity of intensity and continuity of normal flux are not generally exact for non-equilibrium processes. Net evaporation and condensation, which occur simultaneously in different regions of a heat pipe, are by definition non-equilibrium process. There is actually no rigorous justification for requiring, for example, matching liquid and vapor temperatures at the interface. Similarly, the requirement for matching velocities (the so-called no-slip condition) at fluid-fluid boundaries such as the liquid- vapor interface in a heat pipe is not as certain as is the no-slip condition at a solid-fluid interface. Errors introduced by non-equilibrium conditions are dependent on the severity of the departure from equilibrium. In many cases, as is assumed for the heat pipe, departures from local equilibrium are small such that non-equilibrium errors can be neglected. The equilibrium condition can further be justified based on the action of diffusive transport processes. Diffusive forces resist non-equilibrium conditions in proportion to the severity of the departure from equilibrium. Any non-equilibrium condition will tend to be forced back to equilibrium such that non-equilibrium errors will be small.

The full set of conditions for free liquid-vapor interfaces is given by Prosperetti[39] . The interfacial region separating liquid and vapor is assumed to be a massless two dimensional surface across which transport quantities

undergo an abrupt change. The actual physical situation involves a transition layer between liquid and vapor across which there is a rapid but continuous change of transport quantities. The jump conditions approximate the change in flow quantities in the limit of an infinitely thin transition layer. Inconsistencies with the jump conditions can be reconciled by assuming certain surface sources for momentum and energy related to surface tension. The full set of interface conditions are reduced below using the assumptions appropriate for this analysis.

#### A.1 KINEMATIC SURFACE CONDITION

The problem involving a surface free to evolve depending on local conditions requires determination of the shape and position of the surface with respect to time. The kinematic boundary condition is used for this purpose. Let the liquid-vapor interface surface be governed with respect to time by the function  $S$  such that the shape of the surface is given by

$$S(x, t) = 0$$

The kinematic boundary condition is then

$$\frac{\partial S}{\partial t} + \vec{U}_v \cdot \nabla S = 0 \quad \text{on} \quad S = 0 \quad (46)$$

where  $\vec{U}_v$  is the velocity of the liquid vapor interface surface. Systems far removed from equilibrium may have violent evaporation or condensation such that the surface velocity is of the same order of magnitude as the flow field

velocities. Conversely, surfaces in systems close to equilibrium such as is assumed for the heat pipe will have negligible velocity. When the interface is stationary or has negligible velocity, the condition reduces to the usual requirement that the normal component of velocity vanish

$$\vec{U}_h \cdot \vec{n} = 0 \quad (47)$$

## A.2 CONSERVATION OF MASS

The general conservation condition is

$$\rho_l(\vec{U}_{0l} - \vec{U}_h) \cdot \vec{n} = \rho_v(\vec{U}_{0v} - \vec{U}_h) \cdot \vec{n} \quad (48)$$

where  $\vec{U}_{0l}$  and  $\vec{U}_{0v}$  are the surface velocities of the liquid and vapor respectively,  $\rho_l$  and  $\rho_v$  are the liquid and vapor densities, and  $\vec{n}$  is the unit normal to the liquid-vapor interface surface.

Neglecting the velocity of the liquid-vapor interface gives

$$\rho_l \vec{U}_{0l} \cdot \vec{n} = \rho_v \vec{U}_{0v} \cdot \vec{n} \quad (49)$$

Further refinement is achieved by assuming that there is no axial slip at the liquid-vapor interface relative to the wick as discussed in Section A.3, and there is no azimuthal flow. Additional simplification is possible by assuming that  $t_x n_r \gg t_r n_x$  such that  $t_x n_r \simeq 1$ . This assumption is equivalent to approximating the liquid-vapor interface as a cylindrical surface such that velocities at the surface are in the radial direction only. Heat pipe regions with a flooded wick such as portions of the condenser where there is little difference

between liquid and vapor pressure would satisfy this approximation closely, while the regions where liquid recedes into the wick would only approximately satisfy this requirement. Conservation of mass reduces to

$$\rho_l V_{0l} = \rho_v V_{0v} \quad (50)$$

where  $V_{0l}$  and  $V_{0v}$  are the liquid and vapor radial velocities at the surface.

### A.3 CONTINUITY OF TANGENTIAL STRESS

The general condition is

$$\vec{n} \times (\vec{U}_{0v} - \vec{U}_{0l}) [\rho_v (\vec{U}_{0v} - \vec{U}_{0l}) \cdot \vec{n}] - \vec{n} \times [(\vec{\tau}_v - \vec{\tau}_l) \cdot \vec{n}] = \vec{n} \times \nabla_s \sigma \quad (51)$$

where  $\vec{\tau}_v$  and  $\vec{\tau}_l$  are the viscous stresses and  $\nabla_s$  is the surface operator.

The right hand side gives the tangential stress contribution of surface tension gradients. The surface tension of a pure substance is generally a function of temperature. Convective force due to surface tension gradients resulting from local temperature gradients is known as Marangoni Convection. Local temperature gradients in the tiny screen pores at the liquid-vapor interface are assumed small such that Marangoni Convection effects can be neglected so that the right hand is zero.

The first term on the left hand side is also identically zero due to the no-slip condition at the wick discussed later,  $\vec{n} \times (\vec{U}_v - \vec{U}_l) = U_{0v} - U_{0l} = 0$ . The remaining terms of Equation 51 give an expression for tangential stress at the interface due to viscous forces

$$\vec{n} \times [(\vec{\tau}_v - \vec{\tau}_l) \cdot \vec{n}] = 0 \quad (52)$$

The total stress vector  $\vec{P}$  has tensor components

$$P_i = P n_i - \sigma_{ik} n_k \quad (53)$$

The tangential stress is formed by the scalar product of  $\vec{P}$  and the unit tangent vector to the liquid-vapor interface surface  $\vec{t}$

$$\vec{t} \cdot \vec{P} = t_i P_i = P t_i n_i - t_i \sigma_{ik} n_k \quad (54)$$

where tensor summation notation is used.

Note that  $t_i n_i = \vec{t} \cdot \vec{n} = 0$  since the unit normal and tangential vectors are orthogonal. Also for  $i = k$  Equation 54 becomes  $t_k P_k = -\sigma_{kk} t_k n_k$ , but  $t_k n_k = \vec{t} \cdot \vec{n} = 0$  so that the  $i = k$  terms vanish in writing out the components of tangential stress

$$\vec{t} \cdot \vec{P} = -t_x \sigma_{xr} n_r - t_x \sigma_{x\phi} n_\phi - t_r \sigma_{rx} n_x - t_r \sigma_{r\phi} n_\phi - t_\phi \sigma_{\phi x} n_x - t_\phi \sigma_{\phi r} n_r \quad (55)$$

The stress elements are given by Landau and Lifschitz as[40]

$$\sigma_{xr} = \sigma_{rx} = \mu \left( \frac{\partial u}{\partial r} + \frac{\partial v}{\partial x} \right)$$

$$\sigma_{x\phi} = \sigma_{\phi x} = \mu \left( \frac{\partial w}{\partial x} + \frac{1}{r} \frac{\partial u}{\partial \phi} \right)$$

$$\sigma_{r\phi} = \sigma_{\phi r} = \mu \left( \frac{1}{r} \frac{\partial v}{\partial \phi} + \frac{\partial w}{\partial r} - \frac{w}{r} \right)$$

Invoking the assumption that there are no azimuthal flows or gradients for the assumed two dimensional flow gives

$$\sigma_{xr} = \mu \left( \frac{\partial u}{\partial r} + \frac{\partial v}{\partial x} \right)$$

$$\sigma_{x\phi} = 0$$

$$\sigma_{r\phi} = 0$$

Tangential viscous stress is now

$$\vec{t} \cdot \vec{P} = -\sigma_{xr}(t_x n_r + t_r n_x) \quad (56)$$

By using the cylindrical surface approximation, tangential viscous stress is given by

$$\vec{t} \cdot \vec{P} = -\mu \left( \frac{\partial u}{\partial r} + \frac{\partial v}{\partial x} \right) \quad (57)$$

The continuity of tangential stress condition finally reduces to

$$\mu_l \left( \frac{\partial u}{\partial r} + \frac{\partial v}{\partial x} \right)_l = \mu_v \left( \frac{\partial u}{\partial r} + \frac{\partial v}{\partial x} \right)_v \quad (58)$$

Equation 58 provides an important relation for coupling liquid and vapor dynamics, particularly for determining liquid flow reversal and entrainment due to vapor shear forces. However, as discussed in Section 4.4, a vapor model was not available for coupling to the liquid model. In order to perform computations, viscous stress in the vapor is neglected. This assumption is strictly valid only for heat pipe operation at relatively high vapor pressure with



vapor speeds that are low such that entrainment concerns can be neglected. Invoking the assumption of no viscous stress in the vapor reduces the tangential stress condition to the simple result

$$\mu_v \left( \frac{\partial u}{\partial r} + \frac{\partial v}{\partial x} \right)_v = 0 \quad (59)$$

Equation 59 does not in general provide a useful boundary condition for solving the liquid phase dynamics. The tangential stress condition is replaced by the no slip condition at the liquid-vapor interface. This approximation is equivalent to assuming that due to the fineness of pore dimensions involved (e.g., 30 - 50  $\mu\text{m}$  pore diameters [9] ), the no slip condition on screen wires is assumed to dominate over the free slip condition between screen wires. The boundary condition is

$$u_0 = 0 \quad (60)$$

#### A.4 CONTINUITY OF NORMAL STRESS

The general form of the normal stress condition is

$$\rho_v \left[ (\vec{U}_{0v} - \vec{U}_{lv}) \cdot \vec{n} \right] \left[ (\vec{U}_{0v} - \vec{U}_{0l}) \cdot \vec{n} \right] + [\vec{n} \cdot \vec{P}]_v - [\vec{n} \cdot \vec{P}]_l = \sigma \nabla \cdot \vec{n} \quad (61)$$

where  $\nabla \cdot \vec{n}$  is the surface divergence, which is related to meniscus radii of curvature  $R_1$  and  $R_2$  by

$$\nabla \cdot \vec{n} = \frac{1}{R_1} + \frac{1}{R_2} \quad (62)$$

The first term on the left hand side in component form neglecting the surface velocity is

$$\rho_v [\vec{U}_{0v} \cdot \vec{n}] [(\vec{U}_{0v} - \vec{U}_{0l}) \cdot \vec{n}] = \rho_v (u_v n_x + v_v n_r + w_v n_\phi) [(u_v - u_l) n_x + (v_v - v_l) n_r + (w_v - w_l) n_\phi] \quad (63)$$

Applying the no-slip condition at the wick and no azimuthal velocity gives

$$\rho_v [\vec{U}_{0v} \cdot \vec{n}] [(\vec{U}_{0v} - \vec{U}_{0l}) \cdot \vec{n}] = \rho_v (u_v n_x + v_v n_r) (v_v - v_l) n_r \quad (64)$$

Assuming that the liquid-vapor interface is approximately cylindrical gives

$$\rho_v [\vec{U}_{0v} \cdot \vec{n}] [(\vec{U}_{0v} - \vec{U}_{0l}) \cdot \vec{n}] = \rho_v V_{0v} (V_{0v} - V_{0l}) \quad (65)$$

The second term on the left hand side of Equation 61 gives the normal stress contribution from the pressure and viscous forces

$$\vec{n} \cdot \vec{P} = n_i P_i = n_i P n_i - n_i \sigma_{ik} n_k = P - n_i \sigma_{ik} n_k \quad (66)$$

As with tangential stress,  $\sigma_{ik} = 0$  for  $i = \phi$  or  $k = \phi$  and  $\sigma_{xr} = \sigma_{rx}$  so the normal stress components are

$$n_i \sigma_{ik} n_k = \sigma_{xx} n_x^2 + \sigma_{rr} n_r^2 + \sigma_{\phi\phi} n_\phi^2 + 2\sigma_{xr} n_x n_r \quad (67)$$

where

$$\sigma_{xx} = 2\mu \frac{\partial u}{\partial x} \quad (68)$$

$$\sigma_{rr} = 2\mu \frac{\partial v}{\partial r} \quad (69)$$

$$\sigma_{\phi\phi} = 2\mu \left( \frac{1}{r} \frac{\partial w}{\partial r} + \frac{v}{r} \right) = 2\mu \frac{v}{r} \quad (70)$$

Using the cylindrical interface approximation ( $n_x = n_\phi \simeq 0$ ) gives

$$\vec{n} \cdot \vec{P} = P - 2\mu \frac{\partial v}{\partial r} \quad (71)$$

The continuity of normal stress is finally

$$P_v - P_l + \rho_v V_{0v}(V_{0v} - V_{0l}) + 2 \left[ \mu_l \frac{\partial v_l}{\partial r} - \mu_v \frac{\partial v_v}{\partial r} \right] = \sigma \left( \frac{1}{R_1} + \frac{1}{R_2} \right) \quad (72)$$

## A.5 ENERGY BOUNDARY CONDITION

The continuity of thermal energy intensity requires matching temperatures at the liquid-vapor interface

$$T_v = T_l$$

The continuity of thermal flux condition is

$$\begin{aligned} & \rho_v [(\vec{U}_{0v} - \vec{U}_h) \cdot \vec{n}] \left\{ h_v - h_l + \frac{1}{2} [(\vec{U}_{0v} - \vec{U}_h)^2 - (\vec{U}_{0l} - \vec{U}_h)^2] \right\} \\ & + [(\vec{U}_{0l} - \vec{U}_h) \cdot \vec{\tau}_l] \cdot \vec{n} - [(\vec{U}_{0v} - \vec{U}_h) \cdot \vec{\tau}_v] \cdot \vec{n} + (\vec{q}_v - \vec{q}_l) \cdot \vec{n} = \\ & T \left[ \frac{D}{Dt} \frac{d\sigma}{dT} + \frac{d\sigma}{dT} (\vec{U}_h \cdot \vec{n}) \nabla \cdot \vec{n} + \nabla_s \cdot (\vec{U}_h \times \vec{n}) \right] \end{aligned} \quad (73)$$

The first term is the energy required for phase change plus the work to adjust densities and pressures during phase change plus the energy to accelerate from liquid velocity to vapor velocity. The second term is viscous dissipation, taken to be negligible at the low velocities in this analysis. The third term is the thermal energy conduction. The right hand side is the temperature times the

increase of entropy per unit area. The right hand side can be simplified as follows. Surface tension is first considered a function of temperature only for a pure substance<sup>3</sup> so that

$$\frac{D}{Dt} \frac{d\sigma}{dT} = \frac{d^2\sigma}{dT^2} \frac{DT}{Dt} \quad (74)$$

But  $d^2\sigma/dT^2$  is zero, and if the surface has negligible velocity, the terms in parenthesis on the right hand side can be taken as zero so that the entire right hand side vanishes. The energy boundary condition reduces to

$$\rho_v(\vec{U}_{0v} \cdot \vec{n}) \left\{ h_v - h_l + \frac{1}{2} [\vec{U}_{0v}^2 - \vec{U}_{0l}^2] \right\} + (\vec{q}_v - \vec{q}_l) \cdot \vec{n} = 0 \quad (75)$$

but

$$\vec{U}_{0v} \cdot \vec{n} = u_v n_x + v_v n_r + w_v n_\phi \simeq V_{0v}$$

$$h_v - h_l = h_{fg}$$

$$\vec{U}_{0v}^2 - \vec{U}_{0l}^2 = u_v^2 + V_{0v}^2 + w_v^2 - u_l^2 - V_{0l}^2 - w_l^2 = V_{0v}^2 - V_{0l}^2$$

$$(\vec{q}_v - \vec{q}_l) \cdot \vec{n} = q_{vi} n_i - q_{li} n_i$$

---

<sup>3</sup> The surface tension as a function of temperature is given in Appendix F as

$$\sigma = 0.23402 - 1 \times 10^{-4} T$$

Assuming heat conduction by vapor is negligible relative to the latent heat of vaporization gives

$$\begin{aligned}
 (\vec{q}_v - \vec{q}_l) \cdot \vec{n} &= -q_l n_i \\
 &= k_l \left[ \frac{\partial T_l}{\partial x} n_x + \frac{\partial T_l}{\partial r} n_r + \frac{\partial T_l}{\partial \phi} n_\phi \right] \\
 &= k_l \frac{\partial T_l}{\partial r}
 \end{aligned} \tag{76}$$

where the assumption is made that radial heat conduction in the liquid is dominant over heat conduction in other directions. The energy boundary condition reduces to

$$C_w \rho_v V_{0v} \left[ h_{fg} + \frac{1}{2} (V_{0v}^2 - V_{0l}^2) \right] = -k_l \frac{\partial T_l}{\partial r} \tag{77}$$

where  $C_w$  has been added to account for the actual liquid-vapor surface area. The kinetic energy contribution at low velocities is negligible relative to latent heat of vaporization so that the energy boundary condition becomes finally

$$C_w \rho_v V_{0v} h_{fg} = -k_l \frac{\partial T_l}{\partial r} \tag{78}$$

or using the continuity equation to substitute for the vapor parameters,

$$C_w \rho_l V_{0l} h_{fg} = -k_l \frac{\partial T_l}{\partial r} \tag{79}$$

## Appendix B

### AXIAL VELOCITY DETERMINATION

#### B.1 BULK AXIAL VELOCITY

The bulk axial velocity  $\bar{U}$  can be found as a function of axial position from a control volume mass balance. Consider as the control volume the cell shown in Figure 28. Assume the radial interface velocity is uniform along the region from  $i - \frac{1}{2}$  to  $i + \frac{1}{2}$  and is equal to known  $V_0(i)$ . Assuming constant liquid density in the cell, the bulk axial velocity across cell boundary  $i + 1$  is

$$\bar{U}(i + 1) = \bar{U}(i) + \frac{1}{2} \frac{A_{lv}}{A_a} [V_0(i) + V_0(i + 1)] \quad (80)$$

where the cell liquid-vapor interface area  $A_{lv}$  and the annulus cross-section area  $A_a$  are given by

$$A_{lv} = 2\pi R_v h_x C_w$$

$$A_a = \pi(R_l^2 - R_v^2)$$

The term  $C_w$  accounts for wick porosity. A solid boundary exists at  $i = 1$  so that  $\bar{U}(1) = 0$  and the bulk axial flow across grid line  $i = 2$  is

$$\bar{U}(2) = \frac{1}{2} \frac{A_{lv}}{A_a} [V_0(1) + V_0(2)] \quad (81)$$

The bulk flow across  $i = 3$  is

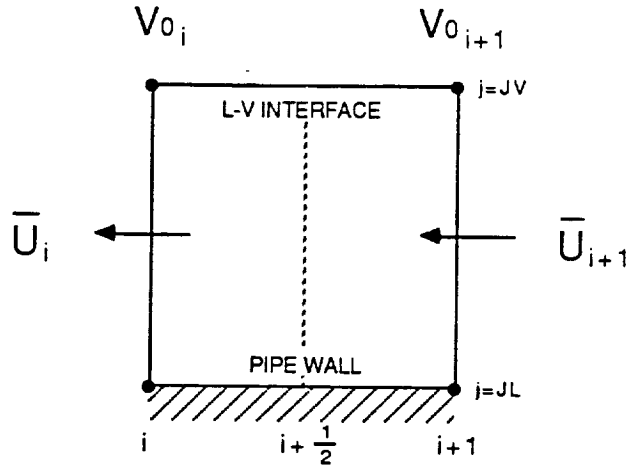


Figure 28: Bulk Axial Velocity Control Volume

$$\bar{U}(3) = \bar{U}(2) + \frac{1}{2} \frac{A_h}{A_a} [V_0(2) + V_0(3)] \quad (82)$$

Substitution of Equation 81 into 82 gives

$$\bar{U}(3) = \frac{1}{2} \frac{A_h}{A_a} [V_0(1) + 2V_0(2) + V_0(3)] \quad (83)$$

The bulk flow across interior grid  $i$  can then be found from the recursion formula

$$\bar{U}(i) = \frac{1}{2} \frac{A_h}{A_a} \left[ V_0(1) + 2 \sum_{n=2}^{i-1} V_0(n) + V_0(i) \right] \quad (84)$$

A solid boundary exists at  $i = N$  so that  $\bar{U}(N) = 0$ .

## B.2 AXIAL VELOCITY DISTRIBUTION

The objective is to define the axial velocity in terms of the bulk axial velocity  $\bar{U}(x)$  and the radial position  $r$ . The velocity profile is assumed to be well approximated by a cubic relation

$$u^* = a + b r^* + c r^{*2} + d r^{*3} \quad (85)$$

where

$$u^* = \frac{u}{\bar{U}}$$

$$r^* = \frac{r - R_v}{\delta}$$

$$\delta = R_l - R_v$$

Apply the no slip condition at the liquid-vapor interface

$$\text{at } r = R_v, r^* = 0,$$

$$u = u^* = 0$$

$$\text{so } a = 0$$

The three unknowns  $b$ ,  $c$ , and  $d$  remain. The no slip condition at the liquid-pipe wall interface is applied

$$\text{at } r = R_l, r^* = 1,$$

$$u = u^* = 0$$

$$\text{so } b + c + d = 0 \quad (86)$$



Equation 86 provides one of the equations required to find the three unknowns. Two additional relations are required. One of the required relations can be derived by taking advantage of the assumption that there is no radial pressure gradient. The axial momentum equation can be solved at the liquid-vapor interface for the pressure gradient. This expression for pressure gradient will explicitly contain the influence of the phase change velocity. This pressure gradient can then be equated to the pressure gradient resulting from integrating the axial momentum equation in the radial direction. The integral formulation will also contain explicit terms for the liquid-vapor interface phase change condition. The resulting expression is the axial momentum compatibility condition. This approach is intended to preserve the influence of the phase change process on the velocity profile. The time dependence of the velocity profile is assumed to be negligible as a first approximation.

The steady, two dimensional momentum equation is

$$u \frac{\partial u}{\partial x} + v \frac{\partial u}{\partial r} = - \frac{1}{\rho} \frac{dP}{dx} + v \left[ \frac{\partial^2 u}{\partial x^2} + \frac{\partial^2 u}{\partial r^2} + \frac{1}{r} \frac{\partial u}{\partial r} \right] \quad (87)$$

Solving at the liquid-vapor interface for pressure gradient gives

$$\frac{1}{\mu} \frac{dP}{dx} = \frac{\partial^2 u}{\partial r^2} \Big|_{R_v} + \left[ \frac{1}{R_v} - \frac{V_0}{v} \right] \frac{\partial u}{\partial r} \Big|_{R_v} \quad (88)$$

Now the axial momentum equation is expressed in integral form corresponding to the heat pipe system of this study. The integration will include the temporal terms for general validity since the integral formulation

is also used for the pressure determination in Appendix D. The temporal terms will then be dropped for the current purpose of determining the axial velocity profile. The conservative form of the axial momentum equation for two dimensional flow is

$$\frac{\partial u}{\partial t} + \frac{\partial u^2}{\partial x} + \frac{\partial uv}{\partial r} + \frac{uv}{r} = -\frac{1}{\rho} \frac{dP}{dx} + v \left[ \frac{\partial^2 u}{\partial x^2} + \frac{\partial^2 u}{\partial r^2} + \frac{1}{r} \frac{\partial u}{\partial r} \right] \quad (89)$$

Integrate between the heat pipe limits  $R_v$  and  $R_l$

$$\begin{aligned} \frac{\partial}{\partial t} \int_{R_v}^{R_l} u r dr + \frac{\partial}{\partial x} \int_{R_v}^{R_l} u^2 r dr + \int_{R_v}^{R_l} \frac{\partial uv}{\partial r} r dr + \int_{R_v}^{R_l} u v dr = \\ -\frac{1}{\rho} \frac{dP}{dx} \int_{R_v}^{R_l} r dr + v \left[ \frac{\partial^2}{\partial x^2} \int_{R_v}^{R_l} u r dr + \int_{R_v}^{R_l} \frac{\partial^2 u}{\partial r^2} r dr + \int_{R_v}^{R_l} \frac{\partial u}{\partial r} dr \right] \end{aligned} \quad (90)$$

Integration by parts and evaluation of integrals produces

$$\begin{aligned} \frac{\partial}{\partial t} \int_{R_v}^{R_l} u r dr + \frac{\partial}{\partial x} \int_{R_v}^{R_l} u^2 r dr = \\ - \left( \frac{R_l^2 - R_v^2}{2\rho} \right) \frac{dP}{dx} + v \left[ \frac{\partial^2}{\partial x^2} \int_{R_v}^{R_l} u r dr + R_l \frac{\partial u}{\partial r} \Big|_{R_l} - R_v \frac{\partial u}{\partial r} \Big|_{R_v} \right] \end{aligned} \quad (91)$$

Assuming now that the temporal terms can be neglected in determining the velocity profile, Equation 91 can be rearranged to give

$$\begin{aligned} \frac{1}{\mu} \frac{dP}{dx} = \\ \left( \frac{2}{R_l^2 - R_v^2} \right) \left\{ \frac{\partial^2}{\partial x^2} \int_{R_v}^{R_l} u r dr + R_l \frac{\partial u}{\partial r} \Big|_{R_l} - R_v \frac{\partial u}{\partial r} \Big|_{R_v} - \frac{1}{v} \frac{\partial}{\partial x} \int_{R_v}^{R_l} u^2 r dr \right\} \end{aligned} \quad (92)$$

Equating expressions 88 and 92 gives after rearranging

$$\begin{aligned} \frac{\partial^2 u}{\partial r^2} \Big|_{R_v} + \left[ \frac{1}{R_v} - \frac{V_0}{v} + \frac{2R_v}{R_l^2 - R_v^2} \right] \frac{\partial u}{\partial r} \Big|_{R_v} = \\ \left( \frac{2}{R_l^2 - R_v^2} \right) \left\{ \frac{\partial^2}{\partial x^2} \int_{R_v}^{R_l} u r dr + R_l \frac{\partial u}{\partial r} \Big|_{R_l} - \frac{1}{v} \frac{\partial}{\partial x} \int_{R_v}^{R_l} u^2 r dr \right\} \end{aligned} \quad (93)$$

Equation 93 is now manipulated by transforming to  $u^*$  and  $r^*$ , substituting  $u^* = b r^* + c r^{*2} + d r^{*3}$ , and rearranging. The result is

$$\begin{aligned} 2c + \left[ \frac{R_l^2 + R_v^2}{R_v(R_l + R_v)} - \frac{\delta V_0}{v} \right] b = \left( \frac{2}{R_l + R_v} \right) \{ R_l(b + 2c + 3d) \\ + \left[ b \left( \frac{1}{3} + \frac{1}{2} \frac{R_v}{\delta} \right) + c \left( \frac{1}{4} + \frac{1}{3} \frac{R_v}{\delta} \right) + d \left( \frac{1}{5} + \frac{1}{4} \frac{R_v}{\delta} \right) \right] \frac{\delta^3}{\bar{U}} \frac{\partial^2 \bar{U}}{\partial x^2} \\ - \left[ b^2 \left( \frac{1}{4} + \frac{1}{3} \frac{R_v}{\delta} \right) + bc \left( \frac{2}{5} + \frac{1}{2} \frac{R_v}{\delta} \right) + bd \left( \frac{1}{3} + \frac{2}{5} \frac{R_v}{\delta} \right) \right. \\ \left. + c^2 \left( \frac{1}{6} + \frac{1}{5} \frac{R_v}{\delta} \right) + cd \left( \frac{2}{7} + \frac{1}{3} \frac{R_v}{\delta} \right) + d^2 \left( \frac{1}{8} + \frac{1}{7} \frac{R_v}{\delta} \right) \right] \frac{2\delta^3}{v} \frac{\partial \bar{U}}{\partial x} \} \end{aligned} \quad (94)$$

After an enormous amount of algebra and using Equation 86, the following is obtained

$$T_{14}b + T_{15}b^2 + T_{16}d + T_{17}d^2 + T_{18}bd = 0 \quad (95)$$

where

$$\begin{aligned} T_{14} &= \left( \frac{R_l^2 - R_v^2}{2} \right) \left[ \frac{1}{R_v} - \frac{V_0}{v} \right] - \left[ \frac{1}{12} + \frac{1}{6} \frac{R_v}{\delta} \right] \frac{\delta^3}{\bar{U}} \frac{\partial^2 \bar{U}}{\partial x^2} \\ T_{15} &= \left[ \frac{1}{60} + \frac{1}{30} \frac{R_v}{\delta} \right] \frac{2\delta^3}{v} \frac{\partial \bar{U}}{\partial x} \end{aligned}$$

$$T_{16} = -2R_l - R_v + \left[ \frac{1}{20} + \frac{1}{12} \frac{R_v}{\delta} \right] \frac{\delta^3}{\bar{U}} \frac{\partial^2 \bar{U}}{\partial x^2}$$

$$T_{17} = \left[ \frac{1}{168} + \frac{1}{105} \frac{R_v}{\delta} \right] \frac{2\delta^3}{v} \frac{\partial \bar{U}}{\partial x}$$

$$T_{18} = - \left[ \frac{2}{105} + \frac{1}{30} \frac{R_v}{\delta} \right] \frac{2\delta^3}{v} \frac{\partial \bar{U}}{\partial x}$$

There are now two equations, 86 and 95, for the three unknowns  $b$ ,  $c$ , and  $d$ .

The third required relation is from the definition of bulk axial flow,

$$\bar{U} = \frac{\int_{R_v}^{R_l} u 2\pi r dr}{\int_{R_v}^{R_l} 2\pi r dr} \quad (96)$$

or

$$\bar{U} = \frac{2}{R_l^2 - R_v^2} \int_{R_v}^{R_l} u r dr \quad (97)$$

Transforming to  $u^*$  and  $r^*$  in Equation 97 gives

$$\frac{R_l^2 - R_v^2}{2\delta} = \delta \int_0^1 u^* r^* dr^* + R_v \int_0^1 u^* dr^* \quad (98)$$

Substitution for  $u^*$  gives

$$\frac{R_l^2 - R_v^2}{2\delta} = \delta \left[ \frac{b}{12} - \frac{d}{20} \right] + R_v \left[ \frac{b}{6} - \frac{d}{12} \right] \quad (99)$$

Rearrangement gives

$$b = 6 + \frac{1}{5} \left[ 3 - \frac{R_v}{R_l + R_v} \right] d \quad (100)$$

Substitution of Equation 100 in Equation 95 and lengthy algebra result in a quadratic equation for  $d$

$$S_1 d^2 + S_2 d + S_3 = 0 \quad (101)$$

where

$$\begin{aligned} S_1 = & \left\{ \frac{1}{25} \left[ 3 - \frac{R_v}{R_l + R_v} \right]^2 \left[ \frac{1}{60} + \frac{1}{30} \frac{R_v}{\delta} \right] + \left[ \frac{1}{168} + \frac{1}{105} \frac{R_v}{\delta} \right] \right. \\ & \left. - \frac{1}{5} \left[ 3 - \frac{R_v}{R_l + R_v} \right] \left[ \frac{2}{105} + \frac{1}{30} \frac{R_v}{\delta} \right] \right\} \left[ \frac{4\delta^2 C_w R_v}{R_l + R_v} \right] \frac{V_0}{v} \\ S_2 = & \frac{1}{5} \left[ 3 - \frac{R_v}{R_l + R_v} \right] \left[ \frac{R_l^2 - R_v^2}{2R_v} \right] - 2(R_l + R_v) \\ & + \left\{ \frac{1}{20} + \frac{1}{12} \frac{R_v}{\delta} - \frac{1}{5} \left[ 3 - \frac{R_v}{R_l + R_v} \right] \left[ \frac{1}{12} + \frac{1}{6} \frac{R_v}{\delta} \right] \right\} \frac{\delta^3}{U} \frac{\partial^2 \bar{U}}{\partial x^2} \\ & - \left\{ \frac{1}{5} \left[ 3 - \frac{R_v}{R_l + R_v} \right] \left[ \frac{R_l^2 - R_v^2}{2} \right] + \left[ \frac{12}{105} + \frac{1}{5} \frac{R_v}{\delta} \right] \right. \\ & \left. - \frac{1}{5} \left( 3 - \frac{R_v}{R_l + R_v} \right) \left( \frac{1}{5} + \frac{2}{5} \frac{R_v}{\delta} \right) \right\} \frac{4\delta^2 C_w R_v}{R_l + R_v} \frac{V_0}{v} \\ S_3 = & \frac{3}{R_v} (R_l^2 - R_v^2) - \left( \frac{1}{2} + \frac{R_v}{\delta} \right) \frac{\delta^3}{U} \frac{\partial^2 \bar{U}}{\partial x^2} \\ & + \left[ \left( 6 + 12 \frac{R_v}{\delta} \right) \frac{2}{5} \frac{\delta^2 C_w R_v}{R_l + R_v} - 3(R_l^2 - R_v^2) \right] \frac{V_0}{v} \end{aligned}$$

Solution of Equation 101 for  $d$  is given by

$$d = \frac{1}{2S_1} \left[ -S_2 \pm \sqrt{S_2^2 - 4S_1S_3} \right] \quad (102)$$

The only remaining issue is selection of the proper  $\pm$  operation in Equation 102. By assuming backflow generally does not occur, the requirement can be imposed that the sign of  $u(x,r)$  and  $\bar{U}(x)$  must be consistent at every axial location  $x$ . Analysis of Equation 102 is not straightforward due to the competing signs of the many terms. Numerical experiments were performed to study the effect of the operation on the profile. The experiments considered using a single operation for the entire pipe, as well as operations dependent on the sign of the phase change velocity. These tests showed that for reasonable velocities, the only operation that produced no backflow was subtraction. Using subtraction in Equation 102 allows the coefficients  $b$ ,  $c$ , and  $d$  to be evaluated from the known geometry parameters and flow conditions  $\bar{U}(x)$  and  $V_0(x)$  using

$$d = \frac{1}{2S_1} \left[ -S_2 - \sqrt{S_2^2 - 4S_1S_3} \right] \quad (103)$$

$$b = 6 + \frac{1}{5} \left[ 3 - \frac{R_v}{R_l + R_v} \right] d \quad (104)$$

$$c = -b - d \quad (105)$$

## Appendix C

### RADIAL VELOCITY DETERMINATION

#### C.1 RADIAL PHASE CHANGE VELOCITY

The objective is to determine the liquid phase change velocity  $V_0$ . A straightforward model of phase change mass flux is given by Schrage as the simple theory of interphase mass transfer of a pure substance [35]

$$\rho_v V_{0v} = \sqrt{\frac{M}{2\pi R_u}} \left[ \frac{P_v}{\sqrt{T_v}} - \frac{P_s}{\sqrt{T_s}} \right] \quad (106)$$

where  $P_s$  and  $T_s$  are values associated with the liquid-vapor interface surface. The sign of velocity as applied to the coordinate system used in this analysis has the convention

$$\begin{aligned} V_0 > 0 & \quad \text{Condensation Occurs} \\ V_0 < 0 & \quad \text{Evaporation Occurs} \end{aligned}$$

Conservation of mass at the interface from Appendix A is given as

$$\rho_v V_{0v} = \rho_l V_{0l}$$

Assume the vapor is saturated at the vapor temperature

$$P_v = P_{sat}|_{T_v}$$

Assume the temperature jump  $\delta T_v$  from the surface to the vapor is small

$$T_s = T_v + \delta T_h$$

$$\delta T_h \ll T_v$$

so that

$$\frac{1}{\sqrt{T_s}} \simeq \frac{1}{\sqrt{T_v}}$$

Equation 106 can now be written as

$$\rho_l V_0 = \sqrt{\frac{M}{2\pi R_u}} \frac{1}{\sqrt{T_v}} [P_{sat}|_{T_v} - P_s] \quad (107)$$

Since the temperature jump  $\delta T_h$  is small, the surface pressure can be approximated as

$$P_s \simeq P_{sat}|_{T_v} - \left. \frac{dP_{sat}}{dT} \right|_{T_v} (T_v - T_s)$$

so that Equation 107 becomes

$$\rho_l V_0 = \sqrt{\frac{M}{2\pi R_u}} \frac{1}{\sqrt{T_v}} \left[ \left. \frac{dP_{sat}}{dT} \right|_{T_v} (T_v - T_s) \right] \quad (108)$$

The slope of a phase curve in a pressure - temperature diagram can be related to the latent heat and to the volume discontinuity by the Clausius-Clapeyron Equation [36]. In terms of molar entropy  $S$  and molar volume  $V$ ,

$$\frac{dP}{dT} = \frac{\Delta S}{\Delta V} \quad (109)$$



Note that  $\Delta S$  and  $\Delta V$  are discontinuities in molar entropy and molar volume associated with phase change. The latent heat of vaporization is defined as

$$h_{fg} \equiv T \Delta S$$

So that Equation 109 can be written as the Clausius-Clapeyron Equation

$$\frac{dP}{dT} = \frac{h_{fg}}{T \Delta V} \quad (110)$$

or

$$\frac{dP}{dT} = \frac{h_{fg}}{T \left( \frac{1}{\rho_v} - \frac{1}{\rho_l} \right)} \quad (111)$$

where the right hand side is evaluated at an appropriate temperature, taken in this case to be the originating temperature. Substituting the Clausius-Clapeyron Equation in Equation 108 produces

$$V_0 = \sqrt{\frac{M}{2\pi R_u}} \left[ \frac{\rho_v h_{fg}}{\rho_l} \right] T_v^{-3/2} (T_v - T_s) \quad (112)$$

or

$$V_0 = h_1 T_v^{-3/2} (T_v - T_s) \quad (113)$$

where the assumption has been used that  $\rho_v \ll \rho_l$ .

## C.2 RADIAL VELOCITY DISTRIBUTION

The objective is to determine the radial velocity as a function of position. The phase change velocity  $V_0(x)$  is assumed to be known from the kinetic formulation of Equation 113. The radial velocity distribution can then be determined by integrating the continuity equation in the radial direction between the limits  $R_v$  and  $r$ ,

$$\int_{R_v}^r \frac{\partial u}{\partial x} 2\pi r' dr' + \int_{R_v}^r \frac{\partial v}{\partial r'} 2\pi r' dr' + \int_{R_v}^r \frac{v}{r'} 2\pi r' dr' = 0 \quad (114)$$

or

$$v(r) = \frac{C_w V_0 R_v}{r} - \frac{1}{r} \frac{\partial}{\partial x} \int_{R_v}^r u r' dr' \quad (115)$$

The screen permeability factor  $C_w$  accounts for the liquid-vapor surface area reduction due to the presence of the screen. Evaluation of Equation 115 at  $r = R_v$  produces the discontinuous result  $\dot{v}(R_v) = C_w V_0$ , so that Equation 115 is not strictly valid at  $r = R_v$ .

Evaluation at  $r = R_l$ , where  $v(R_l) = 0$  due to the impermeable wall boundary condition, produces

$$V_0 = \frac{1}{C_w R_v} \frac{\partial}{\partial x} \int_{R_v}^{R_l} u r' dr' \quad (116)$$

A useful relation can be derived by using the expression for bulk axial velocity developed in Appendix B

$$\bar{U} = \frac{2}{R_l^2 - R_v^2} \int_{R_v}^{R_l} u r' dr'$$

Using  $\bar{U}$  in Equation 116 gives

$$V_0 = \left[ \frac{R_l^2 - R_v^2}{2C_w R_v} \right] \frac{\partial \bar{U}}{\partial x} \quad (117)$$

Returning to Equation 115 and transforming the integral to  $u^*$  and  $r^*$  produces

$$v(r) = \frac{C_w V_0 R_v}{r} - \frac{\delta}{r} \frac{\partial \bar{U}}{\partial x} \left\{ \delta \int_0^{r^*} u^* r^{*'} dr^{*'} + R_v \int_0^{r^*} u^* dr^{*'} \right\} \quad (118)$$

Substituting  $u^* = br^* + cr^{*2} + dr^{*3}$  allows evaluation of the integrals

$$\int_0^{r^*} u^* r^{*'} dr^{*'} = b \frac{r^{*3}}{3} + c \frac{r^{*4}}{4} + d \frac{r^{*5}}{5}$$

$$\int_0^{r^*} u^* dr^{*'} = b \frac{r^{*2}}{2} + c \frac{r^{*3}}{3} + d \frac{r^{*4}}{4}$$

Substitution for the integrals and using Equation 117 for the derivative of bulk axial velocity gives the final result

$$v(x, r) = \frac{C_w V_0 R_v}{r} \left\{ 1 - \frac{2\delta}{R_l + R_v} \left[ b \frac{R_v}{\delta} \frac{r^{*2}}{2} + \left( b + c \frac{R_v}{\delta} \right) \frac{r^{*3}}{3} + \left( c + d \frac{R_v}{\delta} \right) \frac{r^{*4}}{4} + d \frac{r^{*5}}{5} \right] \right\} \quad (119)$$

The parameters  $b$ ,  $c$ , and  $d$  are known from the axial velocity solution of Appendix B so that Equation 119 can be readily solved.

## Appendix D

### PRESSURE DETERMINATION

The objective is to determine the axial pressure distribution in the liquid. The pressure distribution is required to verify that the axial pressure drop does not exceed the maximum capillary pumping capability of the heat pipe.

The axial momentum integral equation developed in Appendix B is

$$\begin{aligned} \frac{\partial}{\partial t} \int_{R_v}^{R_l} u r dr + \frac{\partial}{\partial x} \int_{R_v}^{R_l} u^2 r dr = \\ - \left( \frac{R_l^2 - R_v^2}{2\rho} \right) \frac{dP}{dx} + v \left[ R_l \frac{\partial u}{\partial r} \Big|_{R_l} - R_v \frac{\partial u}{\partial r} \Big|_{R_v} + C_w R_v \frac{\partial V_0}{\partial x} \right] \end{aligned} \quad (120)$$

where the substitution has been made using the result derived in Appendix C

$$C_w R_v V_0 = \frac{\partial}{\partial x} \int_{R_v}^{R_l} u r dr$$

Substitute the bulk axial velocity

$$\bar{U} = \frac{2}{R_l^2 - R_v^2} \int_{R_v}^{R_l} u r dr$$

and rearrange to give

$$\begin{aligned} \rho \frac{\partial \bar{U}}{\partial t} = & -\frac{dP}{dx} - \left( \frac{2\rho}{R_l^2 - R_v^2} \right) \frac{\partial}{\partial x} \int_{R_v}^{R_l} u^2 r dr + \\ & \left( \frac{2\mu}{R_l^2 - R_v^2} \right) \left[ R_l \frac{\partial u}{\partial r} \Big|_{R_l} - R_v \frac{\partial u}{\partial r} \Big|_{R_v} + C_w R_v \frac{\partial V_0}{\partial x} \right] \end{aligned} \quad (121)$$

Transforming to  $u^*$  and  $r^*$ , substitution of  $u^* = br^* + cr^{*2} + dr^{*3}$ , and rearranging gives

$$\rho \frac{\partial \bar{U}}{\partial t} = -\frac{dP}{dx} + \mu \frac{\partial^2 \bar{U}}{\partial x^2} + \gamma \bar{U} \quad (122)$$

where

$$\begin{aligned} \gamma = & \left( \frac{2\mu}{R_l^2 - R_v^2} \right) \left[ b + 2c \frac{R_l}{\delta} + 3d \frac{R_l}{\delta} \right] - \left( \frac{8R_v}{(R_l + R_v)^2} \right) \rho C_w V_0 \\ & \left\{ \frac{1}{12} \left( 3 + 4 \frac{R_v}{\delta} \right) b^2 + \frac{1}{10} \left( 4 + 5 \frac{R_v}{\delta} \right) bc + \frac{1}{15} \left( 5 + 6 \frac{R_v}{\delta} \right) bd \right. \\ & \left. + \frac{1}{30} \left( 5 + 6 \frac{R_v}{\delta} \right) c^2 + \frac{1}{21} \left( 6 + 7 \frac{R_v}{\delta} \right) cd + \frac{1}{56} \left( 7 + 8 \frac{R_v}{\delta} \right) d^2 \right\} \end{aligned}$$

Use the trapezoidal rule to integrate Equation 122

$$\begin{aligned} \rho [\bar{U}^{(n+1)} - \bar{U}^{(n)}] = & \frac{k}{2} \left\{ \left[ -\frac{dP}{dx} + \mu \frac{\partial^2 \bar{U}}{\partial x^2} + \gamma \bar{U} \right]^{(n+1)} + \left[ -\frac{dP}{dx} + \mu \frac{\partial^2 \bar{U}}{\partial x^2} + \gamma \bar{U} \right]^{(n)} \right\} \end{aligned} \quad (123)$$

Assume  $\bar{U}^{(n+1)}$  is known from continuity. Center difference the spatial operator on  $\bar{U}$ ,

$$\frac{\partial^2 \bar{U}}{\partial x^2} = \frac{\bar{U}_{i-1} - 2\bar{U}_i + \bar{U}_{i+1}}{h_x^2}$$

and rearrange to give

$$\begin{aligned} \frac{dP^{(n+1)}}{dx} = & \left[ \frac{\mu}{h_x^2} \bar{U}_{i-1} + \left( \gamma - \frac{2\rho}{k} - \frac{2\mu}{h_x^2} \right) \bar{U}_i + \frac{\mu}{h_x^2} \bar{U}_{i+1} \right]^{(n+1)} + \\ & \left[ \frac{\mu}{h_x^2} \bar{U}_{i-1} + \left( \gamma + \frac{2\rho}{k} - \frac{2\mu}{h_x^2} \right) \bar{U}_i + \frac{\mu}{h_x^2} \bar{U}_{i+1} - \frac{dP}{dx} \right]^{(n)} \end{aligned} \quad (124)$$

Difference the spatial operator on pressure,

$$\frac{dP}{dx} = \frac{P_{i+1} - P_i}{h_x}$$

to give

$$\begin{aligned} [P_{i+1} - P_i]^{(n+1)} = & - [P_{i+1} - P_i]^{(n)} + \\ & \left[ \frac{\mu}{h_x} \bar{U}_{i-1} + \left( \gamma h_x - \frac{2\rho h_x}{k} - \frac{2\mu}{h_x} \right) \bar{U}_i + \frac{\mu}{h_x} \bar{U}_{i+1} \right]^{(n+1)} + \\ & \left[ \frac{\mu}{h_x} \bar{U}_{i-1} + \left( \gamma h_x + \frac{2\rho h_x}{k} - \frac{2\mu}{h_x} \right) \bar{U}_i + \frac{\mu}{h_x} \bar{U}_{i+1} \right]^{(n)} \end{aligned} \quad (125)$$

All terms on the right hand side of Equation 125 are known so that the solution can proceed by specifying pressure at one location in the heat pipe. In general there is a location where the liquid and vapor have equal pressures. This point of matching pressure depends on the operating conditions. At moderate heat fluxes and high vapor pressure this point is at the end of the condenser. In this case, the maximum liquid pressure also occurs at this point. As the axial heat flux, and the vapor speed, increase, the point of matching pressure moves toward the beginning of the condenser. Prediction of the point

of matching pressure requires detailed information of the vapor flow dynamics, which is beyond the scope of this study. The point of matching pressure will be assumed to occur at the end of the condenser. With liquid pressure known at  $x = L$ ,  $i = N$ , Equation 125 can be evaluated as

$$\begin{aligned}
 P_i^{(n+1)} = & P_{i+1}^{(n+1)} + P_{i+1}^{(n)} - P_i^{(n)} \\
 & - \left[ \frac{\mu}{h_x} \bar{U}_{i-1} + \left( \gamma h_x - \frac{2\rho h_x}{k} - \frac{2\mu}{h_x} \right) \bar{U}_i + \frac{\mu}{h_x} \bar{U}_{i+1} \right]^{(n+1)} \\
 & - \left[ \frac{\mu}{h_x} \bar{U}_{i-1} + \left( \gamma h_x + \frac{2\rho h_x}{k} - \frac{2\mu}{h_x} \right) \bar{U}_i + \frac{\mu}{h_x} \bar{U}_{i+1} \right]^{(n)}
 \end{aligned} \tag{126}$$

## Appendix E

### ENERGY EQUATION NUMERICAL SOLUTION

#### E.1 GENERAL NUMERICAL FORMULATION

The two dimensional energy equation in cylindrical coordinates neglecting viscous dissipation is

$$\frac{\partial T}{\partial t} + u \frac{\partial T}{\partial x} + v \frac{\partial T}{\partial r} = \alpha \left[ \frac{\partial^2 T}{\partial x^2} + \frac{\partial^2 T}{\partial r^2} + \frac{1}{r} \frac{\partial T}{\partial r} \right] \quad (127)$$

The energy equation is to be solved subject to the boundary conditions

AXIAL RANGE	RADIAL RANGE	CONDITION
$x = 0$	$R_v \leq r \leq R_w$	$-k \frac{\partial T}{\partial x} = 0$
$x = 1$	$R_v \leq r \leq R_w$	$-k \frac{\partial T}{\partial x} = 0$
$0 \leq x \leq L$	$r = R_v$	$-k_l \frac{\partial T}{\partial r} = q_0$
$0 \leq x \leq L_e$	$r = R_w$	$-k_w \frac{\partial T}{\partial r} = q_{in}$
$L_e < x < L_e + L_a$	$r = R_w$	$-k_w \frac{\partial T}{\partial r} = 0$
$L_e + L_a \leq x \leq L$	$r = R_w$	$-k_w \frac{\partial T}{\partial r} = \varepsilon \sigma (T_w^4 - T_e^4)$



where subscripts  $w$ ,  $l$ , and  $v$  refer to the wall, liquid, and vapor respectively,  $q_{in}$  is the specified input heat flux,  $T_e$  is the radiation environment rejection temperature, and  $q_0$  is the liquid-vapor phase change heat flux given by Equation 30.

Solution of the energy equation is accomplished by the finite difference Peaceman-Rachford Alternating Direction Implicit (ADI) method. The energy equation is rearranged as

$$\frac{\partial T}{\partial t} = \alpha \frac{\partial^2 T}{\partial r^2} + \alpha \frac{\partial^2 T}{\partial x^2} + \left( \frac{\alpha}{r} - v \right) \frac{\partial T}{\partial r} - u \frac{\partial T}{\partial x} \quad (128)$$

Trapezoidal time integration is applied to Equation 128 to give in operator form

$$T^{(n+1)} - T^{(n)} = \frac{k}{2} \left\{ \left[ \alpha D_{0,r}^2 + \alpha D_{0,x}^2 + \left( \frac{\alpha}{r} - v \right) D_{0,r} - u D_{0,x} \right] T \right\}^{(n+1)} + \frac{k}{2} \left\{ \left[ \alpha D_{0,r}^2 + \alpha D_{0,x}^2 + \left( \frac{\alpha}{r} - v \right) D_{0,r} - u D_{0,x} \right] T \right\}^{(n)} \quad (129)$$

Like time levels are combined to give the Crank-Nicolson formulation

$$\left\{ I - \frac{k}{2} \left[ \alpha D_{0,r}^2 + \alpha D_{0,x}^2 + \left( \frac{\alpha}{r} - v \right) D_{0,r} - u D_{0,x} \right] \right\} T^{(n+1)} = \left\{ I + \frac{k}{2} \left[ \alpha D_{0,r}^2 + \alpha D_{0,x}^2 + \left( \frac{\alpha}{r} - v \right) D_{0,r} - u D_{0,x} \right] \right\} T^{(n)} \quad (130)$$

The Crank-Nicolson formulation is second order accurate in space and time.

The left hand side of Equation 130 can be factored in the form

$$\begin{aligned} & \left[ I - \frac{k}{2} \left( \alpha D_{0,r}^2 + \left( \frac{\alpha}{r} - v \right) D_{0,r} \right) \right] \left[ I - \frac{k}{2} \left( \alpha D_{0,x}^2 - u D_{0,x} \right) \right] = \\ & I - \frac{k}{2} \left[ \alpha D_{0,r}^2 + \alpha D_{0,x}^2 + \left( \frac{\alpha}{r} - v \right) D_{0,r} - u D_{0,x} \right] + \\ & \frac{k^2}{4} \left( \alpha D_{0,r}^2 + \left( \frac{\alpha}{r} - v \right) D_{0,r} \right) \left( \alpha D_{0,x}^2 - u D_{0,x} \right) \end{aligned}$$

Similarly the right hand side can be factored as

$$\begin{aligned} & \left[ I + \frac{k}{2} \left( \alpha D_{0,r}^2 + \left( \frac{\alpha}{r} - v \right) D_{0,r} \right) \right] \left[ I + \frac{k}{2} \left( \alpha D_{0,x}^2 - u D_{0,x} \right) \right] = \\ & I + \frac{k}{2} \left[ \alpha D_{0,r}^2 + \alpha D_{0,x}^2 + \left( \frac{\alpha}{r} - v \right) D_{0,r} - u D_{0,x} \right] + \\ & \frac{k^2}{4} \left( \alpha D_{0,r}^2 + \left( \frac{\alpha}{r} - v \right) D_{0,r} \right) \left( \alpha D_{0,x}^2 - u D_{0,x} \right) \end{aligned}$$

Substitution of the factored expressions in Equation 130 gives

$$\begin{aligned} & \left[ I - \frac{k}{2} \left( \alpha D_{0,r}^2 + \left( \frac{\alpha}{r} - v \right) D_{0,r} \right) \right] \left[ I - \frac{k}{2} \left( \alpha D_{0,x}^2 - u D_{0,x} \right) \right] T^{(n+1)} = \\ & \left[ I + \frac{k}{2} \left( \alpha D_{0,r}^2 + \left( \frac{\alpha}{r} - v \right) D_{0,r} \right) \right] \left[ I + \frac{k}{2} \left( \alpha D_{0,x}^2 - u D_{0,x} \right) \right] T^{(n)} + \\ & \frac{k^2}{4} \left\{ \left[ \left( \alpha D_{0,r}^2 + \left( \frac{\alpha}{r} - v \right) D_{0,r} \right) \left( \alpha D_{0,x}^2 - u D_{0,x} \right) \right] T^{n+1} - \right. \\ & \left. \left[ \left( \alpha D_{0,r}^2 + \left( \frac{\alpha}{r} - v \right) D_{0,r} \right) \left( \alpha D_{0,x}^2 - u D_{0,x} \right) \right] T^n \right\} \end{aligned} \quad (131)$$

Equation 131 is consistent with the original Crank-Nicolson form to the last term on the right hand side. This term is the error of the factorization step. The factored equation can be shown in general to preserve the second order accuracy of the original Crank-Nicolson formulation. The Peaceman-Rachford time split of factored Equation 131 results in two coupled equations

$$\left[ I - \frac{k}{2} \left( \alpha D_{0,r}^2 + \left( \frac{\alpha}{r} - v \right) D_{0,r} \right) \right] T^* = \left[ I + \frac{k}{2} \left( \alpha D_{0,x}^2 - u D_{0,x} \right) \right] T^{(n)} \quad (132)$$

$$\left[ I - \frac{k}{2} \left( \alpha D_{0,x}^2 - u D_{0,x} \right) \right] T^{(n+1)} = \left[ I + \frac{k}{2} \left( \alpha D_{0,r}^2 + \left( \frac{\alpha}{r} - v \right) D_{0,r} \right) \right] T^* \quad (133)$$

where  $t^*$  values are evaluated at an intermediate time  $t^n < t^* < t^{n+1}$ . In this case the intermediate time is taken as  $t^* = t^{n+1/2}$ .

Second order accurate centered differencing is used for the spatial operators,

$$D_{0,r}^2 = \frac{T_{i,j-1} - 2T_{i,j} + T_{i,j+1}}{h_r^2} + O(h_r^2)$$

$$D_{0,x}^2 = \frac{T_{i-1,j} - 2T_{i,j} + T_{i+1,j}}{h_x^2} + O(h_x^2)$$

$$D_{0,r} = \frac{T_{i,j+1} - T_{i,j-1}}{2h_r} + O(h_r^2)$$

$$D_{0,x} = \frac{T_{i+1,j} - T_{i-1,j}}{2h_x} + O(h_x^2)$$

Substitution of the spatial operators, rearranging, and defining

$$\theta_r = \frac{2h_r^2}{k}$$

$$\theta_x = \frac{2h_x^2}{k}$$

produces the final result

$$A_1 T_{ij-1}^* + A_2 T_{ij}^* + A_3 T_{ij+1}^* = B_1 T_{i-1,j}^{(n)} + B_2 T_{ij}^{(n)} + B_3 T_{i+1,j}^{(n)} \quad (134)$$

$$A_4 T_{i-1,j}^{(n+1)} + A_5 T_{ij}^{(n+1)} + A_6 T_{i+1,j}^{(n+1)} = B_4 T_{ij-1}^* + B_5 T_{ij}^* + B_6 T_{ij+1}^* \quad (135)$$

where

$$A_1 = -\alpha + \left(\frac{\alpha}{r} - v\right) \frac{h_r}{2}$$

$$A_2 = \theta_r + 2\alpha$$

$$A_3 = -\alpha - \left(\frac{\alpha}{r} - v\right) \frac{h_r}{2}$$

$$B_1 = \left[ \alpha + u \frac{h_x}{2} \right] \frac{\theta_r}{\theta_x}$$

$$B_2 = \theta_r - 2\alpha \frac{\theta_r}{\theta_x}$$

$$B_3 = \left[ \alpha - u \frac{h_x}{2} \right] \frac{\theta_r}{\theta_x}$$

$$A_4 = -\alpha - u \frac{h_x}{2}$$

$$A_5 = \theta_x + 2\alpha$$

$$A_6 = -\alpha + u \frac{h_x}{2}$$

$$B_4 = \left[ \alpha - \left(\frac{\alpha}{r} - v\right) \frac{h_r}{2} \right] \frac{\theta_x}{\theta_r}$$

$$B_5 = \theta_x - 2\alpha \frac{\theta_x}{\theta_r}$$

$$B_6 = \left[ \alpha + \left( \frac{\alpha}{r} - v \right) \frac{h_r}{2} \right] \frac{\theta_x}{\theta_r}$$

Equations 134 and 135 are sparse, tridiagonal matrices suitable for efficient solution by upper-lower decomposition and Gaussian elimination. The procedure is implemented by operating on the entire mesh with Equation 134 to produce time  $t^*$  temperatures. Equation 135 then sweeps the mesh of time  $t^*$  values to produce time  $t^{(n+1)}$  values. The only remaining issue is implementation of boundary conditions.

## E.2 IMPLEMENTATION OF BOUNDARY CONDITIONS

### E.2.1 *Evaporator Endcap Boundary Condition*

$$x = 0 \quad R_v \leq r \leq R_w$$

The boundary condition is

$$\frac{\partial T}{\partial x} = 0$$

Since the solution derivative but not the solution is prescribed on the boundary, difference Equation 127 holds on the boundary. The boundary image point method is used.

Center difference the boundary condition at the boundary  $i = 1$

$$\frac{\partial T}{\partial x} \simeq \frac{T_{2j} - T_{0j}}{2h_x} = 0$$

Solving for the image point  $T_{0j}$  gives

$$T_{0j} = T_{2j}$$

Apply Equation 134 to the boundary

$$A_1 T_{1j-1}^* + A_2 T_{1j}^* + A_3 T_{1j+1}^* = B_1 T_{0j}^{(n)} + B_2 T_{1j}^{(n)} + B_3 T_{2j}^{(n)}$$

Substitute for the image point to give the first time split equation,

$$A_1 T_{1j-1}^* + A_2 T_{1j}^* + A_3 T_{1j+1}^* = B_2 T_{1j}^{(n)} + (B_1 + B_3) T_{2j}^{(n)} \quad (136)$$

In a similar manner, the boundary form of Equation 135 is

$$A_5 T_{1j}^{(n+1)} + (A_4 + A_6) T_{2j}^{(n+1)} = B_4 T_{1j-1}^* + B_5 T_{1j}^* + B_6 T_{1j+1}^* \quad (137)$$

### **E.2.2 Condenser Endcap Boundary Condition**

$$x = L \quad R_v \leq r \leq R_w$$

The boundary condition is

$$\frac{\partial T}{\partial x} = 0$$

Center difference the boundary condition at the boundary  $i = N$

$$\frac{\partial T}{\partial x} \simeq \frac{T_{N+1j} - T_{N-1j}}{2h_x} = 0$$

The image point is  $T_{N+1,j}$ , so that

$$T_{N+1,j} = T_{N-1,j}$$

Following the same procedure as for the evaporator end cap boundary produces the two time split equations for the condenser endcap

$$A_1 T_{N,j-1}^* + A_2 T_{N,j}^* + A_3 T_{N,j+1}^* = (B_1 + B_3) T_{N-1,j}^{(n)} + B_2 T_{N,j}^{(n)}$$

$$(A_4 + A_6) T_{N-1,j}^{(n+1)} + A_5 T_{N,j}^{(n+1)} = B_4 T_{N,j-1}^* + B_5 T_{N,j}^* + B_6 T_{N,j+1}^*$$

### E.2.3 *Liquid-Vapor Interface Boundary Condition*

$$0 \leq x \leq L \quad r = R_v$$

The boundary condition is

$$-k_l \frac{\partial T_l}{\partial r} = q_0$$

where  $q_0$  is given in Appendix A as

$$q_0 = \rho_l h_{fg} C_w V_0$$

The phase change velocity  $V_0$  is determined in Appendix C from kinetic theory as

$$V_0 = \sqrt{\frac{M}{2\pi R_u}} \left[ \frac{\rho_v h_{fg}}{\rho_l} \right] T_v^{-3/2} (T_v - T_s)$$

so that

$$q_0 = C_w \sqrt{\frac{M}{2\pi R_u}} \left[ \rho_v h_{fg}^2 \right] T_v^{-3/2} (T_v - T_s)$$

or

$$q_0 = h_q T_v^{-3/2} (T_v - T_s)$$

The boundary condition becomes

$$-k_l \frac{\partial T}{\partial r} = h_q T_v^{-3/2} (T_v - T_s)$$

Center differencing at the boundary  $j = JV$  and solving for the image point  $T_{i,JV-1}$  gives

$$T_{i,JV-1} = T_{i,JV+1} + \frac{2h_r h_q}{k_l} T_v^{-3/2} (T_v - T_{i,JV})$$

Application of Equation 134 to the boundary  $j = JV$  and substituting for the image point gives

$$\begin{aligned} \left[ A_2 - A_1 \frac{2h_r h_q}{k_l} T_v^{*-3/2} \right] T_{i,JV}^* + (A_1 + A_3) T_{i,JV+1}^* = \\ B_1 T_{i-1,JV}^{(n)} + B_2 T_{i,JV}^{(n)} + B_3 T_{i+1,JV}^{(n)} - A_1 \frac{2h_r h_q}{k_l} T_v^{*-1/2} \end{aligned} \quad (138)$$

Note that in Equation 138,  $T_v^*$  is the vapor temperature at the intermediate time  $t^*$ . This temperature is unknown a priori so that iterations are required between the energy equation solution, the flow dynamic equations, and the vapor determination. Since the unknown vapor temperature terms in



Equation 138 are nonlinear, special treatment is required. Quasilinearization is used to reduce Equation 138 to a relation with only linear unknown terms.

The first nonlinear term is quasilinearized by

$$(T_v^{*m+1})^{-3/2} \simeq (T_v^{*m})^{-3/2} + d(T_v^{*m})^{-3/2}[T_v^{*m+1} - T_v^{*m}]$$

or

$$(T_v^{*m+1})^{-3/2} \simeq \frac{5}{2}(T_v^{*m})^{-3/2} - \frac{3}{2}(T_v^{*m})^{-5/2}T_v^{*m+1}$$

where  $m$  is the iteration counter index. The above is now a linear expression in terms of  $T_v^{*m+1}$ . Similarly, the second nonlinear term becomes

$$(T_v^{*m+1})^{-1/2} \simeq \frac{3}{2}(T_v^{*m})^{-1/2} - \frac{1}{2}(T_v^{*m})^{-3/2}T_v^{*m+1}$$

Substitution for the nonlinear terms in Equation 138 gives the final result for the first time split

$$\left\{ A_2 - A_1 \frac{2h_r h_q}{k_l} \left[ \frac{5}{2}(T_v^{*m})^{-3/2} - \frac{3}{2}(T_v^{*m})^{-5/2}T_v^{*m+1} \right] \right\} T_{i,JV}^* + (A_1 + A_3)T_{i,JV+1}^* = B_1 T_{i-1,JV}^{(n)} + B_2 T_{i,JV}^{(n)} + B_3 T_{i+1,JV}^{(n)} - A_1 \frac{2h_r h_q}{k_l} \left[ \frac{3}{2}(T_v^{*m})^{-1/2} - \frac{1}{2}(T_v^{*m})^{-3/2}T_v^{*m+1} \right]$$

The second time split equation is found by applying Equation 135 to the boundary  $j = JV$  and substituting for the image point  $T_{i,JV-1}$

$$A_4 T_{i-1,JV}^{(n+1)} + A_5 T_{i,JV}^{(n+1)} + A_6 T_{i+1,JV}^{(n+1)} = \left[ B_5 - B_4 \frac{2h_r h_q}{k_l} T_v^{*-3/2} \right] T_{i,JV}^* + (B_4 + B_6) T_{i,JV+1}^* + B_4 \frac{2h_r h_q}{k_l} T_v^{*-1/2}$$

Nonlinear terms in this second time split equation are for time  $t^*$  values, which are known at time  $t^{(n+1)}$  for the second split. Special treatment is not required for these terms.

#### E.2.4 Pipe External Wall Boundary Conditions

$$0 \leq x \leq L \quad r = R_w$$

The boundary condition is

$$-k_w \frac{\partial T}{\partial r} = q_{in} + q_{rad}$$

where the input heat flux  $q_{in}$  and the radiation heat flux  $q_{rad}$  are functions of axial position

Evaporator	$0 \leq x \leq L_e$	$q_{in} \rightarrow \text{specified}$	$q_{rad} = 0$
Adiabat	$L_e < x < L_e + L_a$	$q_{in} = 0$	$q_{rad} = 0$
Condenser	$L_e + L_a \leq x \leq L$	$q_{in} = 0$	$q_{rad} = \varepsilon \sigma (T_w^4 - T_e^4)$

Center differencing the boundary condition and solving for the image point  $T_{i,JW+1}$  gives

$$T_{i,JW+1} = T_{i,JW-1} - \frac{2h_r}{k_w} \left[ q_{in} + \varepsilon \sigma (T_w^4 - T_e^4) \right]$$

where the product  $\varepsilon\sigma$  is taken as zero except for the condenser region. Application of Equation 134 to  $j = JW$  and substituting for the image point gives for the first time split

$$(A_1 + A_3)T_{i,JW-1}^* + \left[ A_2 - A_3 \frac{2h_r \varepsilon \sigma}{k_w} T_{i,JW}^{*3} \right] T_{i,JW}^* = \\ B_1 T_{i-1,JW}^{(n)} + B_2 T_{i,JW}^{(n)} + B_3 T_{i+1,JW}^{(n)} + A_3 \frac{2h_r}{k_w} [q_{in}^* - \varepsilon\sigma T_e^{*4}]$$

The first time split contains the unknown nonlinear term in wall temperature  $T_{i,JW}$  ( the environmental radiation rejection temperature  $T_e$  is assumed known and specified ). Quasilinearization is required

$$(T^{*m+1})^4 \simeq 4(T^{*m})^3 T^{*m+1} - 3(T^{*m})^4$$

Substitution in the first time split and rearrangement gives

$$(A_1 + A_3)T_{i,JW-1}^* + \left[ A_2 - A_3 \frac{8h_r \varepsilon \sigma}{k_w} (T_{i,JW}^{*m})^3 \right] T_{i,JW}^{*m+1} = \\ B_1 T_{i-1,JW}^{(n)} + B_2 T_{i,JW}^{(n)} + B_3 T_{i+1,JW}^{(n)} + A_3 \frac{2h_r}{k_w} \left\{ q_{in}^* - \varepsilon\sigma \left[ 3(T_{i,JW}^{*m})^4 + T_e^{*4} \right] \right\}$$

Application of the second time split equation to the boundary  $j = JW$  and substitution for the image point gives

$$A_4 T_{i-1,JW}^{(n+1)} + A_5 T_{i,JW}^{(n+1)} + A_6 T_{i+1,JW}^{(n+1)} = \\ (B_4 + B_6)T_{i,JW-1}^* + B_5 T_{i,JW}^* - B_6 \frac{2h_r}{k_w} \left\{ q_{in}^* + \varepsilon\sigma \left[ T_{i,JW}^{*4} - T_e^{*4} \right] \right\}$$

The nonlinear terms in the second time split are known since they are from time level  $t^*$  . Special treatment is not required.

### E.2.5 Corner Boundary Conditions

Corner boundary conditions are evaluated by substituting for the image points across the boundary in each of the two boundary directions at the corner. The results are given below.

#### EVAPORATOR END/EXTERNAL WALL CORNER

The first time split equation is

$$(A_1 + A_3)T_{1,JW-1}^* + \left[ A_2 - A_3 \frac{8h_r \varepsilon \sigma}{k_w} (T_{1,JW}^{*m})^3 \right] T_{1,JW}^{*m+1} =$$

$$B_2 T_{1,JW}^{(n)} + (B_1 + B_3)T_{2,JW}^{(n)} + A_3 \frac{2h_r}{k_w} \left\{ q_{in}^* - \varepsilon \sigma \left[ 3(T_{1,JW}^{*m})^4 + T_e^{*4} \right] \right\}$$

The second time split equation is

$$A_5 T_{1,JW}^{(n+1)} + (A_4 + A_6)T_{2,JW}^{(n+1)} =$$

$$(B_4 + B_6)T_{1,JW-1}^* + B_5 T_{1,JW}^* - B_6 \frac{2h_r}{k_w} \left\{ q_{in}^* + \varepsilon \sigma \left[ T_{1,JW}^{*4} - T_e^{*4} \right] \right\}$$

#### CONDENSER END/EXTERNAL WALL CORNER

The first time split equation is

$$(A_1 + A_3)T_{N,JW-1}^* + \left[ A_2 - A_3 \frac{8h_r \varepsilon \sigma}{k_w} (T_{N,JW}^{*m})^3 \right] T_{N,JW}^{*m+1} =$$

$$(B_1 + B_3)T_{N-1,JW}^{(n)} + B_2 T_{N,JW}^{(n)} + A_3 \frac{2h_r}{k_w} \left\{ q_{in}^* - \varepsilon \sigma \left[ 3(T_{N,JW}^{*m})^4 + T_e^{*4} \right] \right\}$$

The second time split equation is

$$(A_4 + A_6)T_{N-1,JW}^{(n+1)} + A_5T_{N,JW}^{(n+1)} = (B_4 + B_6)T_{N,JW-1}^* + B_5T_{N,JW}^* - B_6\frac{2h_r}{k_w}\left\{q_{in}^* + \varepsilon\sigma\left[T_{N,JW}^{*4} - T_e^{*4}\right]\right\}$$

#### EVAPORATOR END/LIQUID-VAPOR INTERFACE CORNER

The first time split equation is

$$\left\{A_2 - A_1\frac{2h_r h_q}{k_l}\left[\frac{5}{2}(T_v^{*m})^{-3/2} - \frac{3}{2}(T_v^{*m})^{-5/2}T_v^{*m+1}\right]\right\}T_{1,JV}^* + (A_1 + A_3)T_{1,JV+1}^* = B_2T_{1,JV}^{(n)} + (B_1 + B_3)T_{2,JV}^{(n)} - A_1\frac{2h_r h_q}{k_l}\left[\frac{3}{2}(T_v^{*m})^{-1/2} - \frac{1}{2}(T_v^{*m})^{-3/2}T_v^{*m+1}\right]$$

The second time split equation is

$$A_5T_{1,JV}^{(n+1)} + (A_4 + A_6)T_{2,JV}^{(n+1)} = \left[B_5 - B_4\frac{2h_r h_q}{k_l}T_v^{*-3/2}\right]T_{1,JV}^* + (B_4 + B_6)T_{1,JV+1}^* + B_4\frac{2h_r h_q}{k_l}T_v^{*-1/2}$$

#### CONDENSER END/LIQUID-VAPOR INTERFACE CORNER

The first time split equation is

$$\left\{A_2 - A_1\frac{2h_r h_q}{k_l}\left[\frac{5}{2}(T_v^{*m})^{-3/2} - \frac{3}{2}(T_v^{*m})^{-5/2}T_v^{*m+1}\right]\right\}T_{N,JV}^* + (A_1 + A_3)T_{N,JV+1}^* = (B_1 + B_3)T_{N-1,JV}^{(n)} + B_2T_{N,JV}^{(n)} - A_1\frac{2h_r h_q}{k_l}\left[\frac{3}{2}(T_v^{*m})^{-1/2} - \frac{1}{2}(T_v^{*m})^{-3/2}T_v^{*m+1}\right]$$

The second time split equation is

$$(A_4 + A_6)T_{N-1,JV}^{(n+1)} + A_5T_{N,JV}^{(n+1)} =$$

$$\left[ B_5 - B_4 \frac{2h_r h_q}{k_l} T_v^{*-3/2} \right] T_{N,JV}^* + (B_4 + B_6)T_{N,JV+1}^* + B_4 \frac{2h_r h_q}{k_l} T_v^{*-1/2}$$

## Appendix F

### THERMOPHYSICAL PROPERTY RELATIONS FOR SODIUM

Selected thermophysical property relations are included in the program to update property values based on temperature conditions. All properties with the exception of surface tension are from Fink and Leibowitz[41] . The relation for surface tension variation with temperature is taken from Foust[42] . The relations that follow have been converted to consistent SI units. Property symbols and units are:

Vapor Temperature	$T$	$K$
Liquid Density	$\rho_l$	$kg/m^3$
Vapor Density	$\rho_v$	$kg/m^3$
Liquid Thermal Conductivity	$k_l$	$W/m K$
Thermal Diffusivity	$\alpha_l$	$m^2/s$
Specific Heat	$c_p$	$J/kg K$
Surface Tension	$\sigma$	$N/m$
Saturation Pressure	$P_{sat}$	$Pa$
Latent Heat of Vaporization	$h_{fg}$	$J/kg$
Dynamic Viscosity	$\mu$	$kg/m s$

The property relations also make use of the following identities:

$$\text{Critical Temperature} \quad T_c \equiv 2509.46 \text{ K}$$

$$\text{Critical Density} \quad \rho_c \equiv 214.1 \text{ kg/m}^3$$

$$\text{Reduced Temperature} \quad T_r \equiv T/T_c$$

### **Liquid Thermal Conductivity**

$$k_l = 105.78 - 5.1767 \times 10^{-2}T + 4.8696 \times 10^{-6}T^2$$

### **Surface Tension**

$$\sigma = 0.23402 - 1 \times 10^{-4}T$$

### **Saturated Liquid Vapor Pressure**

$$P_{sat} = 101,325 \exp \left[ 18.832 - \frac{13113}{T} - 1.0948 \ln T + 1.9777 \times 10^{-4}T \right]$$

### **Latent Heat Of Vaporization**

$$h_{fg} = 1.4487 \times 10^6(1 - T_r) + 3.4860 \times 10^6(1 - T_r)^{0.2}$$



### Dynamic Viscosity

$$\mu = 1.1259 \times 10^{-5} (\rho_l)^{1/3} \exp \left[ 0.74908 \frac{\rho_l}{T} \right]$$

### Liquid Density

Liquid density is dependent on the temperature ranges

$$371K \leq T \leq 1644K$$

$$\rho_l = 1011.8 - 0.22054T - 1.9226 \times 10^{-5}T^2 + 5.6371 \times 10^{-9}T^3$$

$$1644K \leq T \leq 2509K$$

$$\rho_l = \rho_c \left[ 1 + 2.3709(1 - T_r)^{0.31645} + 2.8467 \times 10^{-7}(T_c - T)^2 \right]$$

### Vapor Density

$$\rho_v = \left[ \frac{h_{fg}}{T \left( \frac{dP}{dT} \right)_{sat}} + \frac{1}{\rho_l} \right]^{-1}$$

which is the Clausius-Clapeyron Equation solved for vapor density with  $\left( \frac{dP}{dT} \right)_{sat}$  given under specific heat.

## Specific Heat

$$c_p = \left( \frac{\partial H_l}{\partial T} \right)_{sat} + \frac{\gamma_{sat}}{\rho_l} \left\{ \frac{T}{\rho_l} \left[ \gamma_{sat} \left( \frac{\partial \rho_l}{\partial P} \right)_T - \left( \frac{\partial \rho_l}{\partial T} \right)_{sat} \right] - 1 \right\}$$

where

$$\gamma_{sat} = \left( \frac{dP}{dT} \right)_{sat} =$$

$$101,325 \left[ \frac{13113}{T^2} - \frac{1.0948}{T} + 1.9777 \times 10^{-4} \right]$$

$$\exp \left[ 18.832 - \frac{13113}{T} - 1.0948 \ln T + 1.9777 \times 10^{-4} T \right]$$

$$\left( \frac{\partial \rho_l}{\partial P} \right)_T = \left[ \frac{1.77587 \times 10^{-10}}{b + cT_r + dT_r^2} \right]$$

$$- \left[ 2.15463 \times 10^{-21} T + 1.220408 \times 10^{-24} T^2 \right] P_{sat} + 1.671245 \times 10^{-29} T P^2$$

$$b = 1.2773035$$

$$c = -1.8267670$$

$$d = 0.54946350$$

$$T \leq 1644K$$

$$\left(\frac{\partial H_l}{\partial T}\right)_{sat} = 1.53139 \times 10^3 - 0.613452T + 3.35513 \times 10^{-4}T^2 + \frac{5.40593 \times 10^6}{T^2}$$

$$\left(\frac{\partial \rho_l}{\partial T}\right)_{sat} = -0.22054 - 3.8452 \times 10^{-5}T + 1.6911 \times 10^{-8}T^2$$

$$T \geq 1644K$$

$$\left(\frac{\partial H_l}{\partial T}\right)_{sat} = 805.80 + 304.21(1 - T_r)^{-0.67773}$$

$$\left(\frac{\partial \rho_l}{\partial T}\right)_{sat} = -\frac{\rho_c}{T_c}(.75027)(1 - T_r)^{0.68355} - \rho_c(5.6934 \times 10^{-7})(T_c - T)$$

### Thermal Diffusivity

$$\alpha_l = \frac{k_l}{\rho_l c_p}$$

**Appendix G**  
**COMPUTER CODE LISTING**



```

C
C   SET PROGRAM CONTROL CONSTANTS
C
EPSDLT=1.5D-1
EPSQ=5.D-2
EPSRG1=1.D-2
EPSTS=1.D-5
EPSTV=1.D-5
EPSTW=1.D-4
MAXITR=30
MAXITV=20
ITFLTR=0
IREGIM=1
NCASE=DINT(XPUT(1))

C
C   SET AXIAL PARAMETERS
C
HX=XPUT(2)
HXHALF=HX*0.5D0
IEM1=IE-1
IEP1=IE+1
ICM1=IC-1
ICP1=IC+1
IMM1=IMAX-1
IMM2=IMAX-2
PIL=HX*DFLOAT(IMM1)
EL=HX*DFLOAT(IEM1)
AL=HX*DFLOAT(IC-IE)
CL=HX*DFLOAT(IMAX-IC)
ELPH=HX*(DFLOAT(IE)-0.5D0)
CLPH=HX*(DFLOAT(IMAX-IE)-0.5D0)
DO 40 I=1,IMAX
    X(I)=HX*DFLOAT(I-1)
40  CONTINUE

C
C   SET RADIAL PARAMETERS
C
PI=DATAN(1.D0)*4.D0
HR=XPUT(3)
HRHALF=HR*0.5D0
JVP1=JV+1
JVP2=JV+2
JVP3=JV+3
JLM1=JL-1
JLP1=JL+1
RV=XPUT(4)
RL=RV+HR*DFLOAT(JL-JV)
RW=RV+HR*DFLOAT(JW-JV)
DELTA=RL-RV
DO 50 J=JV,JW
    R(J)=RV+DFLOAT(J-JV)*HR
    RS(J)=(R(J)-RV)/DELTA
    RS1(J)=DELTA/(2.D0*HX*(DELTA*RS(J)+RV))
    RS2(J)=RS(J)*RS(J)/2.D0
    RS3(J)=RS2(J)*RS(J)*2.D0/3.D0
    RS4(J)=RS3(J)*RS(J)*3.D0/4.D0
    RS5(J)=RS4(J)*RS(J)*4.D0/5.D0
50  CONTINUE
DO 55 I=1,IMAX
    RCAP(I)=RV
55  CONTINUE

C
C   SET WICK PARAMETERS
C
PR=XPUT(5)
PD=2.D0*PR
WR=XPUT(6)
CW=PR*PR/((PR+WR)*(PR+WR))

```

```

C
C
C   PIPE FIXED VOLUMES
      VOP=PI*RL*RL*PIL
      VOC=PI*RV*RV*PIL
      VOA=VOP-VOC
      VOLE=PI*RV*RV*ELPH
      VOLC=PI*RV*RV*CLPH
C
C
C   SET TIME PARAMETERS
      HT=XPUT(7)
      IF (NCASE.EQ.1) THEN
        TIME=0.D0
        KTM=0
      ELSE
        READ (12) TIME,KTM
      ENDIF
      KTM0=KTM
      KSTEPS=40000
      KQUIT=KTM+KSTEPS
C
C
C   SET PRINT CONTROL PARAMETERS
      ISKIP1=100
      ISKIP2=2000
      IPRNT1=KTM+ISKIP1
      IPRNT2=KTM+ISKIP2
      IREPT1=1
      IREPT2=1
      IBEGIN=KTM0+1
      IEND=KQUIT-10
C
C
C   SET RADIATION OPTICAL PARAMETERS
      EPS=0.7D0
      SIG=5.67D-8
      EPSIG=EPS*SIG
      TE=XPUT(8)
      TE4=TE**4
      DO 58 I=1,IMAX
        IF (I.LT.IC) THEN
          SRAD(I)=0.D0
        ELSE
          SRAD(I)=EPSIG
        ENDIF
      CONTINUE
58
C
C
C   SET INPUT HEAT TRANSFER PARAMETERS
      QMAX=-1.5D6
      TAU=300.D0
      OMEGA=PI/TAU
      JQFLTR=0
      Q1=2.D0*PI*RW*HX
      Q2=2.D0*PI*RV*HX
      Q3=PI*RV*RV*DSQRT(5.D0*8.314D3/(16.D0*22.9898D0))
      Q4=PI*RV*RV/DSQRT(PD)
      Q5=5.04D-8*PI*(RL*RL-RV*RV)/(PIL*PR)
C
C
C   SET WALL PROPERTIES
      ALPHAW=5.3D-5
      TKW=1.10D2

```

```

C
C
C      SET CONSTANT SODIUM THERMOPHYSICAL PROPERTIES
      TCR=2509.46D0
      RHOCR=214.1D0
      RG=8.314D3/22.9898D0
      VMU=1.4D-5

C
C
C      SET C FACTORS FOR MISCELLANEOUS CALCULATIONS
      C1=CW*RV*HX/(RL*RL-RV*RV)
      C2=DSQRT(1.D0/(2.D0*PI*RG))
      C3=2.D0*HR*C2*CW
      C4=2.D0*HR/TKW

C
C
C      SET V FACTORS FOR VAPOR TEMPERATURE CALCULATIONS
      V1=2.D0*PI*RV*RV*PI*RV*RV
      V2=PI*RV*RV*DSQRT(5.D0*RG/16.D0)
      V3=HT*2.D0*PI*RV*CW*DSQRT(1.D0/(2.D0*PI*RG))/VOLE
      V4=HT*2.D0*PI*RV*CW*DSQRT(1.D0/(2.D0*PI*RG))/VOLC
      V5=-HT*CW*RV*DSQRT(2.D0*PI/RG)/VOC

C
C
C      SET F FACTORS FOR GRID VELOCITY CALCULATIONS (SUBROUTINE SPEED)
      T13=0.2D0*(3.D0-RV/(RL+RV))
      DELTA2=DELTA*DELTA
      DELTA3=DELTA*DELTA*DELTA
      F0=RV/DELTA
      F1=(RL*RL-RV*RV)*3.D0/RV
      F2=-(0.5D0+F0)*DELTA3
      F3=(6.D0+F0*12.D0)*0.4D0*DELTA2*CW*RV/(RL+RV)-3.D0*(RL*RL-RV*RV)
      F4=(RL*RL-RV*RV)*T13*0.5D0/RV-2.D0*(RL+RV)
      F5=(5.D0-2+F0/12.D0-T13*(1.D0/12.D0+F0/6.D0))*DELTA3
      F6=-(12.D0/105.D0+0.2D0*F0-T13*(0.2D0+0.4D0*F0))
1      *4.D0*DELTA2*CW*RV/(RL+RV)-(RL*RL-RV*RV)*T13*0.5D0
      F7=(T13*T13*(1.D0/60.D0+F0/30.D0)+(1.D0/168.D0+F0/105.D0)
1      -T13*(2.D0/105.D0+F0/30.D0))*4.D0*DELTA2*CW*RV/(RL+RV)
      F8=2.D0*DELTA/(RL+RV)

C
C
C      SET Z FACTORS FOR LIQUID PRESSURE CALCS (MAIN AND SUBR. SPEED)
      Z0=RV/DELTA
      Z00=-8.D0*RV*CW/((RL+RV)*(RL+RV))
      Z1=2.D0/(RL*RL-RV*RV)
      Z2=4.D0*RL/(DELTA*(RL*RL-RV*RV))
      Z3=6.D0*RL/(DELTA*(RL*RL-RV*RV))
      Z4=Z00*(3.D0+4.D0*Z0)/12.D0
      Z5=Z00*(4.D0+5.D0*Z0)/10.D0
      Z6=Z00*(5.D0+6.D0*Z0)/15.D0
      Z7=Z00*(5.D0+6.D0*Z0)/30.D0
      Z8=Z00*(6.D0+7.D0*Z0)/21.D0
      Z9=Z00*(7.D0+8.D0*Z0)/56.D0
      Z10=1.D0/HX
      Z11=-2.D0*HX/HT
      Z12=-2.D0/HX
      Z13=4.D0*HX/HT

```



```

C
C
C      SET INITIAL SODIUM THERMOPHYSICAL PROPERTIES
      IF (NCASE.EQ.1) THEN
        T0=XPUT(9)
        TVEP1=T0
        TVCP1=T0
        CALL PROPS
        DUM=PVAP-SIGMA/RV
        DO 80 I=1,IMAX
          PL(I)=DUM
80      CONTINUE
      ELSE
        READ (12) TVEP1,TVCP1,TAV
        READ (12) SIGMA,TKL,HFG,RHOL,RHOV,UMU,UNU,VNU,CP,ALPHAL,PVAP
        READ (12) PVE,PVC,RHOE,RHOC,DPDTE,DPDTC
        READ (12) PG1,PG2,PG3,PG4E,PG4C,PG5E,PG5C,PG6,PG7
        DO 85 I=1,IMAX
          READ (12) PL(I),RCAP(I),ZETAN(I)
85      CONTINUE
      ENDIF
C
C
C      SET ADI NUMERICAL PARAMETERS
      PHIR=2.D0*HR*HR/HT
      PHIX=2.D0*HX*HX/HT
      PHIXOR=PHIX/PHIR
      PHIROX=PHIR/PHIX
      PHIXRH=PHIXOR*HRHALF
      PHIRXH=PHIROX*HXHALF
      DO 90 J=JV,JW
        IF (J.LT.JL) THEN
          ADIA1(J)=-ALPHAL+ALPHAL*HRHALF/R(J)
          ADIA2(J)=PHIR+2.D0*ALPHAL
          ADIA3(J)=-ALPHAL-ALPHAL*HRHALF/R(J)
          ADIA4(J)=-ALPHAL
          ADIA5(J)=PHIX+2.D0*ALPHAL
          ADIA6(J)=-ALPHAL
          ADIB1(J)=ALPHAL*PHIROX
          ADIB2(J)=PHIR-2.D0*ALPHAL*PHIROX
          ADIB3(J)=ALPHAL*PHIROX
          ADIB4(J)=(ALPHAL-ALPHAL*HRHALF/R(J))*PHIXOR
          ADIB5(J)=PHIX-2.D0*ALPHAL*PHIXOR
          ADIB6(J)=(ALPHAL+ALPHAL*HRHALF/R(J))*PHIXOR
        ELSE
          ADIA1(J)=-ALPHAW+ALPHAW*HRHALF/R(J)
          ADIA2(J)=PHIR+2.D0*ALPHAW
          ADIA3(J)=-ALPHAW-ALPHAW*HRHALF/R(J)
          ADIA4(J)=-ALPHAW
          ADIA5(J)=PHIX+2.D0*ALPHAW
          ADIA6(J)=-ALPHAW
          ADIB1(J)=ALPHAW*PHIROX
          ADIB2(J)=PHIR-2.D0*ALPHAW*PHIROX
          ADIB3(J)=ALPHAW*PHIROX
          ADIB4(J)=(ALPHAW-ALPHAW*HRHALF/R(J))*PHIXOR
          ADIB5(J)=PHIX-2.D0*ALPHAW*PHIXOR
          ADIB6(J)=(ALPHAW+ALPHAW*HRHALF/R(J))*PHIXOR
        ENDIF
90      CONTINUE
C
C
C      DETERMINE INITIAL LIQUID AND VAPOR INVENTORIES
      IF (NCASE.EQ.1) THEN
        WL=RHOL*VOA
        WV=RHOV*VOC
        WT=WL+WV
      ELSE
        READ (12) WL,WV,WT
      ENDIF

```

```

C
C   EVALUATE INITIAL OPERATING LIMITS
C
PCMAX=2.D0*SIGMA/PR
QSON=Q3*RHOE*HFG*DSQRT(TVEP1)
QENT=Q4*HFG*DSQRT(SIGMA*RHOV)
QCAP=Q5*SIGMA*HFG/UNU
C
C   SET INITIAL VELOCITIES AND TEMPERATURES
C
IF (NCASE.EQ.1) THEN
DO 110 I=1,IMAX
DO 100 J=JV,JW
U(I,J)=0.D0
V(I,J)=0.D0
T(I,J)=T0
100 CONTINUE
110 CONTINUE
ELSE
DO 140 I=1,IMAX
DO 130 J=JV,JW
READ (12) U(I,J),V(I,J),T(I,J)
130 CONTINUE
140 CONTINUE
ENDIF
C
C   READ ADDITIONAL STARTUP DATA
C
IF (NCASE.NE.1) THEN
READ (12) DELPL
READ (12) QIN,QOT,QEV,QCO,QEVAP,QAX
READ (12) ITER
READ (12) IREGIM
ENDIF
C
C   PRINT SET-UP DATA AND INITIAL CONDITIONS
C
WRITE (6,9003) PIL,RW,RL,RV,VOP,VOC,VOA
WRITE (6,9004) WL,WV,WT
WRITE (6,9002) HR,HX,HT,PHIR,PHIX
WRITE (6,9015)
WRITE (6,9013)
WRITE (6,9014) TIME,KTM
WRITE (6,9031) ITER
WRITE (6,9007) IREGIM
WRITE (6,9005) TVEP1,TVCP1
WRITE (6,9030) DELPL,PCMAX
WRITE (6,9006) QIN,QOT,QEV,QCO,QEVAP,QAX,QSON,QENT,QCAP
WRITE (6,9011) POOL
WRITE (6,9027) SIGMA,TKL,HFG,RHOL,RHOV,UMU,UNU,CP,ALPHAL
WRITE (6,9017)
DO 210 I=1,IE
WRITE (6,9021) I,JV,U(I,JV),V(I,JV),T(I,JV),PL(I),RCAP(I)
DO 200 J=JVP1,JW,4
WRITE (6,9019) I,J,U(I,J),V(I,J),T(I,J)
200 CONTINUE
210 CONTINUE
DO 230 I=IEP1,ICM1
WRITE (6,9021) I,JV,U(I,JV),V(I,JV),T(I,JV),PL(I),RCAP(I)
DO 220 J=JVP1,JW,4
WRITE (6,9019) I,J,U(I,J),V(I,J),T(I,J)
220 CONTINUE
230 CONTINUE
DO 250 I=IC,IMAX,6
WRITE (6,9021) I,JV,U(I,JV),V(I,JV),T(I,JV),PL(I),RCAP(I)
DO 240 J=JVP1,JW,4
WRITE (6,9019) I,J,U(I,J),V(I,J),T(I,J)
240 CONTINUE
250 CONTINUE

```

```

        WRITE (6,9015)
        WRITE (6,9032)
        DO 260 I=1,IMAX
            WRITE (6,9033) I,ZETAN(I)
260    CONTINUE
        WRITE (6,9015)
C
C    BEGIN TIME STEPS
C
500    TSTAR=TIME+0.5D0*HT
        TIME=TIME+HT
        KTM=KTM+1
        ITER=0
C
C    UPDATE PROPERTY DEPENDENT ADI PARAMETERS
C
        DO 505 J=JV,JLM1
            ADIA1(J)=-ALPHAL+ALPHAL*HRHALF/R(J)
            ADIA2(J)=PHIR+2.D0*ALPHAL
            ADIA3(J)=-ALPHAL-ALPHAL*HRHALF/R(J)
            ADIA4(J)=-ALPHAL
            ADIA5(J)=PHIX+2.D0*ALPHAL
            ADIA6(J)=-ALPHAL
            ADIB1(J)=ALPHAL*PHIROX
            ADIB2(J)=PHIR-2.D0*ALPHAL*PHIROX
            ADIB3(J)=ALPHAL*PHIROX
            ADIB4(J)=(ALPHAL-ALPHAL*HRHALF/R(J))*PHIXOR
            ADIB5(J)=PHIX-2.D0*ALPHAL*PHIXOR
            ADIB6(J)=(ALPHAL+ALPHAL*HRHALF/R(J))*PHIXOR
505    CONTINUE
C
C    UPDATE INPUT HEAT TRANSFER
C
        IF (TSTAR.LE.TAU) THEN
            Q0=QMAX*0.5D0*(1.D0-DSIN(TSTAR*OMEGA+0.5D0*PI))
            DO 510 I=1,IE
                QSTR(I)=Q0
510        CONTINUE
            ENDIF
            IF (JQFLTR.EQ.1) THEN
                DO 511 I=IEP1,IC
                    QSTR(I)=0.D0
511        CONTINUE
                QIEM1=0.25D0*(QSTR(IE-2)+2.D0*QSTR(IEM1)+QSTR(IE))
                QIE=0.25D0*(QSTR(IEM1)+2.D0*QSTR(IE)+QSTR(IEP1))
                QIEP1=0.25D0*(QSTR(IE)+2.D0*QSTR(IEP1)+QSTR(IEP1+2))
                QSTR(IEM1)=QIEM1
                QSTR(IE)=QIE
                QSTR(IEP1)=QIEP1
                SUMQIN=0.D0
                DO 515 I=1,IMAX
                    IF (I.EQ.1.OR.QSTR(I+1).EQ.0.D0) THEN
                        SUMQIN=SUMQIN+QSTR(I)*0.5D0
                    ELSE
                        SUMQIN=SUMQIN+QSTR(I)
                    ENDIF
515        CONTINUE
                ELSE
                    SUMQIN=0.5D0*(QSTR(1)+QSTR(IE))
                    DO 517 I=2,IEM1
                        SUMQIN=SUMQIN+QSTR(I)
517        CONTINUE
                ENDIF
                QIN=Q1*SUMQIN

```

```

C
C
C      UPDATE OPERATING REGIME AND AXIAL VAPOR MASS TRANSFER
      IF (DABS(QEVAP).GE.0.98D0*DABS(QSON)) THEN
        IF (IREGIM.EQ.1) THEN
          IPRNT2=KTM
        ENDIF
        IREGIM=2
        VMDOT=V2*RHOE*DSQRT(TVEP1)
      ELSE
        VMDOT=0.D0
        IF (IREGIM.EQ.2) THEN
          IREGIM=3
        ENDIF
        IF (IREGIM.EQ.3) THEN
          IF (DABS(TVEP1-TVCP1).LT.EPSRG1) THEN
            IREGIM=1
            IPRNT2=KTM
          ELSE
            VMDOT=DABS(QEVAP)/HFG
          ENDIF
        ENDIF
      ENDIF
      PSIE=VMDOT*HT/VOLE
      PSIC=VMDOT*HT/VOLC
C
C
C      SAVE PREVIOUS TIME TEMPERATURES
      DO 550 I=1,IMAX
        DO 540 J=JV,JW
          TN(I,J)=T(I,J)
540      CONTINUE
550    CONTINUE
C
C
C      SAVE PREVIOUS TIME VELOCITIES
      DO 600 I=1,IMAX
        DO 590 J=JV,JL
          UN(I,J)=U(I,J)
          VN(I,J)=V(I,J)
590      CONTINUE
600    CONTINUE
C
C
C      INITIAL GUESS TSTAR VELOCITIES AND VAPOR AND WALL TEMPERATURES
      TVES=TVEP1
      TVESM=TVEP1
      TVCS=TVCP1
      TVCSM=TVCP1
      DO 650 I=1,IMAX
        TWS(I)=T(I,JW)
        DO 640 J=JV,JL
          US(I,J)=U(I,J)
          VS(I,J)=V(I,J)
640      CONTINUE
650    CONTINUE
C
C
C      BEGIN ITERATIONS BETWEEN ENERGY AND FLOW
      1000 ITER=ITER+1
C
C
C      RESET TEMPERATURES TO INITIAL VALUES
      DO 1050 I=1,IMAX
        DO 1040 J=JV,JW
          T(I,J)=TN(I,J)
1040      CONTINUE
1050    CONTINUE

```

```

C
C   SOLVE FIRST ADI TIME SPLIT
C
C   ISPLIT=1
C   CALL SPLIT1
C
C   USE LU-DECOMPOSITION TO SOLVE THE FIRST ALGEBRAIC SPLIT SYSTEM
C
C   CALL LORI
C
C   LOAD TIME TSTAR TEMPERATURE RESULTS
C
C   DO 1100 I=1,IMAX
C       DO 1090 J=JV,JW
C           T(I,J)=B(J+JW*(I-1))
1090   CONTINUE
1100   CONTINUE
C
C   APPLY SMOOTHING FILTER IF REQUESTED
C
C   IF (ITFLTR.EQ.1) THEN
C       DELTMX=0.D0
C       DO 1250 I=IE,IC
C           DO 1150 J=JV,JW
C               DELT=DABS(1.D0-T(I-1,J)/T(I,J))
C               IF (DELT.GT.DELTMX) DELTMX=DELT
1150         CONTINUE
C               IF (DELTMX.GT.EPSDLT) THEN
C                   DO 1200 J=JV,JW
C                       TEMP1=0.25D0*(T(I-2,J)+2.D0*T(I-1,J)+T(I,J))
C                       TEMP2=0.25D0*(T(I-1,J)+2.D0*T(I,J)+T(I+1,J))
C                       TEMP3=0.25D0*(T(I,J)+2.D0*T(I+1,J)+T(I+2,J))
C                       T(I-1,J)=TEMP1
C                       T(I,J)=TEMP2
C                       T(I+1,J)=TEMP3
1200                   CONTINUE
C                   GOTO 1250
C               ENDIF
1250         CONTINUE
C       ENDIF
C
C   UPDATE VAPOR TEMPERATURES
C
C   TVESM=TVES
C   TVCSM=TVCS
C   IF (IREGIM.EQ.1) CALL REGIM1(ISPLIT)
C   IF (IREGIM.EQ.2) CALL REGIM2(ISPLIT)
C   TVES=TV1
C   TVCS=TV2
C
C   SAVE T STAR ITERATION WALL TEMPERATURES
C
C   DO 1400 I=1,IMAX
C       TWS(I)=T(I,JW)
1400   CONTINUE
C
C   UPDATE TIME TSTAR VELOCITIES
C
C   CALL SPEED(ISPLIT)
C   DO 1500 I=1,IMAX
C       DO 1450 J=JV,JW
C           US(I,J)=UT(I,J)
C           VS(I,J)=VT(I,J)
1450       CONTINUE
1500   CONTINUE

```

```

C
C      INITIAL GUESS TIME N+1 VELOCITIES AND TEMPERATURES
C
      IF (ITER.EQ.1) THEN
        TVEP1=TVES
        TVCP1=TVCS
        DO 2100 I=1,IMAX
          TS(I)=T(I,JV)
          TW(I)=T(I,JW)
          DO 2050 J=JV,JW
            U(I,J)=US(I,J)
            V(I,J)=VS(I,J)
2050          CONTINUE
2100        CONTINUE
      ENDIF

C
C      SOLVE SECOND ADI TIME SPLIT
C
      ISPLIT=2
      CALL SPLIT2

C
C      USE LU-DECOMPOSITION TO SOLVE THE SECOND ALGEBRAIC SPLIT SYSTEM
C
      CALL LORI

C
C      LOAD TIME N+1 TEMPERATURE RESULTS
C
      DO 2300 J=JV,JW
        DO 2250 I=1,IMAX
          T(I,J)=B(I+IMAX*(J-1))
2250        CONTINUE
2300      CONTINUE

C
C      APPLY SMOOTHING FILTER IF REQUESTED
C
      IF (ITFLTR.EQ.1) THEN
        DELTMX=0.D0
        DO 2500 I=IE,IC
          DO 2350 J=JV,JW
            DELT=DABS(1.D0-T(I-1,J)/T(I,J))
            IF (DELT.GT.DELTMX) DELTMX=DELT
2350          CONTINUE
          IF (DELTMX.GT.EPSDLT) THEN
            DO 2400 J=JV,JW
              TEMP1=0.25D0*(T(I-2,J)+2.D0*T(I-1,J)+T(I,J))
              TEMP2=0.25D0*(T(I-1,J)+2.D0*T(I,J)+T(I+1,J))
              TEMP3=0.25D0*(T(I,J)+2.D0*T(I+1,J)+T(I+2,J))
              T(I-1,J)=TEMP1
              T(I,J)=TEMP2
              T(I+1,J)=TEMP3
2400            CONTINUE
            GOTO 2500
          ENDIF
2500        CONTINUE
      ENDIF

C
C      UPDATE VAPOR TEMPERATURES
C
      IF (IREGIM.EQ.1) CALL REGIM1(ISPLIT)
      IF (IREGIM.EQ.2) CALL REGIM2(ISPLIT)
      TVEP1=TV1
      TVCP1=TV2

```

```

C
C   DETERMINE TIME N+1 VELOCITIES
C
      CALL SPEED(ISPLIT)
      DO 2650 I=1,IMAX
        DO 2600 J=JV,JW
          U(I,J)=UT(I,J)
          V(I,J)=VT(I,J)
        2600   CONTINUE
      2650   CONTINUE
C
C   FIND ITERATION MAX NORM CHANGE OF TN+1 LIQUID SURFACE TEMPERATURE
C
      DELTSM=0.D0
      DO 2700 I=1,IMAX
        DELTS=DABS(1.D0-TS(I)/T(I,JV))
        IF (DELTS.GT.DELTSM) THEN
          DELTSM=DELTS
          ITS=I
        ENDIF
      2700   CONTINUE
C
C   FIND ITERATION MAX NORM CHANGE IN PIPE WALL TEMPERATURE
C
      DELTWM=0.D0
      DO 2750 I=1,IMAX
        DELTW=DABS(1.D0-TW(I)/T(I,JW))
        IF (DELTW.GT.DELTWM) THEN
          DELTWM=DELTW
          ITW=I
        ENDIF
      2750   CONTINUE
C
C   UPDATE TIME N+1 ITERATION WALL AND SURFACE TEMPERATURES
C
      DO 2800 I=1,IMAX
        TS(I)=T(I,JV)
        TW(I)=T(I,JW)
      2800   CONTINUE
C
C   CHECK FOR CONVERGENCE
C
      IF (ITER.GE.MAXITR) THEN
        WRITE (6,9026) ITER,EPSTS,DELTSM,ITS,EPSTW,DELTWM,ITW,IREGIM
        IPRNT2=KTM
        KSTOP=2
        GOTO 2850
      ENDIF
      IF (DELTSM.GT.EPSTS.OR.DELTWM.GT.EPSTW) GOTO 1000
      CONTINUE
C
C   UPDATE THERMOPHYSICAL PROPERTIES
C
      2850   CALL PROPS
C
C   UPDATE HEAT TRANSFER LIMITS
C
      PCMAX=2.D0*SIGMA/PR
      QSON=Q3*RHOE*HFG*DSQRT(TVEP1)
      QENT=Q4*HFG*DSQRT(SIGMA*RHOV)
      QCAP=Q5*SIGMA*HFG/UNU

```

```

C
C      EVALUATE HEAT TRANSFER
C
      SUMQOT=0.D0
      SUMQEV=0.D0
      SUMQCO=0.D0
      SUMQEI=0.D0
      DO 3000 I=1,IMAX
C
C      PHASE CHANGE HEAT TRANSFER
C
      QPC=PG3*V(I,JV)
      IF (I.EQ.1.OR.I.EQ.IMAX) QPC=QPC*0.5D0
      IF (V(I,JV).LT.0.D0) THEN
        SUMQEV=SUMQEV+QPC
      ELSE
        SUMQCO=SUMQCO+QPC
      ENDIF
      IF (I.LE.IE) SUMQEI=SUMQEI+QPC
C
C      OUTPUT HEAT TRANSFER
C
      IF (I.GE.IC) THEN
        QOI=EPS*SIG*(T(I,JW)**4-TE4)
        IF (I.EQ.IC.OR.I.EQ.IMAX) QOI=QOI*0.5D0
        SUMQOT=SUMQOT+QOI
      ENDIF
3000 CONTINUE
      QOT=Q1*SUMQOT
      QEV=Q2*SUMQEV
      QCO=Q2*SUMQCO
      QEVAP=Q2*SUMQEI
      QAX=VMDOT*HFG
C
C      CHECK CAPILLARY LIMIT HEAT TRANSFER
C
      IF (DABS(QEV).GT.QCAP) THEN
        WRITE (6,9000) QEV,QCAP
        IPRNT2=KTM
        KSTOP=2
      ENDIF
C
C      CHECK HEAT TRANSFER FOR STEADY STATE
C
      QTEST=DABS(1.D0+QOT/QIN)
      IF (QTEST.LT.EPSQ) THEN
        WRITE (6,9009)
        KSTOP=2
        IPRNT2=KTM
      ENDIF
C
C      UPDATE LIQUID PRESSURES
C
      DO 3300 I=1,IMAX
        PLN(I)=PL(I)
3300 CONTINUE
      PL(IMAX)=PVAP-SIGMA/RV
      DO 3400 I=IMM1,2,-1
        ZETA(I)=Z10*UMU*(UB(I-1)+UB(I+1))
          +(GAMMA(I)*HX+Z11*RHOL+Z12*UMU)*UB(I)
1      PL(I)=PL(I+1)+PLN(I+1)-PLN(I)-ZETA(I)-ZETAN(I)
        ZETAN(I)=ZETA(I)+Z13*RHOL*UB(I)
3400 CONTINUE
      ZETA(1)=-(UB(3)-2.D0*UB(2))*UMU/HX
      PL(1)=PL(2)+PLN(2)-PLN(1)+ZETA(1)+ZETAN(1)
      ZETAN(1)=ZETA(1)

```



```

C
C      FIND CAPILLARY RADII OF CURVATURE
C
      DO 3500 I=1,IMAX
        GRAD=(-3.D0*V(I,JV)+4.D0*V(I,JVP1)-V(I,JVP2))*UMU/HR
        RCAP(I)=2.D0*SIGMA/(PVAP-PL(I)+PG7*V(I,JV)*V(I,JV)+GRAD)
3500  CONTINUE
C
C      CHECK CAPILLARY LIMIT
C
      DELPL=PL(IMAX)-PL(1)
      IF (DELPL.GT.PCMAX) THEN
        WRITE (6,9001) DELPL,PCMAX
        IPRNT2=KTM
        KSTOP=2
      ENDIF
C
C      MASS INVENTORY ACCOUNTING
C
      POOL=WT-RHOE*VOLE-RHOC*VOLC-RHOL*VOA
C
C      PRINT NEW DATA
C
      IF (KTM.GE.IEND) IPRNT2=KTM
      IF (KTM.EQ.IPRNT1) THEN
        IF (IREPT1.EQ.1) THEN
          IPRNT1=IPRNT1+1
          IREPT1=0
        ELSE
          IPRNT1=IPRNT1+ISKIP1-1
          IREPT1=1
        ENDIF
      IF (KTM.NE.IPRNT2) THEN
        WRITE (6,9022)
        WRITE (6,9014) TIME,KTM
        WRITE (6,9031) ITER
        WRITE (6,9007) IREGIM
        WRITE (6,9005) TVEP1,TVCP1
        WRITE (6,9030) DELPL,PCMAX
        WRITE (6,9006) QIN,QOT,QEV,QCO,QEVAP,QAX,QSON,QENT,QCAP
        WRITE (6,9011) POOL
      ENDIF
    ENDIF
    IF (KTM.EQ.IPRNT2.OR.KTM.LE.IBEGIN) THEN
      IF (KTM.EQ.IPRNT2) THEN
        IF (IREPT2.EQ.1) THEN
          IPRNT2=IPRNT2+1
          IREPT2=0
        ELSE
          IPRNT2=IPRNT2+ISKIP2-1
          IREPT2=1
        ENDIF
      ENDIF
      WRITE (6,9015)
      WRITE (6,9014) TIME,KTM
      WRITE (6,9031) ITER
      WRITE (6,9007) IREGIM
      WRITE (6,9005) TVEP1,TVCP1
      WRITE (6,9030) DELPL,PCMAX
      WRITE (6,9006) QIN,QOT,QEV,QCO,QEVAP,QAX,QSON,QENT,QCAP
      WRITE (6,9011) POOL
      WRITE (6,9027) SIGMA,TKL,HFG,RHOL,RHOV,UMU,UNU,CP,ALPHAL
      WRITE (6,9017)

```

```

C
C      EVAPORATOR DATA
C
      DO 5020 I=1,IE,1
        WRITE (6,9021) I,JV,U(I,JV),V(I,JV),T(I,JV),PL(I),RCAP(I)
        DO 5000 J=JVP1,JL,1
          WRITE (6,9019) I,J,U(I,J),V(I,J),T(I,J)
5000      CONTINUE
          DO 5010 J=JL+2,JW,2
            WRITE (6,9018) I,J,T(I,J)
5010      CONTINUE
5020      CONTINUE
C
C      ADIABAT DATA
C
      DO 5050 I=IEP1,IC+3,1
        WRITE (6,9021) I,JV,U(I,JV),V(I,JV),T(I,JV),PL(I),RCAP(I)
        DO 5030 J=JVP1,JL,1
          WRITE (6,9019) I,J,U(I,J),V(I,J),T(I,J)
5030      CONTINUE
          DO 5040 J=JL+2,JW,2
            WRITE (6,9018) I,J,T(I,J)
5040      CONTINUE
5050      CONTINUE
C
C      CONDENSER DATA
C
      DO 5080 I=IC+4,IMAX-3,3
        WRITE (6,9021) I,JV,U(I,JV),V(I,JV),T(I,JV),PL(I),RCAP(I)
        DO 5060 J=JVP1,JL,1
          WRITE (6,9019) I,J,U(I,J),V(I,J),T(I,J)
5060      CONTINUE
          DO 5070 J=JL+2,JW,2
            WRITE (6,9018) I,J,T(I,J)
5070      CONTINUE
5080      CONTINUE
        DO 5095 I=IMAX-2,IMAX
          WRITE (6,9021) I,JV,U(I,JV),V(I,JV),T(I,JV),PL(I),RCAP(I)
          DO 5085 J=JVP1,JL,1
            WRITE (6,9019) I,J,U(I,J),V(I,J),T(I,J)
5085      CONTINUE
          DO 5090 J=JL+2,JW,2
            WRITE (6,9018) I,J,T(I,J)
5090      CONTINUE
5095      CONTINUE
          WRITE (6,9015)
        ENDIF
C
C      DO NEXT TIME STEP IF TIME HAS NOT EXPIRED
C
      IF (KTM.LT.KQUIT.AND.KSTOP.NE.2) GOTO 500
      WRITE (6,9008) TIME

```

```

C
C   WRITE TO STARTUP FILE
C
      WRITE (13) TIME,KTM
      WRITE (13) TVEP1,TVCP1,TAV
      WRITE (13) SIGMA,TKL,HFG,RHOL,RHOV,UMU,UNU,VNU,CP,ALPHAL,PVAP
      WRITE (13) PVE,PVC,RHOE,RHOC,DPDTE,DPDTC
      WRITE (13) PG1,PG2,PG3,PG4E,PG4C,PG5E,PG5C,PG6,PG7
      DO 7020 I=1,IMAX
        WRITE (13) PL(I),RCAP(I),ZETAN(I)
7020  CONTINUE
      WRITE (13) WL,WV,WT
      DO 7040 I=1,IMAX
        DO 7030 J=JV,JW
          WRITE (13) U(I,J),V(I,J),T(I,J)
7030  CONTINUE
7040  CONTINUE
      WRITE (13) DELPL
      WRITE (13) QIN,QOT,QEV,QCO,QEVAP,QAX
      WRITE (13) ITER
      WRITE (13) IREGIM
8000  STOP
C
C   FORMAT STATEMENTS
C
9000  FORMAT (//////22X,'***** CAUTION *****'
1/17X,'CAPILLARY HEAT TRANSFER LIMIT EXCEEDED'
2/16X,'VAPOR HEAT TRANSFER = ',1PD12.5
3/14X,'CAPILLARY HEAT TRANSFER LIMIT = ',1PD12.5)
9001  FORMAT (//////22X,'***** CAUTION *****'
1/17X,'CAPILLARY PUMPING LIMIT EXCEEDED'
2/16X,'LIQUID PRESSURE DROP = ',1PD12.5
3/14X,'MAX CAPILLARY PRESSURE = ',1PD12.5)
9002  FORMAT (/1X,'NUMERICAL PARAMETERS : '
1//12X,'RADIAL STEP SIZE (M) = ',1PD10.2
2//13X,'AXIAL STEP SIZE (M) = ',1PD10.2
3//14X,'TIME STEP SIZE (S) = ',1PD10.2
4//1X,'ADI NUMERICAL PARAMETERS:'
5/28X,'PHIR = ',1PD10.2
6/28X,'PHIX = ',1PD10.2)
9003  FORMAT ('1',1X,'HEAT PIPE DIMENSIONS:'
1//13X,'INTERNAL LENGTH (M) = ',D12.5
2//16X,'OUTER RADIUS (M) = ',D12.5
3//13X,'INTERNAL RADIUS (M) = ',D12.5
4//17X,'WICK RADIUS (M) = ',D12.5
5/4X,'TOTAL INTERNAL VOLUME (M**3) = ',D12.5
6/8X,'VAPOR CORE VOLUME (M**3) = ',D12.5
7/4X,'LIQUID ANNULUS VOLUME (M**3) = ',D12.5)
9004  FORMAT (/1X,'TIME ZERO HEAT PIPE WORKING FLUID MASSES:'
1//16X,'LIQUID MASS (KG) = ',D12.5
2//17X,'VAPOR MASS (KG) = ',D12.5
3//11X,'TOTAL FLUID MASS (KG) = ',D12.5)
9005  FORMAT (10X,'EVAPORATOR VAPOR TEMPERATURE (K) = ',3PD20.14
1//11X,'CONDENSER VAPOR TEMPERATURE (K) = ',3PD20.14)
9006  FORMAT (19X,'INPUT HEAT TRANSFER (W) = ',1PD12.5
1//18X,'OUTPUT HEAT TRANSFER (W) = ',1PD12.5
2//13X,'EVAPORATION HEAT TRANSFER (W) = ',1PD12.5
3//12X,'CONDENSATION HEAT TRANSFER (W) = ',1PD12.5
4//14X,'EVAPORATOR HEAT TRANSFER (W) = ',1PD12.5
5//19X,'AXIAL HEAT TRANSFER (W) = ',1PD12.5
6//13X,'SONIC HEAT TRANSFER LIMIT (W) = ',1PD12.5
7//7X,'ENTRAINMENT HEAT TRANSFER LIMIT (W) = ',1PD12.5
8//9X,'CAPILLARY HEAT TRANSFER LIMIT (W) = ',1PD12.5)
9007  FORMAT (21X,'OPERATING REGIME FLAG = ',I5)
9008  FORMAT (/1X,'CASE COMPLETED',D12.5)
9009  FORMAT (/1X,'***** STEADY STATE REACHED ** CASE COMPLETED ****')
9010  FORMAT (6X,I2/(4(6X,D12.6)))
9011  FORMAT (21X,'EXCESS MASS POOL (KG) = ',1PD12.5)
9013  FORMAT (/1X,'INITIAL CONDITIONS:')

```

```

9014 FORMAT (10X,'***** TIME = ',1PD12.5,5X,'TIME STEP = ',I8,' *****')
9015 FORMAT (1H1)
9017 FORMAT (/6X,'I',7X,'J',12X,'U',16X,'V',
+15X,'TEMPERATURE')
9018 FORMAT (4X,I3,5X,I3,42X,1PD17.10)
9019 FORMAT (4X,I3,5X,I3,2(6X,1PD12.5),6X,1PD17.10)
9021 FORMAT (4X,I3,5X,I3,2(6X,1PD12.5),6X,1PD17.10,6X,1PD12.5,
16X,1PD12.5)
9022 FORMAT (////)
9026 FORMAT (////////20X,'***** CAUTION *****'
1/12X,'CONVERGENCE WAS NOT REACHED IN ITERATIONS = ',I5
2/15X,'SURFACE TEMP CONVERGENCE TOLERANCE EPSILON = ',1PD12.5
3/9X,'MAX SURFACE TEMPERATURE NORMALIZED CHANGE = ',1PD12.5
4/33X,'INTERFACE GRID POINT = ',I5
5/12X,'WALL TEMPERATURE CONVERGENCE TOLERANCE EPSILON = ',1PD12.5
6/15X,'MAX WALL TEMPERATURE NORMALIZED CHANGE = ',1PD12.5
7/38X,'WALL GRID POINT = ',I5
8/42X,'IREGIM FLAG = ',I5)
9027 FORMAT (15X,'***** THERMOPHYSICAL PROPERTIES *****'
2/9X,'SURFACE TENSION COEFFICIENT SIGMA = ',1PD12.5
3/11X,'LIQUID THERMAL CONDUCTIVITY TKL = ',1PD12.5
4/11X,'LATENT HEAT OF VAPORIZATION HFG = ',1PD12.5
5/23X,'LIQUID DENSITY RHOL = ',1PD12.5
6/24X,'VAPOR DENSITY RHOV = ',1PD12.5
7/14X,'LIQUID DYNAMIC VISCOSITY UMU = ',1PD12.5
8/12X,'LIQUID KINEMATIC VISCOSITY UNU = ',1PD12.5
9/19X,'LIQUID SPECIFIC HEAT CP = ',1PD12.5
1/9X,'LIQUID THERMAL DIFFUSIVITY ALPHAL = ',1PD12.5)
9030 FORMAT (17X,'LIQUID PRESSURE DROP (PA) = ',1PD12.5
1/15X,'MAX CAPILLARY PRESSURE (PA) = ',1PD12.5)
9031 FORMAT (10X,'TIME STEP CONVERGENCE ITERATIONS = ',I5)
9032 FORMAT (/6X,'I',11X,'ZETAN')
9033 FORMAT (4X,I3,5X,1PD12.5)
END

```

```

C *****
C *          BLOCK DATA INITIALIZATION          *
C *****
      BLOCK DATA
      IMPLICIT REAL*8 (A-H,O-Z)
      PARAMETER (IE=3,
1          IC=6,
2          IMAX=21,
3          JV=1,
4          JL=4,
5          JW=12,
6          IJMAX=IMAX*JW)
      COMMON /FLOW/U(IMAX,JV:JW),V(IMAX,JV:JW)
      COMMON /FLOWS/US(IMAX,JV:JW),VS(IMAX,JV:JW)
      COMMON /FLOWN/UN(IMAX,JV:JW),VN(IMAX,JV:JW)
      COMMON /FLOWT/UT(IMAX,JV:JW),VT(IMAX,JV:JW)
      COMMON /UBAR/UB(IMAX),GAMMA(IMAX)
      COMMON /FLUX/QSTR(IMAX),QIN
      COMMON /RAD/R(JW),RS(JW),RS1(JW),RS2(JW),RS3(JW),RS4(JW),RS5(JW)
      DATA U,V/IJMAX*0.D0,IJMAX*0.D0/
      DATA US,VS/IJMAX*0.D0,IJMAX*0.D0/
      DATA UN,VN/IJMAX*0.D0,IJMAX*0.D0/
      DATA UT,VT/IJMAX*0.D0,IJMAX*0.D0/
      DATA UB/IMAX*0.D0/
      DATA GAMMA/IMAX*0.D0/
      DATA R,RS,RS1,RS2/JW*0.D0,JW*0.D0,JW*0.D0,JW*0.D0/
      DATA RS3,RS4,RS5/JW*0.D0,JW*0.D0,JW*0.D0/
      DATA QSTR/IMAX*0.D0/
      END

```



```

C
C
C
C
C
C
EVAPORATOR END BOUNDARY CONDITIONS
IF (I.EQ.1) THEN
  CORNER BETWEEN L/V INTERFACE AND EVAPORATOR END
  IF (J.EQ.JV) THEN
    TVTRM1=2.5D0/(TVESM**1.5)-1.5D0/(TVESM**2.5)*TVES
    TVTRM2=1.5D0/DSQRT(TVESM)-0.5D0/(TVESM**1.5)*TVES
    A(K,1)=0.D0
    A(K,2)=A2-A1*PG4E*TVTRM1
    A(K,3)=A1+A3
    B(K)=B2*T(I,J)+(B1+B3)*T(I,J)-A1*PG4E*TVTRM2
  ENDIF
  EVAPORATOR END BETWEEN CORNERS
  IF (J.NE.JV.AND.J.NE.JW) THEN
    A(K,1)=A1
    A(K,2)=A2
    A(K,3)=A3
    B(K)=B2*T(1,J)+(B1+B3)*T(2,J)
  ENDIF
  CORNER BETWEEN EVAPORATOR END AND AXIAL WALL
  IF (J.EQ.JW) THEN
    A(K,1)=A1+A3
    A(K,2)=A2-A3*4.D0*C4*SRAD(I)*(TWS(I)**3)
    A(K,3)=0.D0
    B(K)=B2*T(I,J)+(B1+B3)*T(I+1,J)
    +A3*C4*(QSTR(I)-SRAD(I)*(3.D0*(TWS(I)**4)+TE4))
  ENDIF
  ENDIF
  CELLS BETWEEN EVAPORATOR AND CONDENSER ENDS
  IF (I.NE.1.AND.I.NE.IMAX) THEN
    LIQUID/VAPOR INTERFACE CELLS
    IF (J.EQ.JV) THEN
      IF (I.LE.IE) THEN
        TVTRM1=2.5D0/(TVESM**1.5)-1.5D0/(TVESM**2.5)*TVES
        TVTRM2=1.5D0/DSQRT(TVESM)-0.5D0/(TVESM**1.5)*TVES
        PG4=PG4E
      ELSE
        TVTRM1=2.5D0/(TVCSM**1.5)-1.5D0/(TVCSM**2.5)*TVCS
        TVTRM2=1.5D0/DSQRT(TVCSM)-0.5D0/(TVCSM**1.5)*TVCS
        PG4=PG4C
      ENDIF
      A(K,1)=0.D0
      A(K,2)=A2-A1*PG4*TVTRM1
      A(K,3)=A1+A3
      DUM=-A1*PG4*TVTRM2
      B(K)=B1*T(I-1,J)+B2*T(I,J)+B3*T(I+1,J)+DUM
    ENDIF
    INTERIOR CELLS
    IF (J.NE.JV.AND.J.NE.JW) THEN
      A(K,1)=A1
      A(K,2)=A2
      A(K,3)=A3
      B(K)=B1*T(I-1,J)+B2*T(I,J)+B3*T(I+1,J)
    ENDIF
  ENDIF

```

```

C
C
C      PIPE AXIAL WALL CELLS
C
C      IF (J.EQ.JW) THEN
C          A(K,1)=A1+A3
C          A(K,2)=A2-A3*4.D0*C4*SRAD(I)*(TWS(I)**3)
C          A(K,3)=0.D0
C          B(K)=B1*T(I-1,J)+B2*T(I,J)+B3*T(I+1,J)
C              +A3*C4*(QSTR(I)-SRAD(I)*(3.D0*(TWS(I)**4)+TE4))
C      +
C      ENDIF
C  ENDIF
C
C      CONDENSER END CELLS
C
C      IF (I.EQ.IMAX) THEN
C
C          CORNER BETWEEN L/V INTERFACE AND CONDENSER END
C
C          IF (J.EQ.JV) THEN
C              TVTRM1=2.5D0/(TVCSM**1.5)-1.5D0/(TVCSM**2.5)*TVCS
C              TVTRM2=1.5D0/DSQRT(TVCSM)-0.5D0/(TVCSM**1.5)*TVCS
C              A(K,1)=0.D0
C              A(K,2)=A2-A1*PG4C*TVTRM1
C              A(K,3)=A1+A3
C              DUM=-A1*PG4C*TVTRM2
C              B(K)=(B1+B3)*T(I,J)+B2*T(I,J)+DUM
C          ENDIF
C
C          CONDENSER END BETWEEN CORNERS
C
C          IF (J.NE.JV.AND.J.NE.JW) THEN
C              A(K,1)=A1
C              A(K,2)=A2
C              A(K,3)=A3
C              B(K)=(B1+B3)*T(IMM1,J)+B2*T(IMAX,J)
C          ENDIF
C
C          CORNER BETWEEN CONDENSER END AND CONDENSER WALL
C
C          IF (J.EQ.JW) THEN
C              A(K,1)=A1+A3
C              A(K,2)=A2-A3*4.D0*C4*SRAD(I)*(TWS(I)**3)
C              A(K,3)=0.D0
C              B(K)=(B1+B3)*T(I-1,J)+B2*T(I,J)
C              +A3*C4*(QSTR(I)-SRAD(I)*(3.D0*(TWS(I)**4)+TE4))
C      +
C      ENDIF
C  ENDIF
C
C      190 CONTINUE
C      199 CONTINUE
C      RETURN
C      END

```



```

C *****
C * SUBROUTINE SPLIT2 - ENERGY EQUATION SOLUTION *
C *
C * THIS ROUTINE USES PEACEMAN-RACHFORD TEMPORAL ADI TO SOLVE THE *
C * SECOND TIME SPLIT OF THE ENERGY EQUATION *
C *
C *
C *****

```

```

C SUBROUTINE SPLIT2
C IMPLICIT REAL*8 (A-H,O-Z)
C PARAMETER (IE=3,
1      IC=6,
2      IMAX=21,
3      JV=1,
4      JL=4,
5      JW=12,
6      IJMAX=IMAX*JW)
COMMON /FLOW/U(IMAX,JV:JW),V(IMAX,JV:JW)
COMMON /FLOWS/US(IMAX,JV:JW),VS(IMAX,JV:JW)
COMMON /FLOWN/UN(IMAX,JV:JW),VN(IMAX,JV:JW)
COMMON /FLOWT/UT(IMAX,JV:JW),VT(IMAX,JV:JW)
COMMON /UBAR/UB(IMAX),GAMMA(IMAX)
COMMON /TEMP1/T(IMAX,JV:JW),TN(IMAX,JV:JW),TWS(IMAX)
COMMON /TEMP2/TV1,TV2,TAV,TE4
COMMON /TEMP3/TVES,TVESM,TVEP1,TVCS,TVCSM,TVCP1
COMMON /LUD/A(IJMAX,3),B(IJMAX)
COMMON /ADIAS1/ADIA1(JW),ADIA2(JW),ADIA3(JW)
COMMON /ADIBS1/ADIB1(JW),ADIB2(JW),ADIB3(JW)
COMMON /ADIAS2/ADIA4(JW),ADIA5(JW),ADIA6(JW)
COMMON /ADIBS2/ADIB4(JW),ADIB5(JW),ADIB6(JW)
COMMON /ADIPAR/PHIR,PHIX,PHIXOR,PHIROX,PHIXRH,PHIRXH
COMMON /FLUX/QSTR(IMAX),QIN
COMMON /LPROP/RHOL,TKL,HFG,ALPHAL,SIGMA,UMU,UNU,CP
COMMON /VPROP1/VMU,VNU,RHOV,PVAP
COMMON /VPROP2/PVE,PVC,RHOE,RHOC,DPDTE,DPDTC,PSIE,PSIC
COMMON /CRIT/TCR,RHOCR
COMMON /WPROP/SRAD(IMAX),ALPHAW,TKW
COMMON /RAD/R(JW),RS(JW),RS1(JW),RS2(JW),RS3(JW),RS4(JW),RS5(JW)
COMMON /R/PI,DELTA,RV,RL,RW,JLM1,JLP1,JVP1,JVP2,JVP3
COMMON /XD/X(IMAX),IEM1,IEM2,IEP1,ICM1,ICP1,IMM1,IMM2
COMMON /XDIM/EL,AL,CL,PIL,ELPH,CLPH
COMMON /DELTAS/HR,HX,HT,HXHALF,HRHALF,KTM
COMMON /ITER/EPSTV,MAXITV,ITRTV
COMMON /WICK/CW
COMMON /PROPG/PG1,PG2,PG3,PG4E,PG4C,PG5E,PG5C,PG6,PG7
COMMON /FGROUP/F0,F1,F2,F3,F4,F5,F6,F7,F8,T13
COMMON /CGROUP/C1,C2,C3,C4
COMMON /VGROUP/V1,V2,V3,V4,V5
COMMON /ZGROUP/Z1,Z2,Z3,Z4,Z5,Z6,Z7,Z8,Z9,Z10,Z11,Z12,Z13

```

```

C
C CALCULATE AT FULL TIME
C

```

```

DO 599 J=JV,JW
DO 590 I=1,IMAX
K=I+IMAX*(J-1)

```

```

C
C CALCULATE ELEMENTS
C

```

```

A4=ADIA4(J)-HXHALF*U(I,J)
A5=ADIA5(J)
A6=ADIA6(J)+HXHALF*U(I,J)
B4=ADIB4(J)-VS(I,J)*PHIXRH
B5=ADIB5(J)
B6=ADIB6(J)-VS(I,J)*PHIXRH

```



```

C
C
C      INTERIOR CELLS
      IF (I.NE.1.AND.I.NE.IMAX) THEN
        A(K,1)=A4
        A(K,2)=A5
        A(K,3)=A6
        B(K)=B4*T(I,J-1)+B5*T(I,J)+B6*T(I,J+1)
      ENDIF
    ENDIF
C
C
C      PIPE AXIAL WALL BOUNDARY CELL
      IF (J.EQ.JW) THEN
C
C
C        EVAPORATOR CORNER CONDITION
        IF (I.EQ.1) THEN
          A(K,1)=0.D0
          A(K,2)=A5
          A(K,3)=A4+A6
          B(K)=(B4+B6)*T(I,J-1)+B5*T(I,J)
          +      -B6*C4*(QSTR(I)+SRAD(I)*(T(I,J)**4-TE4))
        ENDIF
C
C
C        AXIAL WALL CONDITION
        IF (I.NE.1.AND.I.NE.IMAX) THEN
          A(K,1)=A4
          A(K,2)=A5
          A(K,3)=A6
          B(K)=(B4+B6)*T(I,J-1)+B5*T(I,J)
          1      -B6*C4*(QSTR(I)+SRAD(I)*(T(I,J)**4-TE4))
        ENDIF
C
C
C        CORNER BETWEEN AXIAL WALL AND CONDENSER END
        IF (I.EQ.IMAX) THEN
          A(K,1)=A4+A6
          A(K,2)=A5
          A(K,3)=0.D0
          B(K)=(B4+B6)*T(I,J-1)+B5*T(I,J)
          1      -B6*C4*(QSTR(I)+SRAD(I)*(T(I,J)**4-TE4))
        ENDIF
      ENDIF
590      CONTINUE
599      CONTINUE
      RETURN
      END

```

```

C *****
C *
C *          SUBROUTINE LORI
C * THIS SUBROUTINE USES LOWER-UPPER DECOMPOSITION TO SOLVE
C * TRIDIAGONAL LINEAR SYSTEMS OF EQUATIONS OF THE FORM AX=B.
C * DEFINITIONS:
C *
C *          A = TRIDIAGONAL MATRIX (SUPPLIED BY CALLING PROGRAM)
C *          B = RESULTANT VECTOR (SUPPLIED BY CALLING PROGRAM)
C *          X = SOLUTION VECTOR (REPLACES B ELEMENTS IN SOLUTION)
C *          IJMAX = NUMBER OF ELEMENTS IN VECTOR B
C *
C * THE ARRAY NOTATION A(ROW #,BAND #) IS USED
C * BAND # IS ASSIGNED FROM LOWER LEFT CORNER TO UPPER RIGHT
C *****
C
      SUBROUTINE LORI
      IMPLICIT REAL*8 (A-H,O-Z)
      PARAMETER (IE=3,
1             IC=6,
2             IMAX=21,
3             JV=1,
4             JL=4,
5             JW=12,
6             IJMAX=IMAX*JW)
      COMMON /LUD/A(IJMAX,3),B(IJMAX)
      IJM1=IJMAX-1
C
C      CONSTRUCT LOWER AND UPPER MATRICES FROM ELEMENTS OF A
C
      DO 17 I=1,IJMAX
        IF (I.GT.1) THEN
          A(I,2)=A(I,2)-A(I,1)*A(I-1,3)
        ENDIF
        IF (I.LT.IJMAX) THEN
          A(I,3)=A(I,3)/A(I,2)
        ENDIF
17    CONTINUE
C
C      FORWARD SUBSTITUTION IS USED TO SOLVE THE INTERMEDIATE EQUATION LY=B.
C
      B(1)=B(1)/A(1,2)
      DO 20 I=2,IJMAX
        B(I)=(B(I)-A(I,1)*B(I-1))/A(I,2)
20    CONTINUE
C
C      BACK SUBSTITUTION IS USED TO SOLVE FOR X FROM UX=Y. X IS STORED IN B
C
      DO 25 I=1,IJM1
        B(IJMAX-I)=B(IJMAX-I)-A(IJMAX-I,3)*B(IJMAX-I+1)
25    CONTINUE
      RETURN
      END

```

```

C *****
C * SUBROUTINE PROPS - LIQUID THERMOPHYSICAL PROPERTIES *
C * *
C * *
C *****
C

```

```

SUBROUTINE PROPS
IMPLICIT REAL*8 (A-H,O-Z)
PARAMETER (IE=3,
1         IC=6,
2         IMAX=21,
3         JV=1,
4         JL=4,
5         JW=12,
6         IJMAX=IMAX*JW)
COMMON /FLOW/U(IMAX,JV:JW),V(IMAX,JV:JW)
COMMON /FLOWS/US(IMAX,JV:JW),VS(IMAX,JV:JW)
COMMON /FLOWN/UN(IMAX,JV:JW),VN(IMAX,JV:JW)
COMMON /FLOWT/UT(IMAX,JV:JW),VT(IMAX,JV:JW)
COMMON /UBAR/UB(IMAX),GAMMA(IMAX)
COMMON /TEMP1/T(IMAX,JV:JW),TN(IMAX,JV:JW),TWS(IMAX)
COMMON /TEMP2/TV1,TV2,TAV,TE4
COMMON /TEMP3/TVES,TVESM,TVEP1,TVCS,TVCSM,TVCP1
COMMON /LUD/A(IJMAX,3),B(IJMAX)
COMMON /ADIAS1/ADIA1(JW),ADIA2(JW),ADIA3(JW)
COMMON /ADIBS1/ADIB1(JW),ADIB2(JW),ADIB3(JW)
COMMON /ADIAS2/ADIA4(JW),ADIA5(JW),ADIA6(JW)
COMMON /ADIBS2/ADIB4(JW),ADIB5(JW),ADIB6(JW)
COMMON /ADIPAR/PHIR,PHIX,PHIXOR,PHIROX,PHIXRH,PHIRXH
COMMON /FLUX/QSTR(IMAX),QIN
COMMON /LPROP/RHOL,TKL,HFG,ALPHAL,SIGMA,UMU,UNU,CP
COMMON /VPROP1/VMU,VNU,RHOV,PVAP
COMMON /VPROP2/PVE,PVC,RHOE,RHOC,DPDTE,DPDTC,PSIE,PSIC
COMMON /CRIT/TCR,RHOCR
COMMON /WPROP/SRAD(IMAX),ALPHAW,TKW
COMMON /RAD/R(JW),RS(JW),RS1(JW),RS2(JW),RS3(JW),RS4(JW),RS5(JW)
COMMON /R/PI,DELTA,RV,RL,RW,JLM1,JLP1,JVP1,JVP2,JVP3
COMMON /XD/X(IMAX),IEM1,IEP1,ICM1,ICP1,IMM1,IMM2
COMMON /XDIM/EL,AL,CL,PIL,ELPH,CLPH
COMMON /DELTAS/HR,HX,HT,HXHALF,HRHALF,KTM
COMMON /ITER/EPSTV,MAXITV,ITRTV
COMMON /WICK/CW
COMMON /PROPG/PG1,PG2,PG3,PG4E,PG4C,PG5E,PG5C,PG6,PG7
COMMON /FGROUP/F0,F1,F2,F3,F4,F5,F6,F7,F8,T13
COMMON /CGROUP/C1,C2,C3,C4
COMMON /VGROUP/V1,V2,V3,V4,V5
COMMON /ZGROUP/Z1,Z2,Z3,Z4,Z5,Z6,Z7,Z8,Z9,Z10,Z11,Z12,Z13

```

```

UPDATE THERMOPHYSICAL PROPERTIES USING AVERAGE VAPOR TEMP

```

```

TAV=0.5D0*(TVEP1+TVCP1)
PVAP=101325.D0*DEXP(18.832D0-13113.D0/TAV
1  -1.0948D0*DLOG(TAV)+1.9777D-4*TAV)
TR=TAV/TCR
TAV2=TAV*TAV
TAV3=TAV*TAV*TAV
SIGMA=.23402D0-1.D-4*TAV
TKL=1.0578D2-5.1767D-2*TAV+4.8696D-6*TAV2
HFG=1.4487D6*(1.D0-TR)+3.4860D6*((1.D0-TR)**0.2)
DPDT=PVPAP*(13113.D0/TAV2-1.0948D0/TAV+1.9777D-4)

```

```

IF (TAV.LE.1644.D0) THEN
  RHOL=1011.8D0-.22054D0*TAV-1.9226D-5*TAV2+5.6371D-9*TAV3
  DRODT=-.22054D0-3.8452D-5*TAV+1.6911D-8*TAV2
  DHDT=1.53139D3-.613452D0*TAV+3.35513D-4*TAV2+5.40593D6/TAV2
ELSE
  RHOL=RHOCR*(1.D0+2.3709D0*((1.D0-TR)**.31645)
1    +2.8467D-7*((TCR-TAV)**2))
  DRODT=-RHOCR*(.75027D0*((1.D0-TR)**.68355)/TCR
1    +5.6934D-7*(TCR-TAV))
  DHDT=805.8D0+304.21D0*((1.D0/(1.D0-TR))**0.67773)
ENDIF
RHOV=1.D0/(HFG/(TAV*DPDT)+1.D0/RHOL)
UMU=1.1259D-5*(RHOL**((1.D0/3.D0))*DEXP(.74908*RHOL/TAV)
UNU=UMU/RHOL
VNU=VMU/RHOV
DRODP=1.77587D-10/((1.2773035D0-1.8267670*TR+.54946350D0*TR*TR)
1    -(2.15463D-21*TAV+1.220408D-24*TAV2)*PVAP
2    +1.671245D-29*TAV*PVAP*PVAP
CP=DHDT+((DPDT*DRODP-DRODT)*TAV/RHOL-1.D0)*DPDT/RHOL
ALPHAL=TKL/(RHOL*CP)

C
C
C    UPDATE EVAPORATOR REGION VAPOR PROPERTIES
PVE=101325.D0*DEXP(18.832D0-13113.D0/TVEP1
1    -1.0948D0*DLOG(TVEP1)+1.9777D-4*TVEP1)
DPDTE=PVE*(13113.D0/(TVEP1*TVEP1)-1.0948D0/TVEP1+1.9777D-4)
RHOE=1.D0/(HFG/(TVEP1*DPDTE)+1.D0/RHOL)

C
C
C    UPDATE CONDENSER REGION VAPOR PROPERTIES
PVC=101325.D0*DEXP(18.832D0-13113.D0/TVCP1
1    -1.0948D0*DLOG(TVCP1)+1.9777D-4*TVCP1)
DPDTC=PVC*(13113.D0/(TVCP1*TVCP1)-1.0948D0/TVCP1+1.9777D-4)
RHOC=1.D0/(HFG/(TVCP1*DPDTC)+1.D0/RHOL)

C
C
C    UPDATE PROPERTY DEPENDENT PARAMETER GROUPS
PG1=V3*HFG
PG2=V4*HFG
PG3=RHOL*HFG*CW
PG4E=C3*HFG*HFG*RHOE/TKL
PG4C=C3*HFG*HFG*RHOC/TKL
PG5E=C2*HFG*RHOE/RHOL
PG5C=C2*HFG*RHOC/RHOL
PG6=V5*HFG
PG7=RHOL*RHOL*(1.D0/RHOV-1.D0/RHOL)
RETURN
END

```

```

C *****
C * SUBROUTINE REGIM1 - UNIFORM VAPOR CONDITION *
C * * * * *
C *****
C

```

```

SUBROUTINE REGIM1(ISPLIT)
IMPLICIT REAL*8 (A-H,O-Z)
PARAMETER (IE=3,
1         IC=6,
2         IMAX=21,
3         JV=1,
4         JL=4,
5         JW=12,
6         IJMAX=IMAX*JW)
COMMON /FLOW/U(IMAX,JV:JW),V(IMAX,JV:JW)
COMMON /FLOWS/US(IMAX,JV:JW),VS(IMAX,JV:JW)
COMMON /FLOWN/UN(IMAX,JV:JW),VN(IMAX,JV:JW)
COMMON /FLOWT/UT(IMAX,JV:JW),VT(IMAX,JV:JW)
COMMON /UBAR/UB(IMAX),GAMMA(IMAX)
COMMON /TEMP1/T(IMAX,JV:JW),TN(IMAX,JV:JW),TWS(IMAX)
COMMON /TEMP2/TV1,TV2,TAV,TE4
COMMON /TEMP3/TVES,TVESM,TVEP1,TVCS,TVCSM,TVCP1
COMMON /LUD/A(IJMAX,3),B(IJMAX)
COMMON /ADIAS1/ADIA1(JW),ADIA2(JW),ADIA3(JW)
COMMON /ADIBS1/ADIB1(JW),ADIB2(JW),ADIB3(JW)
COMMON /ADIAS2/ADIA4(JW),ADIA5(JW),ADIA6(JW)
COMMON /ADIBS2/ADIB4(JW),ADIB5(JW),ADIB6(JW)
COMMON /ADIPAR/PHIR,PHIX,PHIXOR,PHIROX,PHIXRH,PHIRXH
COMMON /FLUX/QSTR(IMAX),QIN
COMMON /LPROP/RHOL,TKL,HFG,ALPHAL,SIGMA,UMU,UNU,CP
COMMON /VPROP1/VMU,VNU,RHOV,PVAP
COMMON /VPROP2/PVE,PVC,RHOE,RHOC,DPDTE,DPDTC,PSIE,PSIC
COMMON /CRIT/TCR,RHOCR
COMMON /WPROP/SRAD(IMAX),ALPHAW,TKW
COMMON /RAD/R(JW),RS(JW),RS1(JW),RS2(JW),RS3(JW),RS4(JW),RS5(JW)
COMMON /R/PI,DELTA,RV,RL,RW,JLM1,JLP1,JVP1,JVP2,JVP3
COMMON /XD/X(IMAX),IEM1,IEP1,ICM1,ICP1,IMM1,IMM2
COMMON /XDIM/EL,AL,CL,PIL,ELPH,CLPH
COMMON /DELTAS/HR,HX,HT,HXHALF,HRHALF,KTM
COMMON /ITER/EPSTV,MAXITV,I TRTV
COMMON /WICK/CW
COMMON /PROPG/PG1,PG2,PG3,PG4E,PG4C,PG5E,PG5C,PG6,PG7
COMMON /FGROUP/F0,F1,F2,F3,F4,F5,F6,F7,F8,T13
COMMON /CGROUP/C1,C2,C3,C4
COMMON /VGROUP/V1,V2,V3,V4,V5
COMMON /ZGROUP/Z1,Z2,Z3,Z4,Z5,Z6,Z7,Z8,Z9,Z10,Z11,Z12,Z13

C
C SUM SURFACE TEMPERATURE
C
SUM=0.5D0*(T(1,JV)+T(IMAX,JV))
DO 200 I=2,IMM1
SUM=SUM+T(I,JV)
200 CONTINUE

C
C SET PARAMETERS FOR NEWTONS METHOD
C
IF (ISPLIT.EQ.1) TV1=TVES
IF (ISPLIT.EQ.2) TV1=TVEP1
BETA=HX*SUM
DRATIO=-RHOE/RHOL
TERMN=-RHOE*HFG/DPDTE

```

```

C
C      USE NEWTONS METHOD TO FIND VAPOR TEMPERATURE
C
      DO 600 M=1,MAXITV
        TVM1H=1.D0/DSQRT(TV1)
        TVM3H=1.D0/(TV1**1.5)
        AETA=1.D0/(1.D0+PG6*TVM3H*(TV1*PIL-BETA))
        FTV=TV1*(AETA+DRATIO)+TERMN
        FPRIME=AETA*(1.D0-AETA*PG6*0.5D0*(3.D0*BETA*TVM3H-
1      PIL*TVM1H))+DRATIO
        DELTV=-FTV/FPRIME
        TV1=TV1+0.8D0*DELTV
        ITRTV=M
        IF (DABS(DELTV).LT.EPSTV) GOTO 700
600    CONTINUE
700    IF (M.EQ.MAXITV) WRITE (6,9050) M,KTM
        TV2=TV1
9050  FORMAT (//////10X,'***** CAUTION *****'
1/10X,'VAPOR TEMPERATURE DID NOT CONVERGE'
2/15X,'ITERATIONS = ',I3
3/16X,'TIME STEP = ',I3)
        RETURN
      END

```



```

C *****
C * SUBROUTINE REGIM2 - SONIC VAPOR CONDITIONS *
C * *
C * *
C *****
C

```

```

SUBROUTINE REGIM2(ISPLIT)
IMPLICIT REAL*8 (A-H,O-Z)
PARAMETER (IE=3,
1         IC=6,
2         IMAX=21,
3         JV=1,
4         JL=4,
5         JW=12,
6         IJMAX=IMAX*JW)
COMMON /FLOW/U(IMAX,JV:JW),V(IMAX,JV:JW)
COMMON /FLOWS/US(IMAX,JV:JW),VS(IMAX,JV:JW)
COMMON /FLOWN/UN(IMAX,JV:JW),VN(IMAX,JV:JW)
COMMON /FLOWT/UT(IMAX,JV:JW),VT(IMAX,JV:JW)
COMMON /UBAR/UB(IMAX),GAMMA(IMAX)
COMMON /TEMP1/T(IMAX,JV:JW),TN(IMAX,JV:JW),TWS(IMAX)
COMMON /TEMP2/TV1,TV2,TAV,TE4
COMMON /TEMP3/TVES,TVESM,TVEP1,TVCS,TVCSM,TVCP1
COMMON /LUD/A(IJMAX,3),B(IJMAX)
COMMON /ADIAS1/ADIA1(JW),ADIA2(JW),ADIA3(JW)
COMMON /ADIBS1/ADIB1(JW),ADIB2(JW),ADIB3(JW)
COMMON /ADIAS2/ADIA4(JW),ADIA5(JW),ADIA6(JW)
COMMON /ADIBS2/ADIB4(JW),ADIB5(JW),ADIB6(JW)
COMMON /ADIPAR/PHIR,PHIX,PHIXOR,PHIROX,PHIXRH,PHIRXH
COMMON /FLUX/QSTR(IMAX),QIN
COMMON /LPROP/RHOL,TKL,HFG,ALPHAL,SIGMA,UMU,UNU,CP
COMMON /VPROP1/VMU,VNU,RHOV,PVAP
COMMON /VPROP2/PVE,PVC,RHOE,RHOC,DPDTE,DPDTC,PSIE,PSIC
COMMON /CRIT/TCR,RHOCR
COMMON /WPROP/SRAD(IMAX),ALPHAW,TKW
COMMON /RAD/R(JW),RS(JW),RS1(JW),RS2(JW),RS3(JW),RS4(JW),RS5(JW)
COMMON /R/PI,DELTA,RV,RL,RW,JLM1,JLP1,JVP1,JVP2,JVP3
COMMON /XD/X(IMAX),IEM1,IEP1,ICM1,ICP1,IMM1,IMM2
COMMON /XDIM/EL,AL,CL,PIL,ELPH,CLPH
COMMON /DELTAS/HR,HX,HT,HXHALF,HRHALF,KTM
COMMON /ITER/EPSTV,MAXITV,ITRTV
COMMON /WICK/CW
COMMON /PROPG/PG1,PG2,PG3,PG4E,PG4C,PG5E,PG5C,PG6,PG7
COMMON /FGROUP/F0,F1,F2,F3,F4,F5,F6,F7,F8,T13
COMMON /CGROUP/C1,C2,C3,C4
COMMON /VGROUP/V1,V2,V3,V4,V5
COMMON /ZGROUP/Z1,Z2,Z3,Z4,Z5,Z6,Z7,Z8,Z9,Z10,Z11,Z12,Z13

```

```

C
C
C FIND EVAPORATOR VAPOR TEMPERATURE

```

```

IF (ISPLIT.EQ.1) TV1=TVES
IF (ISPLIT.EQ.2) TV1=TVEP1
SUM=T(1,JV)*0.5D0
DO 200 I=2,IE
    SUM=SUM+T(I,JV)
200 CONTINUE
BETA=HX*SUM
RATIO=-RHOE/RHOL
TERM1=-PSIE/RHOE
TERM2=-RHOE*HFG/DPDTE

```

```

DO 300 M=1,MAXITV
  TM1H=1.D0/DSQRT(TV1)
  TM3H=1.D0/TV1**1.5
  AETA=1.D0/(1.D0-PG1*ELPH*TM1H+PG1*BETA*TM3H+TERM1)
  FTV=AETA*TV1+RATIO*TV1+TERM2
  FPRIM=AETA*(1.D0-0.5D0*AETA*PG1*(ELPH*TM1H-3.D0*BETA*TM3H))
+
  DELTV=-FTV/FPRIM
  TV1=TV1+0.8D0*DELTV
  ITRTV=M
  IF (DABS(DELTV).LT.EPSTV) GOTO 400
300 CONTINUE
  IF (M.EQ.MAXITV) WRITE (6,9050) M,KTM
C
C FIND CONDENSER VAPOR TEMPERATURE
C
400 IF (ISPLIT.EQ.1) TV2=TVCS
  IF (ISPLIT.EQ.2) TV2=TVCP1
  SUM=T(IMAX,JV)*0.5D0
  DO 500 I=IE+1,IMAX-1
    SUM=SUM+T(I,JV)
500 CONTINUE
  BETA=HX*SUM
  RATIO=-RHOC/RHOL
  TERM1=PSIC/RHOC
  TERM2=-RHOC*HFG/DPDTC
  DO 600 M=1,MAXITV
    TM1H=1.D0/DSQRT(TV2)
    TM3H=1.D0/TV2**1.5
    AETA=1.D0/(1.D0-PG2*CLPH*TM1H+PG2*BETA*TM3H+TERM1)
    FTV=AETA*TV2+RATIO*TV2+TERM2
    FPRIM=AETA*(1.D0-0.5D0*AETA*PG2*(CLPH*TM1H-3.D0*BETA*TM3H))
+
    DELTV=-FTV/FPRIM
    TV2=TV2+0.8D0*DELTV
    ITRTV=M
    IF (DABS(DELTV).LT.EPSTV) GOTO 700
600 CONTINUE
700 IF (M.EQ.MAXITV) WRITE (6,9050) M,KTM
  RETURN
9050 FORMAT (//////10X,'***** CAUTION *****'
1/10X,'VAPOR TEMPERATURE DID NOT CONVERGE'
2/15X,'ITERATIONS = ',I3
3/16X,'TIME STEP = ',I3)
  END

```

```

C *****
C * SUBROUTINE SPEED - LIQUID VELOCITIES *
C * *
C * *****
C

```

```

C SUBROUTINE SPEED(ISPLIT)
C IMPLICIT REAL*8 (A-H,O-Z)
C PARAMETER (IE=3,
1 IC=6,
2 IMAX=21,
3 JV=1,
4 JL=4,
5 JW=12,
6 IJMAX=IMAX*JW)
COMMON /FLOW/U(IMAX,JV:JW),V(IMAX,JV:JW)
COMMON /FLOWS/US(IMAX,JV:JW),VS(IMAX,JV:JW)
COMMON /FLOWN/UN(IMAX,JV:JW),VN(IMAX,JV:JW)
COMMON /FLOWT/UT(IMAX,JV:JW),VT(IMAX,JV:JW)
COMMON /UBAR/UB(IMAX),GAMMA(IMAX)
COMMON /TEMP1/T(IMAX,JV:JW),TN(IMAX,JV:JW),TWS(IMAX)
COMMON /TEMP2/TV1,TV2,TAV,TE4
COMMON /TEMP3/TVES,TVESM,TVEP1,TVCS,TVCSM,TVCP1
COMMON /LUD/A(IJMAX,3),B(IJMAX)
COMMON /ADIAS1/ADIA1(JW),ADIA2(JW),ADIA3(JW)
COMMON /ADIBS1/ADIB1(JW),ADIB2(JW),ADIB3(JW)
COMMON /ADIAS2/ADIA4(JW),ADIA5(JW),ADIA6(JW)
COMMON /ADIBS2/ADIB4(JW),ADIB5(JW),ADIB6(JW)
COMMON /ADIPAR/PHIR,PHIX,PHIXOR,PHIROX,PHIXRH,PHIRXH
COMMON /FLUX/QSTR(IMAX),QIN
COMMON /LPROP/RHOL,TKL,HFG,ALPHAL,SIGMA,UMU,UNU,CP
COMMON /VPROP1/VMU,VNU,RHOV,PVAP
COMMON /VPROP2/PVE,PVC,RHOE,RHOC,DPDTE,DPDTC,PSIE,PSIC
COMMON /CRIT/TCR,RHOCR
COMMON /WPROP/SRAD(IMAX),ALPHAW,TKW
COMMON /RAD/R(JW),RS(JW),RS1(JW),RS2(JW),RS3(JW),RS4(JW),RS5(JW)
COMMON /R/PI,DELTA,RV,RL,RW,JLM1,JLP1,JVP1,JVP2,JVP3
COMMON /XD/X(IMAX),IEM1,IEP1,ICM1,ICP1,IMM1,IMM2
COMMON /XDIM/EL,AL,CL,PIL,ELPH,CLPH
COMMON /DELTAS/HR,HX,HT,HXHALF,HRHALF,KTM
COMMON /ITER/EPSTV,MAXITV,ITRTV
COMMON /WICK/CW
COMMON /PROPG/PG1,PG2,PG3,PG4E,PG4C,PG5E,PG5C,PG6,PG7
COMMON /FGROUP/F0,F1,F2,F3,F4,F5,F6,F7,F8,T13
COMMON /CGROUP/C1,C2,C3,C4
COMMON /VGROUP/V1,V2,V3,V4,V5
COMMON /ZGROUP/Z1,Z2,Z3,Z4,Z5,Z6,Z7,Z8,Z9,Z10,Z11,Z12,Z13

C FIND FIRST TIME SPLIT L-V I/F RADIAL VELOCITIES
C
C IF (ISPLIT.EQ.1) THEN
C DO 100 I=1,IE
C VT(I,JV)=(TVES-T(I,JV))*PG5E/TVES**1.5
100 CONTINUE
C DO 150 I=IEP1,IMAX
C VT(I,JV)=(TVCS-T(I,JV))*PG5C/TVCS**1.5
150 CONTINUE
C ENDIF

```

```

C
C   FIND SECOND TIME SPLIT L-V I/F RADIAL VELOCITIES
C
  IF (ISPLIT.EQ.2) THEN
    DO 200 I=1,IE
      VT(I,JV)=(TVEP1-T(I,JV))*PG5E/TVEP1**1.5
200    CONTINUE
      DO 250 I=IEP1,IMAX
        VT(I,JV)=(TVCP1-T(I,JV))*PG5C/TVCP1**1.5
250    CONTINUE
      ENDIF
C
C   FIND MEAN AXIAL VELOCITIES
C
    SUM=VT(1,JV)
    DO 400 I=2,IMM1
      UB(I)=C1*(SUM+VT(I,JV))
      SUM=SUM+2.D0*VT(I,JV)
400    CONTINUE
C
C   FIND GRID VELOCITIES
C
    DO 700 I=2,IMM1
      IF (UB(I).NE.0.D0) THEN
        IF (VT(I,JV).NE.0.D0) THEN
          DU2DX=(UB(I-1)-2.D0*UB(I)+UB(I+1))/(HX*HX)
          S1=F7*VT(I,JV)/UNU
          S2=F4+F5*DU2DX/UB(I)+F6*VT(I,JV)/UNU
          S3=F1+F2*DU2DX/UB(I)+F3*VT(I,JV)/UNU
          DD=(-S2-DSQRT(S2*S2-4.D0*S1*S3))*0.5D0/S1
        ELSE
          DD=0.D0
        ENDIF
        BB=6.D0+T13*DD
        CC=-BB-DD
      ENDIF
      DO 600 J=JVP1,JLM1
        UT(I,J)=UB(I)*(BB*RS(J)+2.D0*CC*RS2(J)+3.D0*DD*RS3(J))
        VT(I,J)=CW*VT(I,JV)*(1.D0-F8*(BB*F0*RS2(J)+(BB+CC*F0)
1          *RS3(J)+(CC+DD*F0)*RS4(J)+DD*RS5(J)))*RV/R(J)
        IF (ISPLIT.EQ.2) THEN
          GAMMA(I)=UMU*(Z1*BB+Z2*CC+Z3*DD)+RHOL*VT(I,JV)
1          *(Z4*BB*BB+Z5*BB*CC+Z6*BB*DD+Z7*CC*CC
2          +Z8*CC*DD+Z9*DD*DD)
        ENDIF
600      CONTINUE
700    CONTINUE
    RETURN
    END
C
C*****
C INPUT DATA
C   NUM          NCASE          HX          HR          RV
C               PR              WR          HT          TE
C               TV
C*****

```

```

C
C      FIND SECOND TIME SPLIT L-V I/F RADIAL VELOCITIES
C
      IF (ISPLIT.EQ.2) THEN
        DO 200 I=1,IE
          VT(I,JV)=(TVEP1-T(I,JV))*PG5E/TVEP1**1.5
200      CONTINUE
          DO 250 I=IEP1,IMAX
            VT(I,JV)=(TVCP1-T(I,JV))*PG5C/TVCP1**1.5
250      CONTINUE
        ENDIF
C
C      FIND MEAN AXIAL VELOCITIES
C
      SUM=VT(1,JV)
      DO 400 I=2,IMM1
        UB(I)=C1*(SUM+VT(I,JV))
        SUM=SUM+2.D0*VT(I,JV)
400      CONTINUE
C
C      FIND GRID VELOCITIES
C
      DO 700 I=2,IMM1
        IF (UB(I).NE.0.D0) THEN
          IF (VT(I,JV).NE.0.D0) THEN
            DU2DX=(UB(I-1)-2.D0*UB(I)+UB(I+1))/(HX*HX)
            S1=F7*VT(I,JV)/UNU
            S2=F4+F5*DU2DX/UB(I)+F6*VT(I,JV)/UNU
            S3=F1+F2*DU2DX/UB(I)+F3*VT(I,JV)/UNU
            DD=(-S2-DSQRT(S2*S2-4.D0*S1*S3))*0.5D0/S1
          ELSE
            DD=0.D0
          ENDIF
          BB=6.D0+T13*DD
          CC=-BB-DD
        ENDIF
        DO 600 J=JVP1,JLM1
          UT(I,J)=UB(I)*(BB*RS(J)+2.D0*CC*RS2(J)+3.D0*DD*RS3(J))
          VT(I,J)=CW*VT(I,JV)*(1.D0-F8*(BB*F0*RS2(J)+(BB+CC*F0)
1          *RS3(J)+(CC+DD*F0)*RS4(J)+DD*RS5(J)))*RV/R(J)
          IF (ISPLIT.EQ.2) THEN
            GAMMA(I)=UMU*(Z1*BB+Z2*CC+Z3*DD)+RHOL*VT(I,JV)
1            *(Z4*BB*BB+Z5*BB*CC+Z6*BB*DD+Z7*CC*CC
2            +Z8*CC*DD+Z9*DD*DD)
          ENDIF
600      CONTINUE
700      CONTINUE
      RETURN
      END
C
C*****
C INPUT DATA
C      NUM          NCASE          HX          HR          RV
C              PR          WR          HT          TE
C              TV
C*****

```

